信州大学審査学位論文

Anisotropic Properties of Fiber-embedded Soft Materials

September, 2011

Jian Zhou

信州大学審査学位論文

Anisotropic Properties of Fiber-embedded Soft Materials

September, 2011

Department of Bioscience and Textile Technology, Interdisciplinary Graduate School of Science and Technology, Shinshu University

Jian Zhou

Table of Contents

List of Figures

List of Tables

Anisotropic Properties of Fiber-embedded Soft Materials

by

Jian Zhou

Submitted to the Interdisciplinary Division of Science and Technology
in Partial Fulfillment of the Requirements for the Degree of
Doctor of Philosophy in Bioscience and Fiber Engineering
at the
Shinshu University

Abstract

The field of anisotropic control using active materials has received great attention in recent years. One way of improving the level of actuator is the use of anisotropic actuators. In this thesis, electroactive composites incorporated aligned cellulose fibers or aligned electrospun nanofibers into conductive polymer matrix, were investigated for a highly anisotropic actuator material.

We first used cellulose fiber-based paper as the substrate for the anisotropic motion of actuators. The papers coated with highly conductive PEDOT/PSS showed a reversible generation of stress and anisotropic motion under electric fields, which leads to low-cost printable paper-based actuators.

Then we selected aligned electrospun nanofibers for anisotropic actuation of conductive polymers. We fabricated aligned PVP/PMMA nanofiber assemblies up to several centimeters in length to realize anisotropic motion of PEDOT/PSS films which cover the nanofiber assemblies. The aligned nanofiber assemblies displayed anisotropic wettability due to the high alignment degree of the nanofibers. We then demonstrated anisotropic electromechanical actuation of PEDOT/PSS film by using the aligned PVP/PMMA nanofibers. The composites with incorporated aligned nanofiber assemblies offer new opportunities to achieve anisotropic electromechanical actuation in soft materials.

Finally, we enhanced the electromechanical actuation property of PEDOT/PSS film by creating channels in the film. PEDOT/PSS aqueous dispersion penetrates into the nanofiber mat and all nanofibers are decorated with PEDOT/PSS. The nanofibers are robust enough to

retain its morphology during the deposition process and can be easily removed by the solvent extraction process. The channels in PEDOT/PSS film provide an adsorption interface of water vapors because of its large surface area and improve the actuation properties. It is possible to manipulate the diameter, shape, density and alignment of the channels in conductive polymer films by controlling the template nanofibers through different electrospinning conditions. Construction of aligned channels in conductive polymer can also realize anisotropic bending actuation with improved responsibility.

Thesis Supervisor: Dr. Mutsumi Kimura, Ph.D of Engineering

Title: Associate Professor of Functional Polymer

Chapter 1

General Introduction

Chapter 1 General Introduction

1.1 Motivation

Living things have acquired special anisotropic functions based on directional orientations of micro- and nanostructures during their evolution. Anisotropic structures in nature make possible directional motion, adhesion, friction or wetting.[1-5] These natural structures provide important insights for constructing artificial materials. Thus, bio-inspired advanced materials have been developed to mimic natural anisotropic structures.[6-9]

Long, fibrous structures such as collagens and celluloses are a major component of the extracellular matrix that supports most tissues by maintaining their strength and elasticity.[10] Moreover, composite materials with incorporated highly dense fibrous assemblies have been widely developed, and these materials show significantly different physical and chemical properties, which remain separate and distinct at the macroscopic or microscopic scale in the finished material structure.[11, 12] Several anisotropic functions of aligned fiber assemblies have been reported in the literature. Vertically aligned multi-walled carbon nanotube assemblies show strong adhesion to vertical surfaces, similar to gecko legs.[13] Anisotropic hydrophobic properties have been demonstrated by aligned nanofiber assemblies.[14] Fiber orientation within natural and artificial composites is a key factor in determining final properties.

Inspired by biological systems, artificial muscles have continued to grab the attention of the world. Biology contains especially rich knowledge for artificial muscles in diciplines such as animal physiology, systems biology and bimechanics.[15-20] The major goals for artificial muscles are movement, orientation, manipulation. In order to improve the control flexibility of artificial muscles, this thesis focuses on using nonaligned or aligned fibers which will be embedded in artificial muscles in controlling their anisotropic properties. Figure 1.1 shows the conceptual structure of fiber-embedded airtificial muscles. By embedding nonaligned or

aligned fibers into artificial muscles, it may generate anisotropic motions, which will provide flexible design ability for engineers.

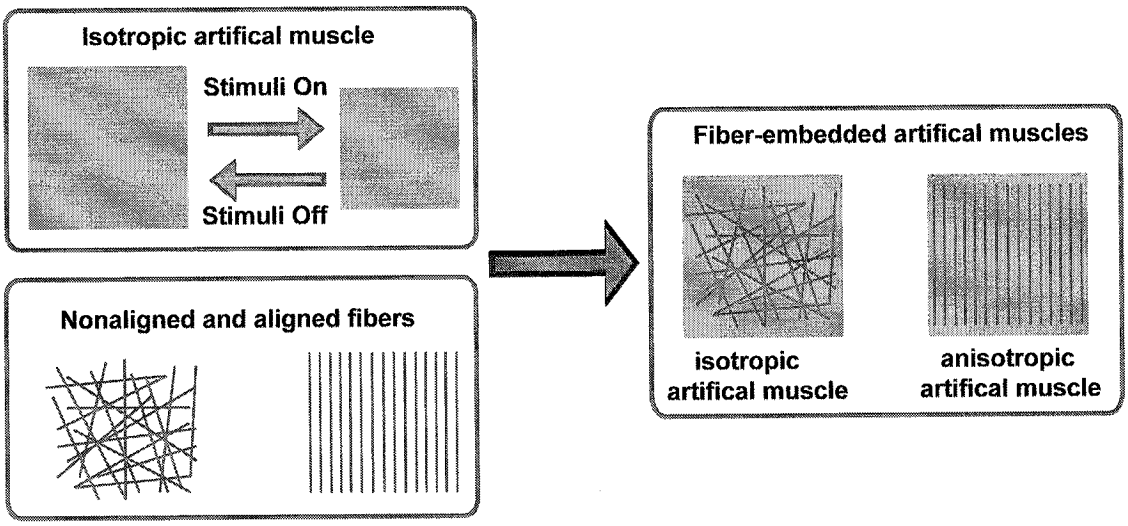

Figure 1.1 Conceptual structure of fiber-embedded airtificial muscles

Fiber reinforced composites are a strategy for producing advanced materials that take advantage of enhanced properties of fibers.[21-27] The matrix acts as an adhesive, binding the fibers and leading solidity to the material. It also protects the fibers from environment stress and damages. The modern use of fiber reinforced composites began in the 1945, with early applications being rocket motor cases and radomes using glass fibers.[24] Fiber reinforced composites used today have continued to grab the attention of materials technology, with performance and costs appropriate to lots of applications such as automobiles, space craft, architectures and so forth.[24, 25] However, heterogeneous materials combining the advantages of dissimilar constituents have been used by nature for millions of years. Natural fibres such as jute, coir and sisal can be considered as naturally occurring composites consisting mainly of cellulose fibrils embedded in lignin matrix.[23, 24] Due to their supporting function in the plant they are naturally endowed with good mechanical properties. Trees also employ cellulosic fibrous components to reinforce a lignin matrix, and arrange the strong fibers in the

right direction to withstand loads from wind and natural disasters. These natural fibres, with low density and acceptable specific mechanical properties, are more economical that man-made fibers such as glass fibers and carbon fibers. In this context, the application in composite materials of natural fibres obtained from plants offers an interesting alternative to industrial products. Present products range from the cladding of tailgates, columns, boots to covers for baggage compartments and door panels and the first structural elements for external applications are being tested.[28]

Not only natural plant fibers, but also human muscle fibers also play important parts for the human functions work out smoothly. Muscle fibers are not the strongest, fastest, but a certain combination of performance advantages and versatile characteristics makes it suitable for locomotion. Inspired by the working mechanism of muscle fibers, the incredible achievements of successive lifelike robots provide insight into challenges of using conventional actuators to drive machines that mimic human muscle and motions.[29] Many materials have been investigated as candidates for artificial muscle, including such as shape memory alloy, piezoelectric fibers, electroactive polymer and magnetostrictive materials.[15-20] Take conductive polymer fibers for examples. Baohua Qi reported electrochemical linear actuation of polyaniline fiber working in various aqueous electrolytes.[30] G. M. Spinks demonstrated carbon nanotube reinforced polyaniline fibers for high strength artificial muscles.[31] Plesse also displayed conductive polymer artificial muscle fibres with an open air linear actuation.[32] These conductive polymer fibers could really mimic human muscles and their motions with superior properties than human muscles.

The fiber materials play an important role in nature and also engineering materials. There are various fibers with specific properties we could choose for the reinforcement of composites.[21-27] Fibers are principal constituents in fiber reinforced composites. They have

the largest volume fraction in the composite and share the major portion of load in a composite.[28] It is crucial to understand not only the material site but also the structure site of fiber materials in composites. For fiber reinforced composites to be isotropic in specific properties, such as Young's modulus, all reinforcing fibers, have to be randomly oriented. This is not easy for discontinuous fibers due to the normal processing methods tend to impart a certain orientation to the fibers.[21] Aligned fiber reinforced composites typically exhibit anisotropy, which means some properties vary depending on which geometric axis or plane they are measured along. The anisotropic nature of fiber reinforced composites create a unique opportunity of tailoring is properties according to the design requirements. The design flexibility can be reinforce a structure in the direction of major stresses or increase its stiffness in preferred direction.[33] Recently, Li described highly anisotropic properties of thermoplastic elastomer composites with aligned hierarchical structures. This highly anisotropic properties may induce new applications for the novel elastomer composites.[34] Chen reported a fibrous composites with anisotropic distribution of mechanical properties be potential as bone substitutes and repairing devices.[35]

As the application of fiber reinforced composite becomes more widespread, there is a desire to add functionality not only simple enhancement of mechanical properties but also development of smart materials. In 1993, a new concept for actuator and sensing structure, "active fiber composite"(AFC) was first introduced by Hagood and Bent.[36] The composite incorporated unidirectional Piezoelectric Transducer (PZT) fibers into hybrid matrix, producing a highly conformable and anisotropic actuator material.[36, 37] With the combination of interdigital electrode on piezoceramics with PZT fiber composites in 1997, this lead to the realization of an actuation material superior to other commercial actuators at that time.[38, 39] This is a great success to realize the anisotropic actuation by incorporating unidirectional

fibers. It is well known that glass fiber reinforced polymer composites exhibit good performance combined with high strength, high fatigue resistance. and high corrosion resistance.[21, 22] Apart from these superior performance, Julie Etches et al followed by "active fiber composite" concept, and demonstrated hollow glass fibers were effectively used as containers for magnetic material, thus, composites reinforced by these fibers can achieve magnetically active structures.[40, 41] Moreover, Williams used macrofiber composites (MFC) to improve many of the limitations encountered with monolithic piezoceramic devices used to control structural dynamics.[42] The MFC retains the advantageous features of high strain energy density, anisotropic actuation, conformability and durability. It also incorporates of using an unifrom and repeatable high-yield fabrication process.[43-48] Hiroshi Asanuma reported a aluminum matrix composite by embedding Ti oxide/Ti fibers for generation of heat for actuation and sensing temperature/deformation.[49] Yun Lu developed electric heating actuators using SiC fiber reinforced aluminum composite, which could be used at elevated temperature.[50] These anisotropic actuators have been used to improve the level of anisotropic control for structural control applications.[51-61] These anisotropy features are advantageous in that they provide a great deal of design flexibility for engineers.

Despite the past successes in AFC and MFC, there are material issues in piezoelectric materials, associated with the generic properties of ceramic materials. As for sintered ceramic, the material is very brittle and easily damaged, which will result in further difficulties when integrate into structural applications. A further problem is the instinctive nature of piezoceramics, which of course creates good stiffness, but increase a significant mass to the total material.[62] Thus, distribution of light-weight soft fiber materials into polymer matrix to form an active composite may provide a solution to solve this issue.

Table 1.1 Materials with Anisotropic actuation

Materials	Configuration	Actuation motion	Working Medium	References
Polypyrrole	Film	Linear actuation	Electrolyte	63
Nafion/ionic polymer -metal composites	Film, microfiber	Bending actuation	Air	64
Electroclinic elastomer	Film	Linear actuation	Air	66
Electroactive cellulose paper	Trilayer(Au layer/cellulose paper/Au layer)	Bending actuation	Air	65

There are only a few reports in the literature on anisotropic actuation by using soft materials (Table 1.1). Anisotropic actuation of polypyrrole films was achieved by orientation of polymer backbones through directional stretching.[63] Uniaxial orientation of nafion, and the subsequent formation of electrode layers to create ionic polymer-metal composites, can also yield anisotropic actuation upon electrical stimulation.[64] Anisotropic bending actuation of cellulose/Au bilayer was demonstrated by cutting the bilayers in different directions.[65] Anisotropic response of a freestanding, electroclinic liquid crystal elastomer to an applied electrical field was also reported.[66] Theses anisotropic actuations allow more efficient control of independent structure and could largely improve structural control performance. Compare with the AFC and MFC, these actuators have a great flexibility and some of them even have anisotropic bend actuations.[62-66] For soft material like conductive polymer, studies have highlighted the difficulties with conductive polymers in anisotropic actuation control. Due to the isotropic nature of conductive polymer film, the material actuates all normal components of in-plane actuation equally.[19] Thus, there is a need for development of anisotropic actuation of conductive polymer based actuators. Inspired by active fiber composite configuration, there is potential for controlling anisotropic actuation of conductive polymer film by using natural fibers and synthetic fibers.

1.2 Objectives

The major goal of this work is to control anisotropic properties of soft materials which comprise polymeric fibers in conductive polymer matrix. This approach needed to confirm two major issues including the wetting properties of the fiber-based substrate and orientation of the fibers. Supporting tasks, which highlight the major goal of this thesis, are the following:

(1) Develop methods for characterizing actuation of PEDOT/PSS-based actuators.

(2) Identify the key issues and challenges in design of anisotropic actuators.

(3) Develop the ability to fabricate hydrophilic surfaces with anisotropic structures.

(4) Demonstrate the anisotropic actuators with biomimetic motions.

(5) Control the output of the actuators by varying different factors like applied voltage, relative humidity, frequency, weight of PEDOT/PSS.

(6) Improve the response speed of PEDOT/PSS film by construction channel structures using electrospun nanofibers.

1.3 Approach to Realize Anisotropic Actuation of PEDOT/PSS Film

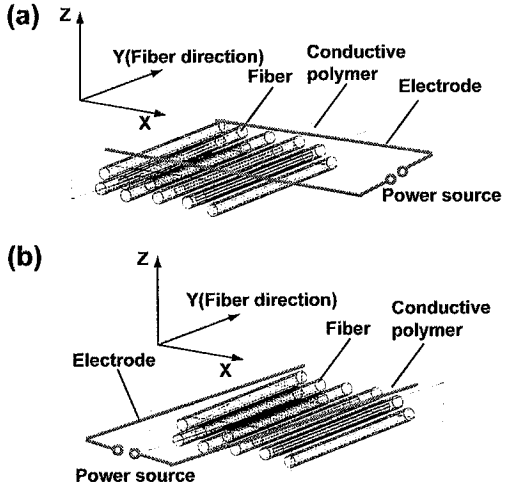

Figure 1.2 Approach to build up anisotropic PEDOT/PSS film actuator: (a) Loading direction parallel with fiber direction, (b) Loading direction parpendicular to fiber direction.

One means of improving the anisotropic actuation control is the use of aligned fiber assemblies. The aligned fiber assemblies give us added freedom to vary the mechanical properties by incorporating the aligned fibers into conductive polymer films. The conductive polymer act as host and active structure while the aligned fiber assemblies produce the desired degree of anisotropy by restricting the isotropic deformation of conductive polymer film. Figure 1.2 shows the approach to build up anisotropic PEDOT/PSS film actuators by using aligned fiber assemblies. In design process of this fiber reinforced conductive polymers, simple replacement of the component is not enough. There are two major issues that are important to the design of the fiber composite actuators. These can be separated into two categories: issues at the fiber material level, and issues at the structure level. Issues at the material level deal primarily with the wettability of the fiber material. The fiber material should have a good wettability that PEDOT/PSS dispersion could easily penetrate into the fiber substrate and coat onto the surface of all fibers. Issues at the structure level deal with the orientation degree of the fiber assemblies. The fiber assembly candidates should be carefully fabricated and characterized to ensure a high degree of orientation. If these two major issues are solved, the fiber composite incorporate electroactive PEDOT/PSS with aligned fiber assemblies could be used to realize anisotropic actuation. The benefits derived from such anisotropic structure will be elucidated in the next three chapters.

1.4 Backgrounds

1.4.1 Conductive Polymers

The fundamental discovery of conductive polymer by Shirakawa, MacDiarmid, and Heeger in 1977 marked the beginning of a dramatic growth in a field that earned its pioneers the Nobel Prize in Chemistry in 2000.[67, 68] The number of publications granted in the field has grown steadily over the last 30 years, and within the last 15 years inherently conductive polymers

(ICPs) have developed from laboratory researches into real commercial applications. Early versions of ICPs, mostly based on oxidatively doped polyacetylenes (PAcs) which discovered by the Nobel Prize winners in Chemistry, faced several intrinsic obstacles that prevented their industrial commercialization. The material degrades readily in air, and no known good methods exist for making easily processable PAc polymers. These obstacles led to the investigation of alternate polymer backbone structures in the search for stable, processable, high conductivity ICPs. Over these years, several promising polymer types have emerged as potentially useful replacement to PAc for commercial applications, including polypyrroles, polyanilines, and polythiophenes and so forth.[19, 69-76]

Based on the steady development of conductive polymers, there has been a great flow of new ideas, new understanding, new conducing polymer structures and devices with enhanced performance. Several breakthroughs have been made in the design and fabrication technology of the organic devices.[19, 77-79] Almost all properties, mechanical, electrical, and optical, are important in organics. Great advances have been made in the understanding of the transport of charge carriers in the conducting organics. High performance LEDs, lasers, solar cells and transistors have also been developed.[80-85] The performance of organic transistors has become comparable to that of the amorphous Si transistors while the performance and stability of the organic LEDs have become so good that they have already reached the market place. The reported efficiency of the bulk heterojunction organic solar cells is already more than 5%.[86]

1.4.2 Conductive Polymer Actuators

An actuator is a mechanical device for moving or controlling a mechanism or system. It is operated by a source of energy, usually in the form of an electric current, pH, pressure, light and converts that energy into some kind of motion.[15-20, 87-90] So an actuator can be simplified as a system that establishes a flow of energy between an input port and an output (mechanical)

port. The actuator is transducing input power in to mechanical power.[87-90] The application of actuator technologies is identified specifically for robots that are biomimetic in form. The incredible achievements and limitations of humanoid robots provide insight in to the challenges of using conventional actuators to drive machines that mimic human or animal form and motion. [15-20, 87-90] The development of responsive materials such as shape memory alloy actuators, piezoelectric actuators, electroactive polymer actuators and magnetostrictive actuator have given investigators lots of possibilities to engineer.

Conductive polymer actuator, which is one kind of the electroactive polymer actuators, has continued to grab considerable attention as a good candidate for artificial muscles, robotics and biomedical applications due to their outstanding advantages including light-weight, flexible, biocompatible, large strain and stress under low operating voltages (~10 V).[19] To date, many conductive polymers like polypyrroles, [19, 38] polyanilines[16, 91-93] and polythiophenes[94, 95] have been mainly investigated as self-standing film, bilayer or even multilayer actuators (Table 1.2).

Table 1.2 Conductive polymer-based actuators

Materials	Configurations	Working Medium	References
Polypyrrole	Film, bilayer and trilayer	Electrolyte and air	19, 63
Polyanilines	Film and microfiber	Electrolyte	19, 91-93
Poly(3,4-ethylenedioxythiophene)(PEDOT)	Film, fiber	Electrolyte and air	19, 32
PEDOT/PSS	Film	air	94

Through suitable design and fabrication, linear actuation could be achieved by free-standing film actuators or fiber actuators, while bending deformations could be produced by bilayer or multilayer actuators under appropriate external stimulus.[15-20, 87-95] These conjugated polymers undergo changes in volume caused by the movement of ions in and out of the polymer.[19, 96] Recently, the actuation of solid-state conjugated polymers under ambient

conditions has received attention because such actuators would further expand the range of applications, and can be operated without immersion in a liquid.[94-96]

1.4.3 Synthesis, Properties and Applications of PEDOT/PSS.

Early development in polythiophene chemistry like mono- and dialkoxythiophenes exhibited low conductivity in the oxidized or doped state. During the second half of 1980s, a breakthrough in this area was the synthesis of polymers of the bicyclic 3, 4-ethylenedioxythiophene (EDOT) and its derivatives by the scientists at the Bayer AG research laboratories in Germany. The new derivative, poly (3, 4-ethylenedioxythiophene) (PEDOT), has a very stable and highly conductive cationic doped state (Figure 1.2). The low HOMO-LUMO bandgap of the PEDOT allowed the formation of tremendously stable, highly conductive ICP.[19, 97, 98]

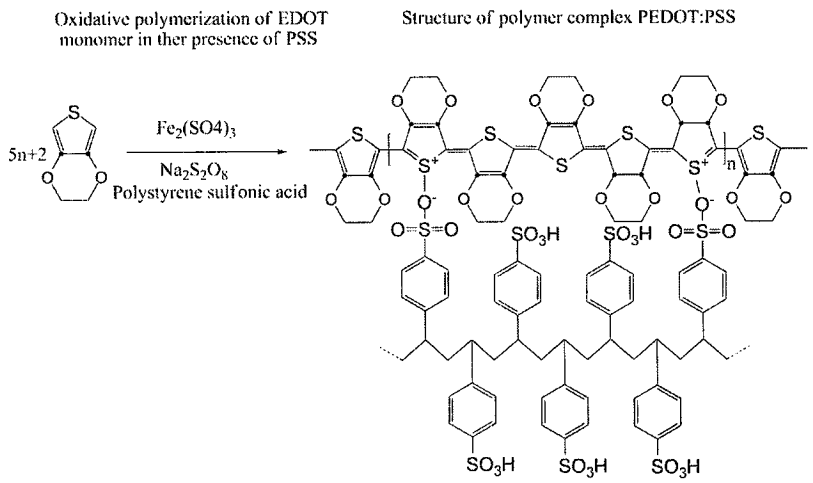

Figure 1.3 Synthesis and structure of PEDOT/PSS

Prepared using standard oxidative chemical or electrochemical polymerization methods, PEDOT was found to be insoluble in most commonly used solvents. Thus, it cannot be easily made into a processable solution. However, an industrially useful form of oxidized PEDOT can be made by aqueous oxidative polymerization of EDOT monomer in the presence of a template polymer, poly (styrene sulfonic acid) (PSS). PSS can be used as the

charge-balancing dopant during the polymerization with the oxidant sodium peroxodisulfate to yield PEDOT:PSS-complex in its conductive, cationic form (Figure 1.3). The PSS in this complex has two functions which are important for the final properties of PEDOT/PSS. The first function is to serve as the charge-balancing counterion to PEDOT.[19] The second function is to disperse PEDOT segments in water. In PEDOT/PSS aqueous dispersion, PEDOT/PSS segments are tightly attached to PSS chains of much higher molecular weight. Since the PEDOT stacks with monomeric counterions, highly conductivity of PEDOT/PSS is attributed to stacked arrangements of PEDOT chains.[19, 97-100] These particles consist about 90% to 95% of water. The PEDOT/PSS dispersion used in this research is Clevios P from H. C. Starck with a solid content of 1.3%. An interesting aspect of Clevio P is that, after drying, the remaining PEDOT/PSS films are conductive, transparent, flexible, mechanically durable and thermally stable. Due to these excellent properties, PEDOT/PSS have become the most successful conductive polymer in terms of commercial applications.[101, 102] For instance, it has been widely used as antistatic coatings, transparent conductor in electroluminescent devices, conductive layer in transistors and so forth.[19, 103-107]

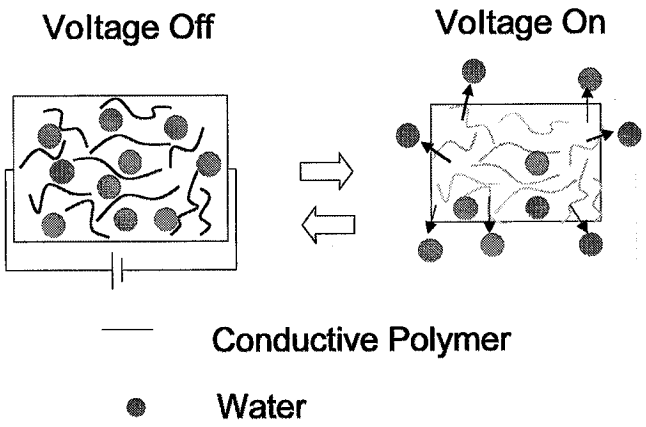

Figure 1.4 The mechanism of the PEDOT/PSS film actuator

Except for the aforementioned applications, researchers also found the potential of PEDOT/PSS for sensors and actuators. The hygroscopic properties of PEDOT/PSS from its

PSS groups allow uses, such as a humidity sensor, which was fabricated by inkjet printing PEDOT/PSS on a flexible polyimide substrate.[108] The humidity sensor shows not only fully reversible and repeatable capacity but also has a good sensitivity with an accuracy of 1% relative humidity (RH). Recently, Okuzaki and coworkers reported a PEDOT/PSS film actuator that exhibits large contraction strain under an applied electric field in ambient conditions.[94] The mechanism of this PEDOT/PSS film actuator was not driven by the electrochemical doping and dedoping but lies in the desorption of water vapor sorbed in the film through Joule heating, where the equilibrium of water vapor sorption can be controlled by an applied electrical field (Figure 1.4). While these PEDOT/PSS film actuators undergo isotropic dimensional changes, anisotropic motions have not been as extensively explored.

1.5 Scope of the Work

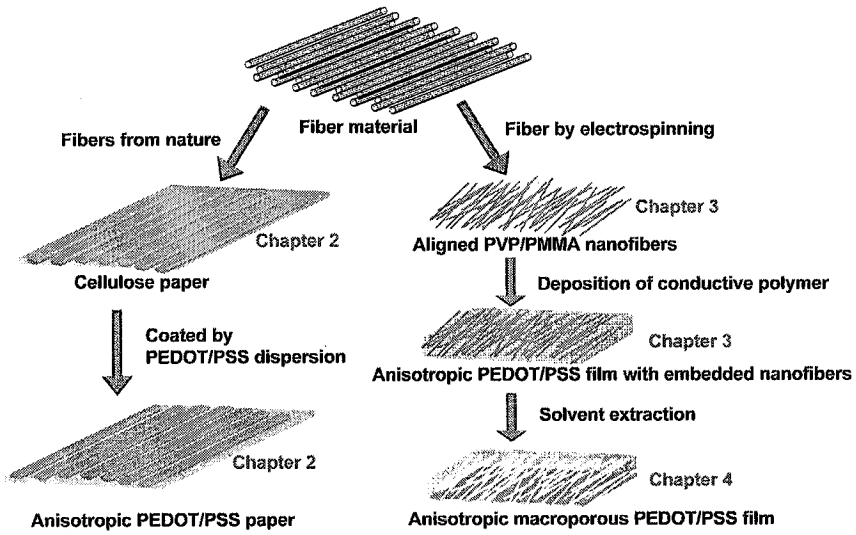

Figure 1.5 Scope of the thesis, illustrating concept to realize the anisotropic actuation of conductive polymers.

Figure 1.5 offers a pictorial scope of this thesis, breaking down the items by chapter. The first chapter has served as a general introduction into fiber reinforced composites. It provided a motivation for carrying out this work by reviewing fiber reinforced composite and showed the objective of realizing anisotropic actuation of conductive polymers by using fiber materials.

Then it followed by general approach to design anisotropic structures to realize the anisotropic actuation of PEDOT/PSS films. The background section provide a framework for building upon the goals by discussing previous research in related areas like different conductive polymer actuators and their working mechanisms, actuator design and fabrication, basic properties of PEDOT/PSS and their applications. Finally, the scope of work section briefly introduces the contents of each chapter of this thesis.

Chapter 2 contains the anisotropic properties of PEDOT/PSS coated cellulose paper. This chapter focus on an anisotropic actuation of cellulose fiber based composites. The merit of introducing cellulose paper is discussed. The dependence of electromechanical actuation on the orientation of cellulose fibers, applied voltage, relative humidity, weight of PEDOT/PSS, frequency are investigated. Furthermore, a butterfly-like reversible bending/unbending motion of the PEDOT/PSS coated paper are demonstrated when the voltage switching between on and off.

Chapter 3 demonstrates directional electromechanical properties of PEDOT/PSS composite films containing aligned poly(vinyl pyrrolidone)/poly(methyl methacrylate) (PVP/PMMA) nanofiber assemblies. In this chapter, electrospun nanofiber mats were use as reinforement material to control the anisotropic properties of PEDOT/PSS films. The aligned nanofiber assemblies showed anisotropic wettability based on the high alignment degree of the nanofibers. This is a prerequisite for the following procedure to deposit the PEDOT/PSS dispersion onto the nanofiber mats. The PEDOT/PSS composite film containing aligned nanofibers displayed an anisotropic actuation response when a voltage was applied in air. The orientation of the embedded nanofibers within the PEDOT/PSS matrix leads to the control of actuation direction due to the difference of anisotropic mechanical properties in the composite films.

Chapter 4 contains enhancement of electromechanical properties of PEDOT/PSS by construction of the empty channels in PEDOT/PSS film. The method of construction of nonaligned channels in PEDOT/PSS film using electrospun nanofiber templates is demonstrated. The anisotropic actuations of these macroporous film or bilayer were also demonstrated. The mechanism of the enhancement in electromechanical properties is discussed.

Chapter 5 drawn the conclusions from this thesis and their implications to conductive polymer based actuators are discussed. Possible areas of future work are also discussed.

References

1. K. Autumn, M. Sitti, Y. A. Ling, A. M. Peattie, W. R. Hansen, S. Sponberg, T. W. Keny, R. Fearing, J. N. Israelachvili, R. J. Full, Evidence for Van Der Waals Adhesion in Gecko Setae, *Proc. Nat. Aca. Sci.* **2002**, *99*, 12252-12256.
2. H. M. Whitney, M. Kolle, P. Andrew, L. Chittka, U. Steiner, B. J. Glover, Floral Iridescence, Produced by Diffractive Optics, Acts As a Cue for Animal Pollinators, *Science* **2009**, *323*, 130-133.
3. Y. M. Zheng, X. F. Gao, L. Jiang, Directional Adhesion of Superhydrophobic Butterfly Wings, *Soft. Matter.* **2007**, *3*, 178-182.
4. T. Binzoni, C. Courvoisier, R. Giust, G. Tribillon, T. Gharbi, J. C. Hebden, T. S. Leung, J. Roux, D. T. Delpy, Anisotropic Photon Migration in Human Skeletal Muscle, *Phys. Med. Biol.* **2006**, *51*, 79-90.
5. D. Y. Xia, S. R. J. Brueck, Strongly Anisotropic Wetting on One-Dimensional Nanopatterned Surfaces, *Nano Lett.* **2008**, *8*, 2819-2824.
6. N. A. Malvadkar, M. J. Hancock, K. Sekeroglu, W. J. Dressick, M. C. Demirel, An Engineered Anisotropic Nanofilm with Unidirectional Wetting Properties, *Nat. Mater.* **2010**, *9*, 1023-1028.
7. K. H. Chu, R. Xiao, E. N. Wang, Unidirectional Liquid Spreading on Asymmetric Nanostructured Surfaces, *Nat. Mater.* **2010**, *9*, 413-417.
8. J. Y. Chung, J. P. Youngblood, C. M. Stafford, Anisotropic Wetting on Tunable Micro-Wrinkled Surfaces, *Soft. Mater.* **2007**, *3*, 1163-1169.
9. D. Wu, Q. D. Chen, J. Yao, Y. C. Guan, J. N. Wang, L. G. Niu, H. H. Fang, H. B. Sun, A Simple Strategy to Realize Biomimetic Surfaces with Controlled Anisotropic Wetting, *Appl. Phys. Lett.* **2010**, *96*, 0537041-0537043.
10. P. Fratzl, Cellulose and Collagen: From Fibers to Tissues, *Curr. Opin. Coll. Interface. Sci.* **2003**, *8*, 32-39.
11. J. Dryden, A. Deakin, F. Zok, Effect of Cracks on the Thermal resistance of Aligned Fiber Composites, *J. Appl. Phys.* **2002**, *92*, 1137-1142.
12. B. K. Gu, Y. A. Ismail, G. M. Spinks, S. I. Kim, I. So, S. J. Kim, A Linear Actuation of Polymeric Nanofibrous Bundle for Artificial Muscles, *Chem. Mater.* **2009**, *21*, 511-515

13. L. T. Qu, L. M. Dai, M. Stone, Z. H. Xia, Z. L. Wang, Carbon Nanotube Arrays with Strong Shear Binding-On and Easy Normal Lifting-Off, *Science* **2008**, *322*, 238-242

14. H. Wu, R. Zhang, Y. Sun, D. L. Lin, Z. Q. Sun, W. Pan, P. Downs, Biomimetic Nanofiber Patterns with Controlled Wettability, *Soft. Matter.* **2008**, *4*, 2429-2433.

15. Y. Ma, J. Q. Sun, Humido- and Thermo-Responsive Free-Standing Films Mimicking the Petals of the Morning Glory Flower, *Chem. Mater.* **2009**, *21*, 898.

16. T. Mirfakhrai, J. D. Madden, R. H. Baughman, Polymer Artificial Muscles, *Mater. Today* **2007**, *10*, 30-38.

17. B. C. Yoseph, *Proc. SPIE Smart Structures and Materials Symposium, EAPAD Conference*, San Diego, CA, March 18-21, 2002.

18. J. D. Madden, Mobile Robots: Motor Challenges and Materials Solutions, *Science* **2007**, *318*, 1094-1097.

19. T. A. Skotheim, J. R. Reynolds, *Handbook of Conducting Polymers*,3rd edition, CRC Press, Boca Raton, 2007; Volume I, pp 308-309.

20. K. J. Kim, S. Tadokoro, *Electroactive Polymer for Robotic Application*: Springer-Verlag Limited: London 2007.

21. P. K. Mallick, *Fiber Reinforced Composites: Materials, Manufacturing, and Design,* 3rd ed.; CRC Press: Boca Raton, London, New York, 2007.

22. R. W. Cahn, E. A. Davis, I. M. Ward, *Microstructural design of fiber composites*, 1st ed.; Cambridge University Press: Cambridge, New York, Port Chester, Melbourne, Sydney, 1992.

23. S. Taj, M. A. Munawar, S. Khan, Natural Fiber-reinforced Polymer Composites, *Proc. Pakistan Acad. Sci.* **2007**, *44*, 129-144.

24. R. R. Fran, *Bast and other plant fibers,* Woodhead Publishing Limited and CRC Press: Abington, 2005.

25. P. Zugenmaier. *Crystalline Cellulose and Derivatives*, 3rd ed.; CRC Press: Boca Raton, London, New York, 2007.

26. H. Holik, *Handbook of Paper and Board*, 1st ed.; WILEY-VCH Press: Weinheim, 2006

27. A. A. Klyosov, *Wood-Plastic Composites,* 1st ed.; John Wiley & Sons, Inc: Hoboken, New Jersey, 2007

28. R. E. Mark, C. C. Habeger, J. Borch, M. B. Lyne, *Handbook of Physical Testing of Paper, Volume 1*, 2nd ed.; CRC Press:, 2001.

29. R. M. Alexander, *Exploring Biomimetics: Animals in Motion,* W. H. Freeman and Company Publish, New York, p.260,1992.

30. B. H. Qi, W. Lu, B. R. Mattes, Strain and Energy Efficiency of Polyaniline Fiber Electrochemical Actuators in Aqueous Electrolytes, *J. Phys. Chem. B.* **2004**, *108*, 6222-6227.

31. G. M. Spinks, V. Mottaghitalab, M. Bahrami-Samani, P. G. Whitten, G. G. Wallace, Carbon-Nanotube-Reinforced Polyaniline Fibers for High-Strength Artificial Muscles, *Adv. Mater.* **2006**, *18*, 637-640.

32. C. Plesse, F. Vidal, D. Teyssie and C. Chevrot, Conducting Polymer Artificial Muscle Fibres: Toward an Open-air Linear Actuation, *Chem. Commun.* **2010**, *46*, 2910-2912.

33. E. Car, S. Oller, E. Onate, A large Strain Plasticity Model for Anisotropic Materials: Composite Material Application, *Int. J. Plasticity*, **2001**, *17*, 1437-1463.

34. Y. Li, Y. Iwakura, K. Nakayama, H. Shimizu, Highly anisotropic Properties of Thermoplastic Elastomer Composites with Aligned Hierarchical Structures, *Composite. Sci. Tech.* **2007**, *67*, 2886-2891.

35. J. Chen, X. Li, W. Cui, C. Xie, J. Zou, B. Zou, Fibrious Composites with Anisotropic Distribution of Mechanical Properties After Layer-by-Layer Deposition of Aligned Electrospun Fibers, *Adv. Eng. Mater.* **2010**, *12*, 529-538.

36. A. A. Bent, N. W. Hagood, Development of Piezoelectric Fiber Composites for Structural Actuation, *Proceedings of the 34th AIAA/ASME/AHS Structures, Structural Dynamic and Materials Conference*, La Jolla, CA, April, 1993.

37. N. W. Hagood, A. Pizzochero, Residual Stiffness and Actuation of Piezoelectric Fiber Composites: Theory and Experiment, *J. Intell. Mater. Syst. Struct.* **1997**, *8*, 724-737.

38. A. A. Bent, N. W. Hagood, Piezoelectric Fiber Composites with Interdigitated Electrodes, *J. Intell. Mater. Syst. Struct.* **1997**, *8*, 903-912.

39. A. A. Bent, Active Fiber Composite Material Systems for Structural Control Applications, *Proc. SPIE.* **1999**, *3674*, 166-177.

40. J. Etches, I. Bond, P. Mellor, Manufacture of Maganetically Active Fibre Reinforced Composites for Use in Power Generation, Proc. SPIE. 2004, 5387, 54; doi:10.1117/12.543901

41. J. Etches, I. Bond, P. Mellor, Application of Maganetically Active Fibre Reinforced Composites, Proc. SPIE. 2005, 55761, 127-137.

42. R. B. Williams, D. J. Inman, W. K. Wilkie, Electromechanical Property Characterization of the Macro Fiber Composite Actuator, *Proc. ISMA*. 2005, September 27th - 28th 2005, Dresden.
43. W. Wilkie, J. High, P. Mirick, R. Fox, B. Little, R. Bryant, R. Hellbaum, A. Jalink, Low-Cost Piezocomposite Actuator for Structural Control Applications, Proceedings, SPIE's 7th International Symposium on Smart Structures and Materials, Newport Beach, California, March 5-9, 2000.
44. J. High, W. Wilkie, Method of Fabricating NASA-Standard Macro-Fiber Piezocomposite Actuators, NASA/TM-2003-212427, ARL TR 2833, June 2003.
45. W. K. Wilkie, Piezoelectric Macro-Fiber Composite Actuator and Method for Making Same, U.S. Patent No. 6,629,341, October 7, 2003.
46. P. Wierach, MFC-Actuators for Active Twist Control of a Model Rotor Blade, ISMA 2005 September 27th - 28th 2005, Dresden, Proceedings
47. J. L. Gaspar, Vibration Testing of Gossamer Space Structures with Macro Fiber Composite Actuators, ISMA 2005, September 27th - 28th 2005, Dresden, Proceedings
48. M. R. Shultz, Piezocomposite Actuators for Shape Control of Multistable Structures, ISMA 2005 September 27th.
49. H. Asanuma, Development of Active Material Systems Based on Fiber reinforced Metals, *Proc. SPIE*, **2006**, *6173*, 617315-1-617315-12.
50. Y. Lu, M. Hirohashi, Development of Electric Heating Actuators of Fiber Reinforced Metal Composite, *J. Mater. Sci.* **2004**, *39*, 969-973.
51. J. Etches, I. Bond, P. Mellor, Manufacture of Maganetically Active Fibre Reinforced Composites for Use in Power Generation, Proc. SPIE. 2004, 5387, 54; doi:10.1117/12.543901
52. J. Etches, I. Bond, P. Mellor, Application of Maganetically Active Fibre Reinforced Composites, Proc. SPIE. 2005, 55761, 127-137.
53. R. B. Williams, D. J. Inman, W. K. Wilkie, Electromechanical Property Characterization of the Macro Fiber Composite Actuator, *Proc. ISMA*. 2005, September 27th - 28th 2005, Dresden.
54. W. Wilkie, J. High, P. Mirick, R. Fox, B. Little, R. Bryant, R. Hellbaum, A. Jalink, Low-Cost Piezocomposite Actuator for Structural Control Applications, Proceedings, SPIE's 7th International Symposium on Smart Structures and Materials, Newport Beach,

California, March 5-9, 2000.

55. J. High, W. Wilkie, Method of Fabricating NASA-Standard Macro-Fiber Piezocomposite Actuators, NASA/TM-2003-212427, ARL TR 2833, June 2003.
56. W. K. Wilkie, Piezoelectric Macro-Fiber Composite Actuator and Method for Making Same, U.S. Patent No. 6,629,341, October 7, 2003.
57. P. Wierach, MFC-Actuators for Active Twist Control of a Model Rotor Blade, ISMA 2005 September 27th - 28th 2005, Dresden, Proceedings
58. J. L. Gaspar, Vibration Testing of Gossamer Space Structures with Macro Fiber Composite Actuators, ISMA 2005, September 27th - 28th 2005, Dresden, Proceedings
59. M. R. Shultz, Piezocomposite Actuators for Shape Control of Multistable Structures, ISMA 2005 September 27th.
60. H. Asanuma, Development of Active Material Systems Based on Fiber reinforced Metals, *Proc. SPIE*, **2006**, *6173*, 617315-1-617315-12.
61. Y. Lu, M. Hirohashi, Development of Electric Heating Actuators of Fiber Reinforced Metal Composite, *J. Mater. Sci.* **2004**, *39*, 969-973.
62. A. A. Bent, Active Fiber Composites for Structural Actuation, PhD thesis, 1997.
63. R. Pytel, E. Thomas, I. Hunter, Anisotropy of Electroactive Strain in Highly Stretched Polypyrrole Actuator, *Chem. Mater.* **2006**, *18*, 861-863.
64. J. K. Park, R. B. Moore, Influence of Ordered Morphology on the Anisotropic Actuation in Uniaxially Oriented Electroactive Polymer Systems, *ACS App. Mater. Interfaces.* **2009**, *1*, 697-702.
65. H. S. Kim. Y. X. Li, J. Kim, Electro-mechanical Behavior and Direct Piezoelectricity of Cellulose Electro-active Paper, *Sens. Actuators. A.* **2008**, *147*, 304-309.
66. C. M. Spillmann, B. R. Ratna, J. Naciri, Anisotropic Actuation of Electroclinic Liquid Crystal Elastomers, *Appl. Phys. Lett.* **2007**, *90*, 0219911-1-0219911-3.
67. H. Shirakawa, E. Louis, A.G. MacDiarmid, C. K. Chiang, and A. J. Heeger. Synthesis of Electrically Conducting Organic Polymers: Halogen Derivatives of Polyacetylene, $(CH)_x$, *J. Chem. Soc., Chem. Commun.* **1977**, (16), 578-580.
68. C. K. Chiang, C. R. Fincher, Jr., Y. W. Park, A. J. Heeger, H. Shirakawa, E. J. Louis, S. C. Gau, A. G. MacDiarmid, Electrical Conductivity in Doped Polyacetylene, *Phys. Rev. Lett.* **1977**, *39*, 1098-1101.

69. J. H. Burroughes, D. D. C. Bradley, A. R. Brown, R. N. Marks, K. MacKay, R. H. Friend, P. L. Burn, A. B. Holmes. Light-emitting Diodes Based on Conjugated Polymers. *Nature* **1990**, *347*, 539-541.

70. A. O. Patil, A. J. Heeger, and F. Wudl, Optical Properties of Conducting Polymers. *Chem. Rev.* **1988**, *88*, 183-200.

71. J. Roncali, Conjugated Poly(thiophenes): Synthesis, Functionalization and Applications, *Chem. Rev.* **1992**, *92*, 711-738.

72. G. Barbarella, M. Melucci, G. Sotgiu, The Versatile Thiophene: An overview of Recent Research on Thiophene-based Materials, *Adv. Mater.* **2005**,*17*, 1581-1593.

73. J. Roncali, Synthetic Principle for Bandgap Control in Linear P-conjugated Systems. *Chem. Rev.* **1997**, *97*, 173-205.

74. H. A. Ho, H. Brisset, E. H. Elandaloussi, P. Frere, and J. Roncali, Thiophene-based Conjugated Oligomers and Polymers with High Electron Affinity. Adv. Mater. **1996**, *8*, 990-994.

75. G. Casalbore-Miceli, N. Carmaioni, M. C. Galazzi, L. Albertin, A. M. Fichera, A. Geri, E. M. Girotto. Photoelectrical Properties in poly(alky/alkoxy-terthiophenes): Dependance of the Alkyl-chain Length. *Synth. Met.* **2002**, *125*, 307-311.

76. G. Zotti, R. Salmaso, M. C. Gallazzi, R. A. Marin. In Situ Conductivity of a Polythiophene from a Branched Alkoxy-substituted Tetrathiophene. Enhancement of Conductivity by Conjugated Cross-linking of Polymers chains. *Chem. Mater.* **1997**, *9*, 791-795.

77. J. Ouyang, C. W. Chu, F. C. Chen, Q. Xu, Y. Yang, High-Conductivity Poly(3,4-ethylenedioxythiophene):Poly(styrene sulfonate) Film and Its Application in Polymer Optoelectronic Devices, *Adv. Funct. Mater.* **2005**, *15*, 203-208.

78. S. Sakamoto, M. Okamura, Z. Zhao, Y. Furukawa, Raman Spectral Changes of PEDOT-PSS in Polymer Light-Emitting Diodes upon Operation, *Chem. Phys. Lett.* **2005**, *412*, 395-398.

79. B. Zhang, J. Sun, H. E. Katz, F. Fang, R. L. Opila, Promising Thermoelectric Properties of Commercial PEDOT:PSS Materials and Their Bi_2Te_3 Powder Composites, *ACS Appl. Mater. Interfaces*. **2010**, *2*, 3170-3178.

80. V. Cimrova, Polarized Light Emission from LEDs Prepared by the Langmuir–Blodgett Technique, *Adv. Mater.* **1996**, *8*, 146-149.

81. N. Tessler, Lasers Based on Semiconducting Organic Materials. *Adv. Mater.* **1999**, *11*, 363-370.

82. C. J. Brabec, N. S. Sariciftci, J. C. Hummelen, Plastic Solar Cells. *Adv. Funct. Mater.* **2001**, *11*, 15-26.

83. S. Karg, Characterization of Light Emitting Diodes and Solar Cells Based on Polyphenylene-vinylene. *Synth. Met.* **1993**, 4186, 56-57.

84. W. Reiss, Electroluminescence and Photovoltaic Effect in PPV Schottky Diodes. *J. Lumin.* **1994**, *906*, 60-61.

85. A. C. Arias, Doped Conducting-polymer–semiconducting-polymer Interfaces: Their Use in Organic Photovoltaic Devices, *Phys. Rev. B.* **1999**, *60*, 1854-1860.

86. H. Hoppe, N.S. Sariciftci. Organic Solar Cells: An Overview. *J. Mater. Res.* **2004**, *19*, 1924-1945.

87. Y. Bar-cohen, *Biomimetics-Biologically Inspired Technologies*, 1st ed.; CRC Press: Boca Raton, 2006.

88. G. G. Wallace, G. M. Spinks, L. A. P. Kane-Maguire, P. B. Teasdale, *Conductive Electroactive Polymers:Intelligent Polymer Systems*, 3rd ed.; CRC Press: Boca Raton, London, New York, 2009.

89. M. Shahinpoor, K. J. Kim, M. Mojarrad, *Artificial Muscles: Applications of Advanced Polymeric Nanocomposites*, 3rd ed.; CRC Press: Boca Raton, London, New York, 2007.

90. L. Dai, *Intelligent Macromolecules for Smart Devices: From Materials Synthesis to Device Applications,* 1st ed.; Springer-Verlag: London, Berlin, Heidelberg, New York, Hong Kong, Milan, Paris, Tokyo, 2004.

91. W. Lu, E. Smela, P. Adams, G. Zuccarello, B. R. Mattes, Development of Solid-in-Hollow Electrochemical Linear Actuator Using Conductive Polyaniline, *Chem. Mater.* **2004**, *16*, 1615-1621.

92. A. Mazzoldi, C. Deglinnocenti, M. Michelucci, D. De Rossi, Actuative Properties of Polyaniline Fibers Under Electrochemical Stimulation, *Mater. Sci. Eng. C.* **1998**, *6*, 65-72.

93. W. Lu, A. G. Fadeev, B. Qi, E. Smela, B. R. Mattes, J. Ding, G. M. Spink, J. Mazurkiewicz, D. Zhou, G. G. Wallace, D. R. MacFarlane, S. A. Forsyth, M. Forsyth, Use of Ionic Liquids for π-Conjugated Polymer Electrochemical Devices, *Science* **2002**, *297*, 983-987.

94. H. Okuzaki, H. Suzuki, T. Ito. Electromechanical Properties of

Poly(3,4-ethylenedioxythiophene)/poly(4-styrene sulfonate) Films. *J. Phys. Chem. B.* **2009**, *113*, 11378.

95. C. Plesse, F. Vidal, D. Teyssie and C. Chevrot, Conducting Polymer Artificial Muscle Fibres: Toward an Open-air Linear Actuation, *Chem. Commun.* **2010**, *46*, 2910-2912.
96. E. Smela, Conjugated Polymer Actuator for Biomedical Applications, *Adv. Mater.* **2003**, *15*, 481-494.
97. L. Groenendaal, F. Jonas, D. Freitag, H. Pielartzik, J. R. Reynolds, Poly(3,4-ethylenedioxythiophene) and Its Derivatives: Past, Present, and Future, *Adv. Mater.* **2000**, *12*, 481-494.
98. S. Kirchmeyer, K. Reuter. Scientific Importance, Properties and Growing Applications of Poly(3,4-ethylenedioxythiophene), *J. Mater. Chem.* **2005**, *15*, 2077-2088.
99. U. Lang, E. Muller, N. Naujoks, J. Dual, Microscopical Investigations of PEDOT:PSS Thin Films, *Adv. Funct. Mater.* **2009**, *19*, 1-6.
100. U. Lang, N. Naujoks, J. Dual, Mechanical Characterization of PEDOT:PSS Thin Films, *Synth. Met,* **2009**, 159, 473-479.
101. P. Tehrani, L. O. Hennerdal, A. L. Dyer, J. R. Reynolds, M. Berggren. Improving the Contrast of All-printed Electrochromic Polymer on Paper Displays, *J. Mater. Chem.* **2009**, *19*, 1799-1802.
102. X. Crispin, F. L. E. Jakobsson, A. Crispin, P. C. M. Grim, P. Andersson, A. Volodin, C. Van Haesendonck, M. Van der Auweraer, W. R. Salaneck, M. Berggren, The Origin of the High Conductivity of Poly(3,4-ethylenedioxythiophene)–Poly(styrenesulfonate) (PEDOT–PSS) Plastic Electrodes, *Chem. Mater.* **2006**, *18*, 4354-4360.
103. D. Hohnholz, H. Okuzaki, A. G. MacDiarmid, Plastic Electronic Devices Through Line Patterning of Conducting Polymers, *Adv. Funct. Mater.* **2005**, *15*, 51-66.
104. Y. S. Hsiao, W. T. Whang, C. P. Chen, Y. C. Chen, High Conductivity Poly(3,4-ethylenedioxythiophene):Poly(styrenesulfonate) Film for Use in ITO-free Polymer Solar Cells. *J. Mater. Chem.* **2008**, *18*, 5948-5955.
105. S. Sakamoto, M. Okamura, Z. Zhao, Y. Furukawa, Raman Spectral Changes of PEDOT-PSS in Polymer Light-Emitting Diodes upon Operation, *Chem. Phys. Lett.* **2005**, *412*, 395-398.
106. D. Y. Kim, Y. S. Kim, K. W. Choi, J. C. Grunlan, C, H. Yu, Improved Thermoelectric Behavior of Nanotube-filled Polymer Composites with

Poly(3,4-ethylenedioxythiophene)/poly(styrenesulfonate), *ACS Nano*. **2010**, *4*, 513-523.

107. B. Zhang, J. Sun, H. E. Katz, F. Fang, R. L. Opila, Promising Thermoelectric Properties of Commercial PEDOT:PSS Materials and Their Bi_2Te_3 Powder Composites, *ACS Appl. Mater. Interfaces*. **2010**, *2*, 3170-3178

108. H. C. Lim, Y. F. Hor, Y. L. Hor, J. L, Zunino III, J. F. Federici, Poly(3,4-ethylenedioxythiophene):Poly(styrenesulfonate) for humidity Sensing Using Ink-jet Printing Technique on Flexible Polyimide Substrate, *Sensor. Tranducers. J.* **2009**, *101*, 52-59.

Chapter 2

Anisotropic Actuation of PEDOT/PSS-coated Cellulose Papers

Chapter 2 Anisotropic Actuation of PEDOT/PSS-coated Cellulose Papers

Abstract: This chapter describes actuation of electro-active cellulose papers by using poly (3, 4-ethylenedioxythiophene):poly(4-styrene sulfonate), (PEDOT/PSS) in ambient air. PEDOT/PSS coated papers were prepared by coating of concentrated PEDOT/PSS aqueous dispersion on cellulose papers. The electro-active papers generated contractile stress repeatedly by applying voltage, and they exhibited different stresses within the plain of the paper in accordance with the orientation of cellulose fibers. The dependence of electromechanical actuation on the orientation of cellulose fibers, applied voltage, relative humidity, weight of PEDOT/PSS, frequency have been investigated. The repeatability of the actuation is confirmed by generation of a stable stress more than 2000 times under ambient conditions. Furthermore, the PEDOT/PSS paper underwent intensive bending/unbending motion and showed a dependence on relative humidity. We also demonstrated that a butterfly-like reversible bending motion of the PEDOT/PSS coated paper occurred when the voltage switching between on and off. The present study suggests that PEDOT/PSS papers can be highly scalable for high-performance electromechanical devices in ambient air.

2.1 Introduction

While polymer-based actuators undergo isotropic dimensional changes, anisotropic motions have not been as extensively explored. One way to achieve the anisotropic motion of the actuators would be to use composites of actuation materials with a suitable substrate.

Cellulose fiber-based paper is a versatile material because of the abundance of its composite raw materials and its many uses involving printed media, as well as packaging and cleaning materials. Cellulose fiber-based paper is produced in modern continuous flow

processes and cellulose fibers in papers are aligned parallel to the direction of paper flow through the paper machine (machine direction).[1] Paper is also a suitable substrate material for building devices as it is widely available, easily patterned by cutting or drawing/printing, as well as being lightweight, and low cost.[2] During recent years, solution-processible nanomaterials such as metal nanoparticles, carbon nanotubes, organic semi-conductive materials, and conductive polymers have expected to be active materials for low-cost electronic devices.[3] In this context, the combination between nanomaterials and paper substrates through solution-processes allow the realization of active matrix displays,[4] organic thin-film transistors[5], organic photodiodes[6], lithium ion batteries[7, 8], circuits[9], and diagnostic devices.[10-13] Three-dimensional hierarchical porous fiber structure and functional groups in paper results in the strong adhesion of nanomaterials onto paper and the deposition of nanomaterials produce high-quality and stable films on paper.

In this Chapter, we used a mechanically robust cellulose fiber-based paper as the substrate for the anisotropic motion of actuators and the papers coated with highly conductive PEDOT/PSS showed a reversible generation of stress and anisotropic motion under electric fields, which leads to low-cost printable natural fiber-based actuators. [14-18]

2.2 Experimental Section

2.2.1 Materials

PEDOT/PSS aqueous dispersion (Clevios P AG) was purchased from H. C. Starck, Inc. Cellulose paper with a basis weight of 15.6 g/m^2 (25 μm thickness) was used as a substrate of paper actuators. Ethylene glycol was purchased from Wako chemicals in analytical grade.

2.2.2 Preparation of PEDOT/PSS Paper

The aqueous dispersion of PEDOT/PSS was evaporated at 120 °C for 3 hours to increase its viscosity. The solid content of the concentrated solution of PEDOT/PSS was ca. 3.1% estimated from the change in weight, and its absolute viscosity was 170 mPa·s at 25 °C, as measured by a viscometer (VA-10A, CBC Co. Ltd., Japan). Coating and drying processes were carried out in a labcoater/drier (LTE-S E-06, Werner Mathis AG, Switzerland). PEDOT/PSS papers were obtained by bar-coating the concentrated PEDOT/PSS solution onto cellulose paper with dimensions of 21 × 27 cm with a doctor blade and then the coated papers were dried at 120 °C. Five different thicknesses of PEDOT/PSS-coated paper were obtained by controlling the distance between the doctor blade and the paper at 0.04, 0.06, 0.08, 0.1 and 0.13 mm. The coated papers were immersed in EG (100 ml) for 20 min and then dried at 100 °C for 60 min in air.

2.2.3 Measurements

The average thickness of Cellulose paper and PEDOT/PSS coated paper were measured by a micrometer(the paper material was folded for 4 times and the measured value will be divided by 16).Mechanical properties were performed with a tension tester (RTC-1250A, A&D Co., Ltd) at a constant strain rate of 100 % min^{-1} (chuck distance 30 mm). Tensile specimen were prepared in size of 30 × 2 mm. Young's modulus was calculated from the stress-strain curves and represented average values of at least 10 tests.

Conductivity measurements of the papers were measured with a source meter (Model 2400, Keithley) with a universal four-probe (four proved electrode, BAS Co., tip diameter 0.1 mm, probe spacing 1 mm). The sheet resistances (R_{spuare}) of PEDOT/PSS-coated papers were calculated from the following equation[19];

$$R_{spuare}\ (\Omega/\text{square}) = K \times (U / I)$$

where K: a constant depending on the geometry (In this case, K = log (2/Ω) = 4.532), U (V) : the measured voltage, and I (A): the set current. The electrical contacts were made by applying the four probes with an insulated weight of 200g on the PEDOT/PSS papers. To minimize errors, 10 measurements were taken on surface on each sample.

The actuation performance of PEDOT/PSS coated papers was tested on a force gauge (ZP-2N, Imada Co., Ltd.). Actuation specimen was prepared in size of 140 × 2 mm and settled into a humidity-controlled chamber. The electric field was applied to the paper with a computer-driven DC power supply (PK-80, Matsusada Co., Ltd.) through a pair of copper wires (170 m) attached to the paper with silver paste, the distance between the electrode was 100 mm. The electric currents were monitored by a digital multimeter (U1252A, Agilent). Temperature and humidity in the measuring chamber were monitored by a humidity and temperature sensor (HMI 31, VAISALA Co., Ltd). The force and current changes were collected through USB communication to the computer. The force was converted into stress by dividing the cross section area of the PEDOT/PSS coated papers.

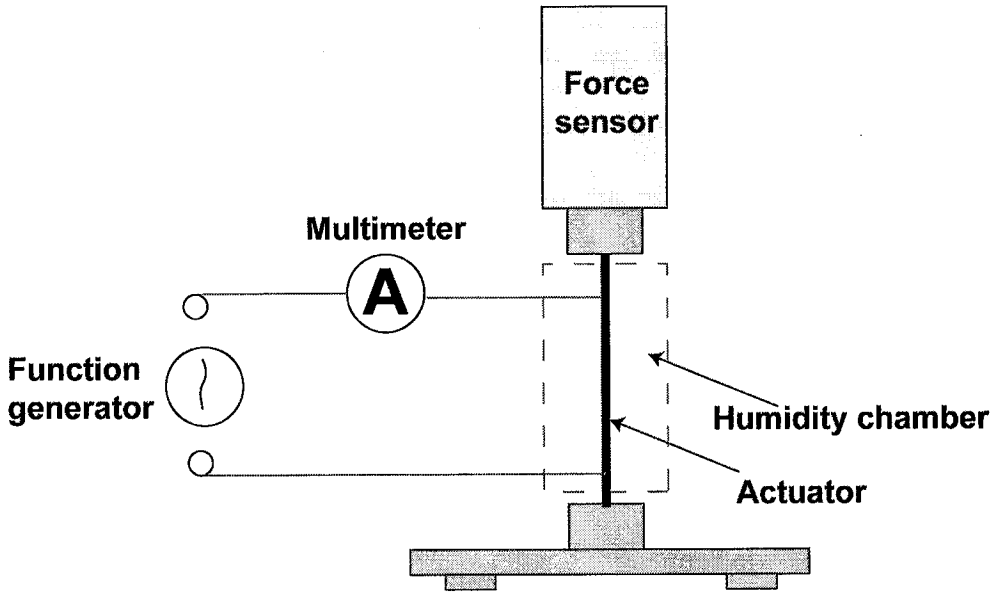

Figure 2.1 Illustration of actuation measurement system.

2.3 Results and Discussion

2.3.1 Fabrication and Characterization of Conductive PEDOT/PSS Papers

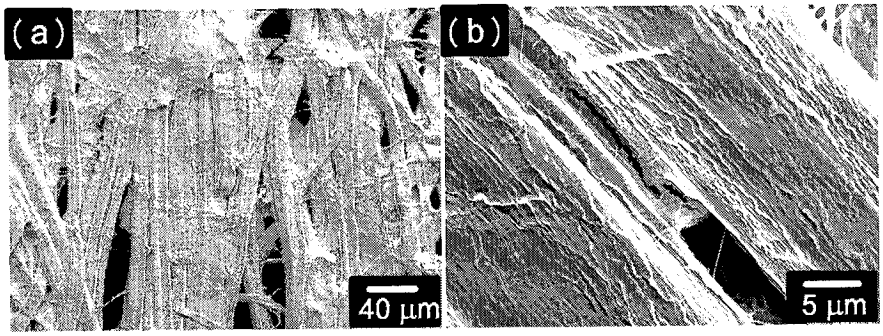

Figure 2.2 SEM images of cellulose paper

Cellulose paper has been used in many ways due to its good mechanical strength and printing quality. We used this paper as a substrate for fabricating paper-based actuators. As shown in the scanning electron microscope (SEM) image in Figure 2.2a, the cellulose paper is composed of long belt-like cellulose fibers with an average width of 15.6 ± 3.7 μm and an average thickness of 3.5± 0.7 μm. Each cellulose fiber is comprised of multiple individual fibrils that are rich in hydroxyl groups (Figure 2.2b). This hierarchical structure has high porosity, which allows the cellulose paper to absorb large amounts of water or other polar solvents.[8, 20] The cellulose fibers are laid down with their axes parallel to the plane of the sheet. The mean orientation angle of Cellulose paper was 0.16 degree against the machine direction and over 70% of fibers was found to be in the angular range of -15 to +15 degrees obtained by the statistical analysis of fiber distribution orientation.[21] The observed structural anisotropy in the plain of the paper may affect the properties of paper-based devices.

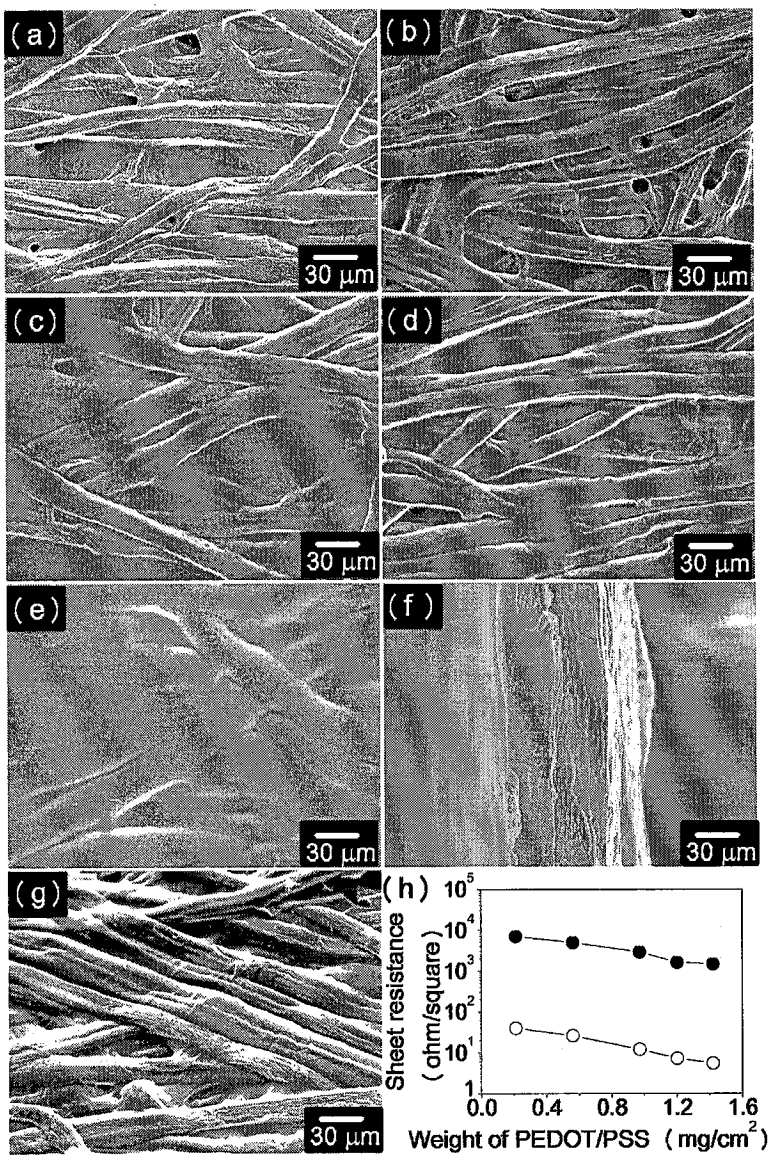

Figure 2.3 SEM images of PEDOT/PSS papers containing different weights of PEDOT/PSS: (a) 0.21 mg/cm^2, (b) 0.56 mg/cm^2, (c) 0.97 mg/cm^2, (d) 1.21 mg/cm^2, (e) 1.42 mg/cm^2, (f) cross-section of (e), (g) uncoated side of (e) and (h) sheet resistance of PEDOT/PSS papers containing different weights of PEDOT/PSS: (●) as-prepared PEDOT/PSS paper, (○) EG-treated PEDOT/PSS paper.

The paper became dark blue once the PEDOT/PSS ink had been applied onto cellulose paper by conformal coating. Five different thicknesses of PEDOT/PSS coated paper were obtained by controlling the distance between the doctor blade and the paper to 0.04, 0.06, 0.08, 0.1 and 0.13 mm. The PEDOT/PSS coated papers were baked at 100 °C for 60 min in air. The

density of the PEDOT/PSS layer in the coated papers was determined to be 0.21, 0.56, 0.97, 1.21 and 1.42 mg/cm^2, respectively, from the change in weight after coating. SEM images (Figure 2.3a-e.) show the morphology of the coated side of PEDOT/PSS papers. For the thinnest PEDOT/PSS paper (Figure 2.3a), some parts of the cellulose fibers and microfibrils can still be clearly seen. However, as the distance between the doctor blade and paper increased, the fibers in the paper and the interspace between fibers gradually became well coated with PEDOT/PSS. For the sample with a weight of 1.42 mg/cm^2, the PEDOT/PSS coatings are continuous and possess good homogeneity on the coated side (Figure 2.3e). No obvious cellulose fiber structure is observed in the cross section which indicated the PEDOT/PSS penetrated to the uncoated side (Figure 2.3f-g). Mechanical adhesion tests to assess the strength of the interaction between PEDOT/PSS and the cellulose paper were performed by immersion in water. The PEDOT/PSS papers were immersed in water for 60 min, and then baked at 100 °C for 60 min. After this process, there was no PEDOT/PSS present in the water, so PEDOT/PSS adhered well to the cellulose paper without peeling or dissociation in water. These results suggest that PEDOT/PSS adheres very strongly to the cellulose fibers, which is critical for electronic paper devices. Such strong binding may be caused by large capillary forces, as well as, hydrogen bonding between PEDOT/PSS and the cellulose fibers.

Figure 2.3h shows that the sheet resistance (R_s) of the as-prepared PEDOT/PSS papers decreases as the weight of PEDOT/PSS increases. Immersing the PEDOT/PSS papers in EG for 20 min followed by drying decreased their R_s by approximately three orders of magnitude. The R_s of the EG-treated PEDOT/PSS papers were as low as 5.5 Ω/□, corresponding to a conductivity of 150 S/cm in the PEDOT/PSS layer. Many studies reported the conductivity enhancement of PEDOT/PSS films by treatment with polar solvents such as dimethyl

sulfoxide, dimethylformamide, tetrahydrofuran, or polyalcohols.[22-25] The enhancement in conductivity was caused by the benzoid structure of PEDOT transforming into a quinoid structure. Thus, PEDOT/PSS papers with a large range of R_s could be obtained by tuning the weight of PEDOT/PSS and treatment with EG. It has also been reported that excess PSS was washed away from the surface region of the PEDOT/PSS grains by the EG treatment.[26] The phase segregation occurred in PEDOT/PSS system and PSS was predominant in the surface region, where the layer of excess PSS surrounding the PEDOT/PSS grains was estimated to be about 37 Å using XPS and UPS.[27] These methods may allow the actuation of PEDOT/PSS papers to be realized at low electrical field.

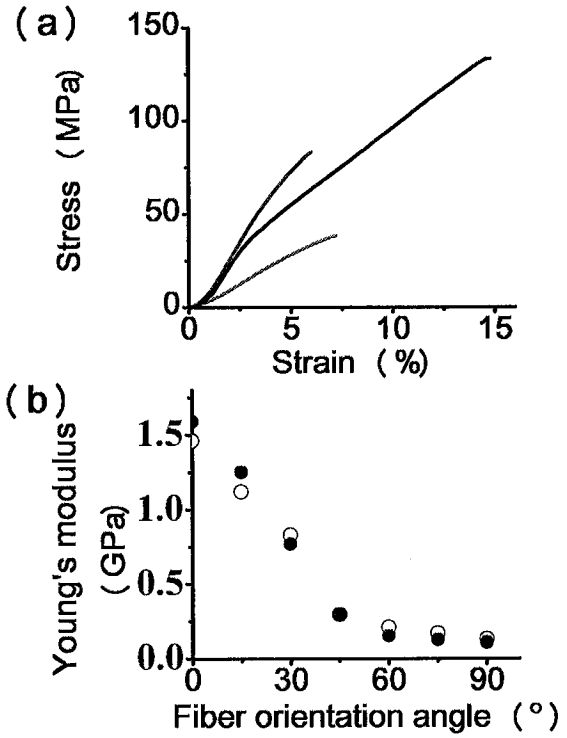

Figure 2.4 (a) Stress-strain curves of cellulose paper (black line), PEDOT/PSS film (red line) and PEDOT/PSS paper (blue line). (b) Dependence of Young's modulus on fiber orientation angle: (○) cellulose paper,(●)PEDOT/PSS paper.

We investigated the mechanical properties of these papers at 65% relative humidity (RH) (Figure 2.4a). The Young's modulus of the PEDOT/PSS-coated paper was 1.6±0.1 GPa,

which is almost the same as that of uncoated paper (1.5±0.1 GPa). The obtained Young's modulus of the paper was about twice of that of PEDOT/PSS thin film (0.8±0.1 GPa), showing that the combination of PEDOT/PSS with cellulose paper had higher mechanical properties than those of PEDOT/PSS thin film.[25, 28] Furthermore, Young's modulus of PEDOT/PSS-coated paper depends on the orientation angle of cellulose fibers in paper, and this profile is compatible with that of the Cellulose paper (Figure 2.4b).

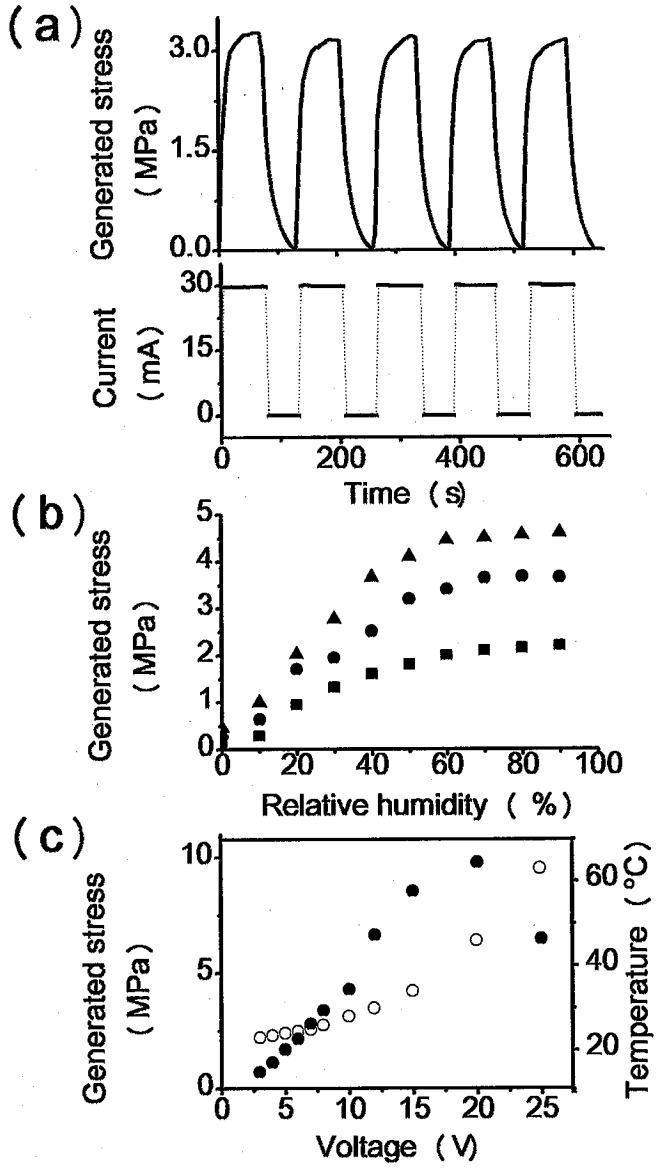

Figure 2.5 (a) Time profiles of the generated stress and electronic current of PEDOT/PSS coated paper at 50% relative humidity and 25 °C. (b) Generated stress under different relative humidity levels at 5V (■), 8V (●), 10V (▲). (c) Dependence of generated stress (●) and temperature (○) of PEDOT/PSS coated paper on applied voltage.

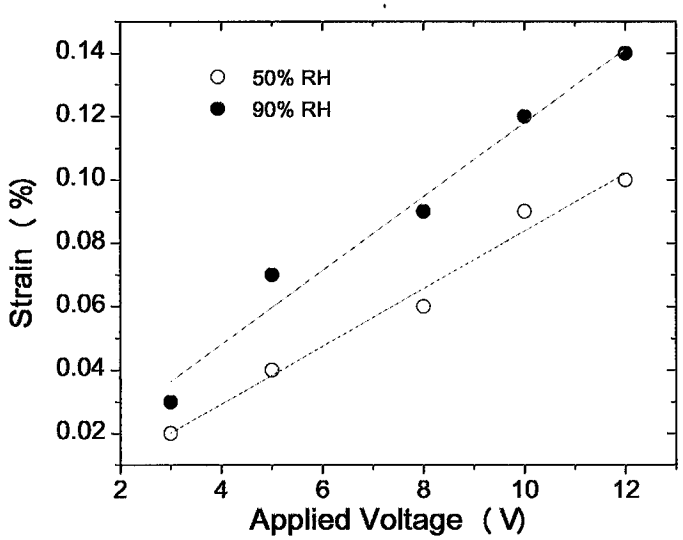

Figure 2.6 Strain-voltage curve of PEDOT/PSS coated paper different relative humidity levels: 90% RH (●),50% RH (○). Fiber orientation is agree with the loading direction.

2.3.2 Electromechanical Properties of Conductive PEDOT/PSS Papers

Time profiles of the generated stress and electronic current of PEDOT/PSS-coated papers at 50% RH and 25 °C are shown in Figure 2.5a. When a direct current of 8V was applied to the coated paper, the paper generated significant stress in response to the electric field. Turning off the applied voltage returned the stress to zero. The generated stress after 400 cycles of this experiment was almost unaltered, which indicates good repeatability of actuation properties. The electronic current was 30 mA and the temperature at the surface of the coated paper increased from 25 to 30 °C due to the Joule heating. The relative humidity within the chamber increased by about 2% by applying voltage, which suggests desorption of water vapor from the PEDOT/PSS coated paper. The actuation strain by applying voltage was shown in Figure 2.6. Large deformation could be achieved by applying a higher voltage or at a relative higher RH. Okuzaki et al. found that water vapor sorption from PEDOT/PSS film resulted in the stress generation. [25] We also found that the generated stress increased with both applied voltage and relative humidity (Figure 2.5b). While the coated paper exhibited a generated stress of 0.27 MPa in dry N_2 atmosphere under the applied voltage of 8V, the generated stress

was enhanced to be 3.6±0.2 MPa at 50% RH. The generated stress increases with the applied voltage until 20 V (Figure 2.5c). The temperature of the coated paper increased with voltage because of the Joule heating. A further increase of the voltage over 20V results in a decrease of the generated stress value, which might be explained by thermal expansion of the coated paper.[25]

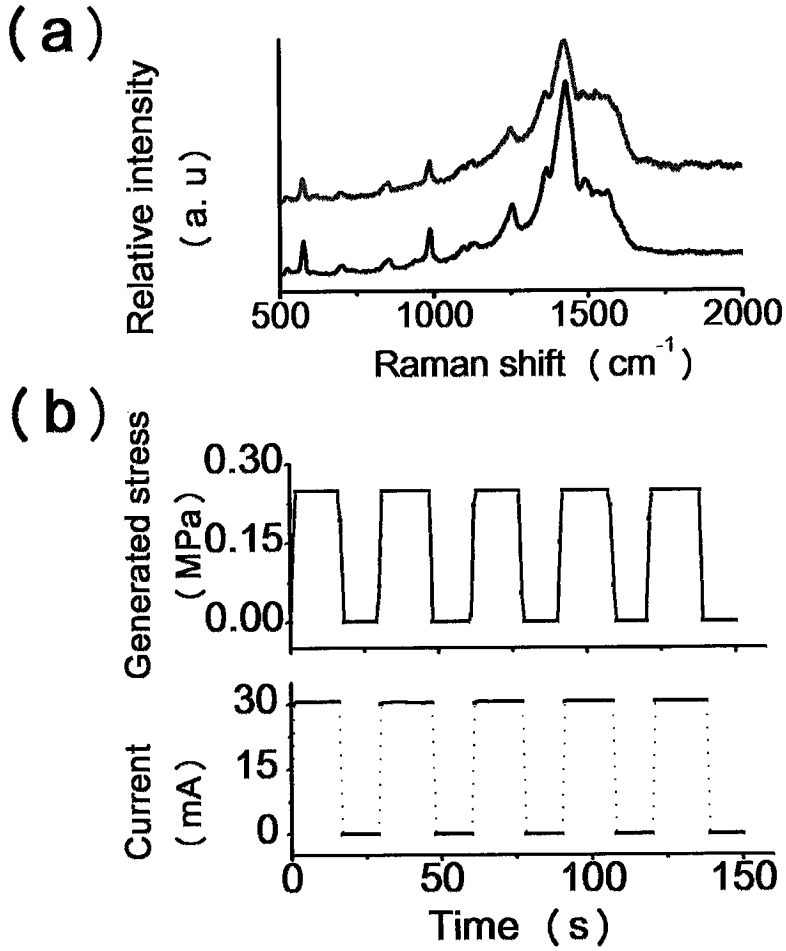

Figure 2.7 (a) Raman spectral changes of a PEDOT/PSS paper between 0V (blue line) and 8 V (black line). (b) Time profiles of the generated stress and electronic current of PEDOT/PSS coated paper in dry N_2 and 25 °C.

To understand the mechanism of actuation properties on a molecular level, the PEDOT/PSS-coated papers were studied by Raman spectroscopy.[29-33] Figure 2.7a shows the Raman spectral change of PEDOT/PSS-coated papers by applying voltage. Raman spectroscopic analysis of PEDOT/PSS-coated paper at 0 V revealed an intense peak at 1430

cm^{-1}, which can be assigned to symmetric C-C stretching deformation in the aromatic thiophene ring.[29-33] Upon applying voltage at 8 V, the peak position of this band was slightly shifted toward lower frequency and the Raman intensity was decreased. This spectral change between 0 and 8 V was reversible. Raman spectral change at 8 V can be attributed to the change in the conjugation length of PEDOT segment and the orientation of PEDOT chains.[29-33] Figure 2.7b shows time profiles of the generated stress and electronic current of PEDOT/PSS-coated papers in dry N_2 atmosphere and 25 °C. The coated paper in dry N_2 generated small stress repeatedly in response to the electrical field, but electric current at 8 V was almost same as that at 50% RH. This indicates that the coated paper generates stress without water vapor due to structural changes of PEDOT/PSS. We also observed that the response time of reaching the maximum stress after applying voltage is 2.0 seconds and the recovering time for the paper after turning off voltage is 1.8 seconds. The observed response times are faster than those at 50% RH (see Figure 2.3a). The principles of the actuation for coated papers lies in the control of water vapor desorption and adsorption and the conformational change in PEDOT chains caused by the electric field. Thus, the coated papers composed of conductive PEDOT/PSS and cellulose fibers exhibit the actuation property in ambient air in response to the voltage and relative humidity.

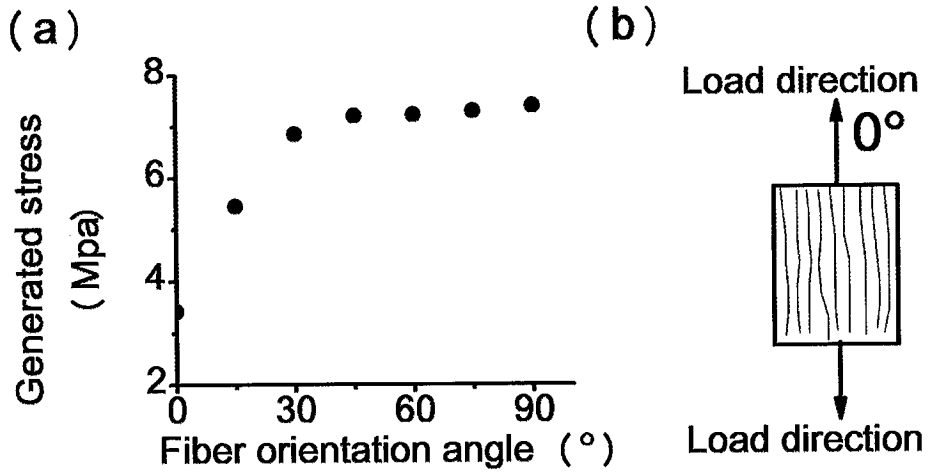

Figure 2.8 (a) Dependence of generated stress at 8V on fiber orientation angle measured at 50% relative humidity and 25 °C. (b) Schematic representation of cellulose fibers orientation in paper.

The dependence of generated stress under the applied voltage of 8 V on the fiber orientation angle measured at 50% RH and 25 °C is shown in Figure 2.8a. The fiber orientation angle is between the orientation direction of cellulose fibers in the tested paper and the loading direction, zero degree means that most of cellulose fibers are oriented along with the loading direction as shown in Figure 2.78. The stress for PEDOT/PSS coated paper having 45 degree of fiber orientation angle is 2.3 times of that for the paper with zero degree of fiber orientation. The observed stress profile can be explained by the dependence of Young modulus on the fiber orientation angle. It is known that the Young modulus in the machine direction where the fibers are mainly oriented is much higher than that in the cross direction. The relation between Young's modulus and fiber orientation angle of the coated paper has already been confirmed in Figure 2.3b. It indicated that the coated paper has a higher degree of compliance at cross direction than the machine direction. The generated stress transformation will turn out to be easier when the testing is carried out to the off-principal directions where the main fiber orientation does not coincide with the loading direction. The largest generated stress is only half of the Okuzaki's value, which is attributed to the

introduction of cellulose paper. The thickness of PEDOT/PSS paper is almost twice than PEDOT/PSS film. If we only calculated the thickness of PEDOT/PSS layer in PEDOT/PSS paper, our value is at the same level with the PEDOT/PSS film.[25] The coated paper can generate different stresses within the plain of the paper in accordance with the fiber orientation.

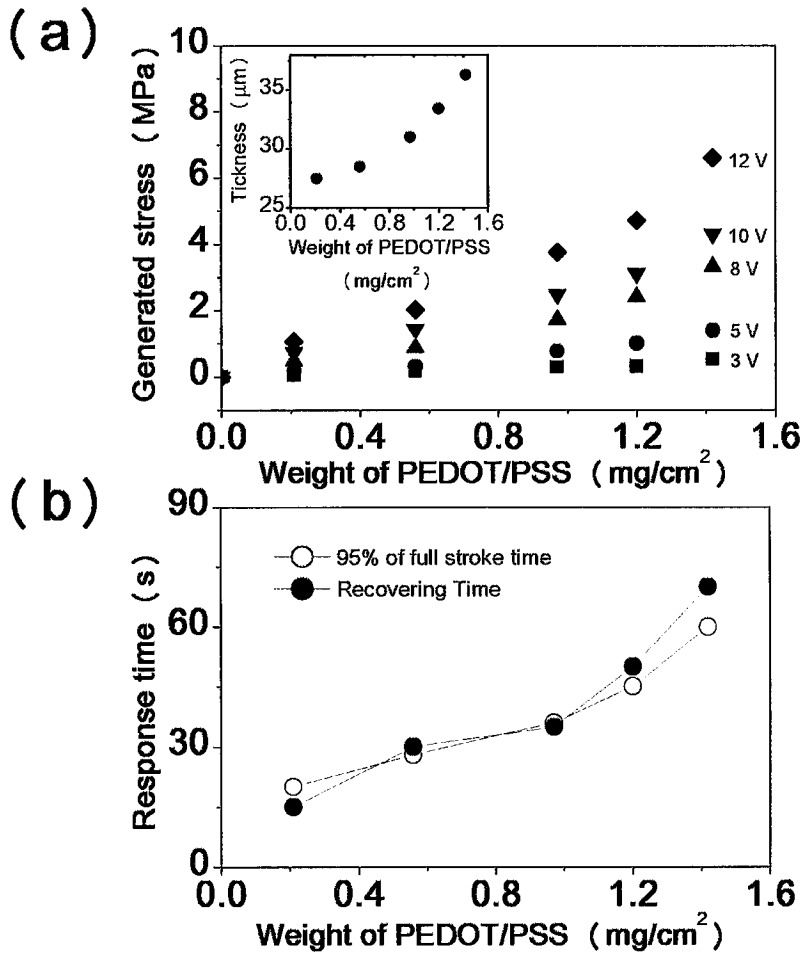

Figure 2.9 (a) The dependence of the weight of PEDOT/PSS on stress generated under different applied voltages at 50% RH and 25 °C: (■) 3 V, (●) 5 V, (▲) 8 V, (▼) 10 V, (◆) 12 V. Inset: dependence of the thickness of the PEDOT/PSS paper on the weight of PEDOT/PSS. (b) The dependence of response time on the weight of PEDOT/PSS: (○) 95% full stroke time after applying a voltage, (●) recovery time after turning off the voltage.

Figure 2.9a shows the effect of the weight of PEDOT/PSS on the electromechanical properties of the paper. To clarify the effect of the electrical potential on the electroactive behavior of the conductive papers in more detail, each sample was measured at five voltages

(3, 5, 8, 10, and 12 V) at 25 °C and 50% RH. For each of the five different applied voltages, the stress generated increased linearly with the weight of the PEDOT/PSS paper. For the thickest PEDOT/PSS paper, the stress reaches 3.5 and 4.5 MPa under an applied voltage of 10 and 12 V, respectively. These stresses are more than 10 times that produced in the skeletal muscle of animals (about 0.3 MPa).[34] When a voltage of 8 V was applied to the samples, a clear indication of the importance of the weight of PEDOT/PSS on the papers on the change in response time was observed (Figure 2.9b). The 95% full stroke time is the time that it takes the PEDOT/PSS paper to reach 95% of the maximum stress after applying a voltage. The 95% full stroke time increases with the weight of PEDOT/PSS coated on the cellulose paper, as did the recovery time after turning off the applied voltage. This is because the thickness of the conductive paper increased with the weight of PEDOT/PSS coated on paper, as shown in the inset in Figure 2.9a. For the thinner samples, the surfaces of the cellulose paper were not completely coated with PEDOT/PSS. The resulting porous structures in the paper allow water vapor to be absorbed readily by PEDOT/PSS inside the paper. For the thicker samplers, both desorption and absorption is more difficult for the PEDOT/PSS inside the paper. Meanwhile, the charge density increases more rapidly in the thinner film than in the thicker film, which results in faster actuation in the thinner film. Thus, the weight of PEDOT/PSS influences the actuation properties of the cellulose paper. The electromechanical properties of the PEDOT/PSS papers can therefore be adjusted simply by tuning the weight of PEDOT/PSS in the paper.

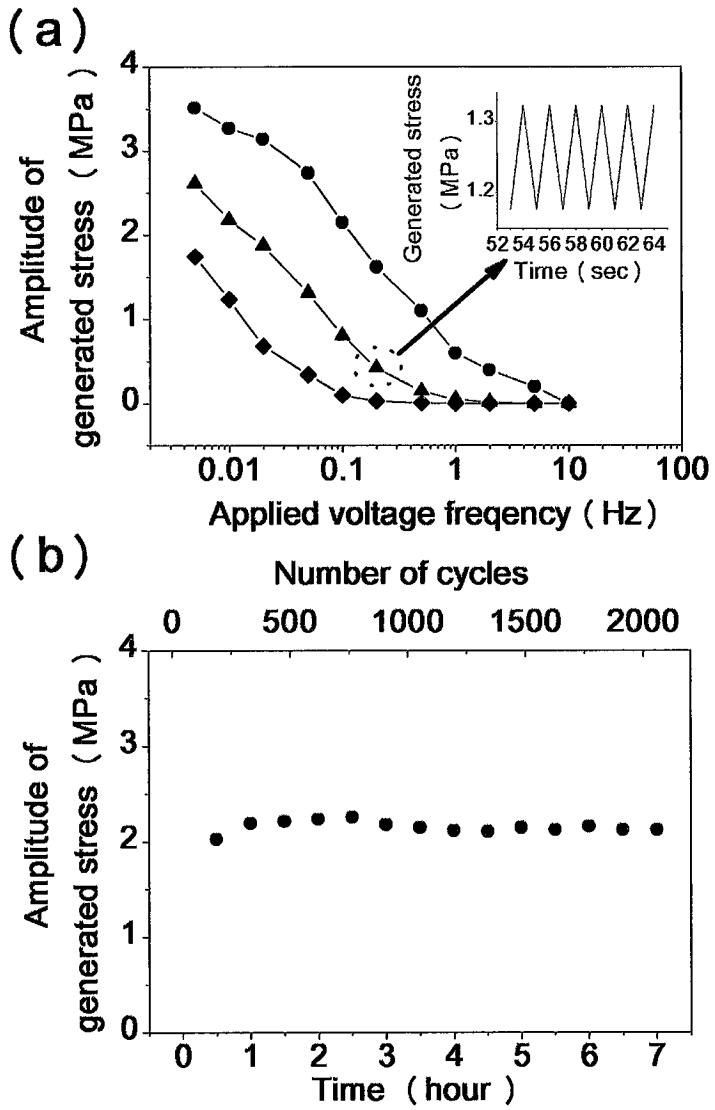

Figure 2.10 (a) The amplitude of stress generated in PEDOT/PSS papers under applied rectangular voltages (0-8V) with different frequencies: weight of PEDOT/PSS of (●) 1.42 mg/cm2, (▲) 0.97 mg/cm2, (◆) 0.56 mg/cm2. Inset: The dependence of stress generated on time under an applied voltage frequency of 0.5 Hz. (b) Cycle life of PEDOT/PSS paper with a weight of 1.42 mg/cm2 and dimensions of 2 mm × 100 mm × 36 μm under a square wave voltage of (0-8V) with a frequency of 0.1 Hz. Measurements were obtained at 50% RH and 25 °C.

The electromechanical actuation of the PEDOT/PSS papers under rectangular voltages (0-8 V) with different frequencies is shown in Figure 2.10a. The duty of all square wave signals was 50%. The amplitude of the stress generated was calculated from the highest peak and lowest peak as shown in Figure 2.10a (inset). It can be seen that at the same applied

voltage frequency, the amplitude of stress generated increased with the weight of PEDOT/PSS. However, as the voltage frequencies increased, the amplitude of stress generated decreased significantly. For the sample with a higher weight of PEDOT/PSS (1.42 mg/cm^2), a response was not detected when the frequency was higher than 10 Hz. For the lighter sample (weight of PEDOT/PSS of 0.56 mg/cm^2), an electromechanical response was not detected when the frequency was higher than 0.5 Hz.

The repeatability and reliability of the actuation of the PEDOT/PSS papers was examined by applying a continuous alternating square wave voltage (0.1 Hz, 0-8 V). After more than 2000 cycles, no significant degradation in performance was found, as shown in Figure 2.9b. These results indicate that the actuation of PEDOT/PSS papers is both repeatable and reliable. They also show that the amplitude of the stress generated can be controlled by the weight of PEDOT/PSS in the paper and the application of different voltage frequencies.

2.3.3 Butterfly-like Motion Based on PEDOT/PSS Papers

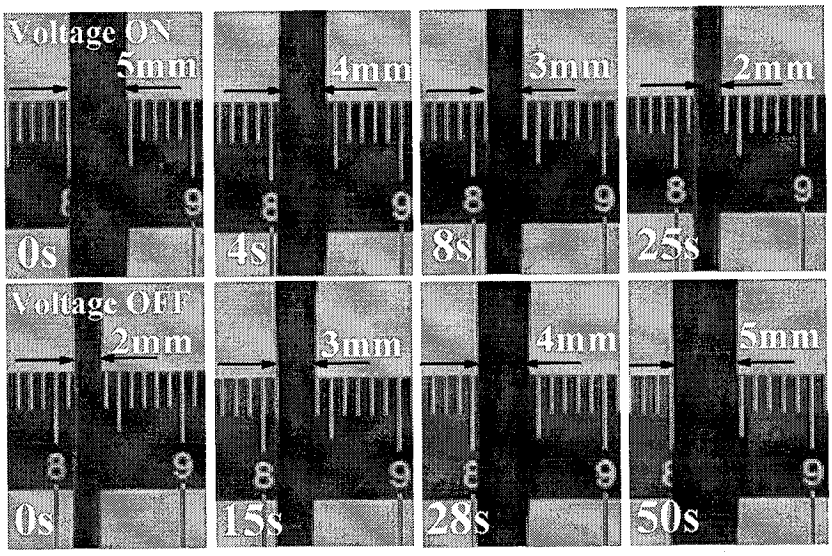

Figure 2.11 Bending motion of PEDOT/PSS coated paper upon voltage switching between on and off.

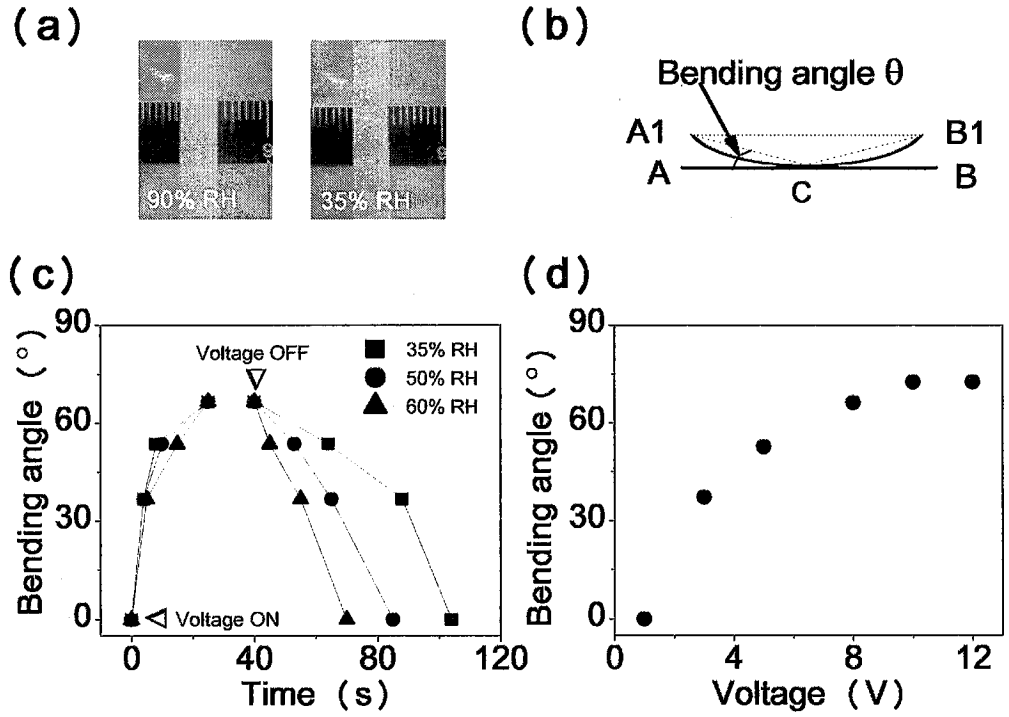

Figure 2.12 (a) Configuration of cellulose paper at 90% and 35% RH (b) Schematic illustration of the bending/unbending movement of a PEDOT/PSS paper. (c) Time-dependent bending angles of PEDOT/PSS paper at different RH at 8 V and 25 °C: (■) 35% RH, (●) 50% RH, (▲) 60% RH. (d) Voltage-dependent bending angles of PEDOT/PSS paper at 50% RH and 25 °C.

Both edges of the coated paper (100 mm long between the two copper electrodes and 5 mm wide) bend towards the middle upon applying voltage at 50% RH (Figure 2.10). The edges of the paper in the cross section bend and the width of the paper changed from 5 to 2 mm within 25 seconds by being applied at 8 V. When the voltage was turned off, the curled PEDOT/PSS-coated paper reverted to its original straight shape after 50 seconds and this motion was reversible. Since the main orientation of cellulose fibers in paper coincides with the load direction, the electromechanical motion in the loading direction was limited. The bending direction was occurred at the coated side of PEDOT/PSS-coated paper, in which PEDOT/PSS was embedded within the cellulose fiber network with a high density. We propose that the difference of PEDOT/PSS density on two sides of cellulose paper results in the bending direction of PEDOT/PSS paper. The PEDOT/PSS layer will shrink under

electrical potential due to desorption of water vapor by Joule heating and the cellulose paper moves as a result of the shrinking of the PEDOT/PSS layer. The shrinking of the layer on its coated side significantly affects the bending effect compared to the uncoated side. The anisotropic electromechanical motion can be induced from the orientation of cellulose fibers and the density difference of PEDOT/PSS across the thickness in the coated paper. Figure 2.11a shows that the cellulose paper did not show obvious bending motions when the RH was reduced from 90% to 35%. Thus, the bending/unbending motion of the PEDOT/PSS paper mainly results from the shrinking or expansion of the PEDOT/PSS film. Figure 2.11b shows a schematic illustration of the bending movement of the PEDOT/PSS paper. The cross-section of bilayer AB will bend into an arc A_1B_1 by applying electrical field. If C is the midpoint of AB, and supposing that arc A_1C equals line A_1C, the bending angle (θ) of the PEDOT/PSS paper can be estimated from the equation (1);

$$\cos \theta = A_1B_1/AB \qquad (1)$$

where AB=5 mm, and A_1B_1 can be measured using a camera recorder. Figure 2.11c shows the dependence of the bending angle of the PEDOT/PSS paper on the response time under applied square voltages (0-8V). The bending was recorded when the PEDOT/PSS paper started to bend. After applying an electrical field, it took 25 s for the paper to reach a θ of 68.4° .When the electrical field was turned off at 40 s, it took another 50 s for the paper to unbend from θ = 68.4° to 0° at RH = 50%. A lower RH of 35% results in a slower unbending movement, while a higher RH of 60% results increases the rate of unbending. Furthermore, θ can be adjusted by applying different voltages, as shown in Figure 2.11d. Thus, the bending/unbending movements of the PEDOT/PSS papers can be controlled by adjusting the applied voltage and the RH around the paper.

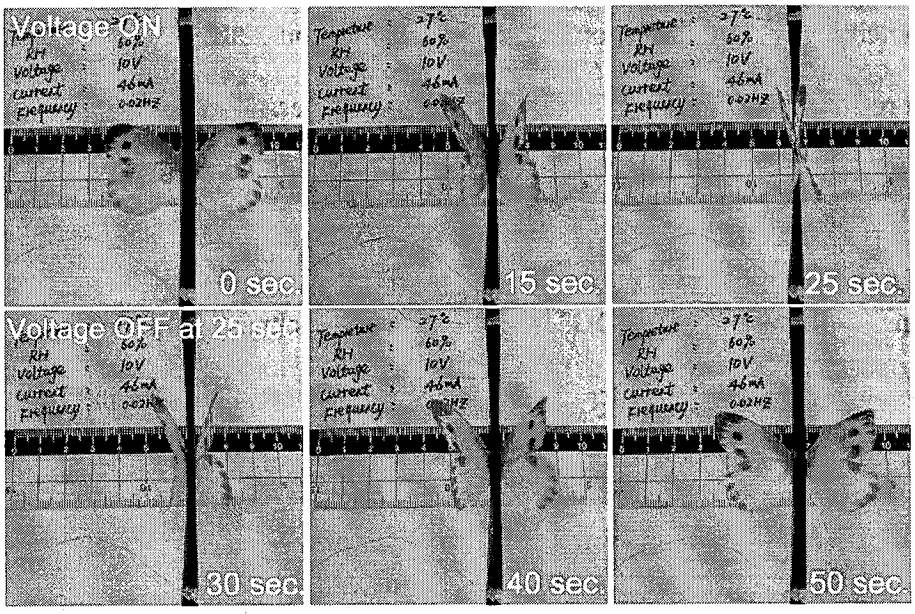

Figure 2.13 Time profiles of butterfly-like biomimetic motion based on PEDOT/PSS paper at 60% RH and 27 °C. The applied voltage (10 V) is switching between on and off with a frequency of 0.02 Hz.

The intensive bending/unbending movement of the PEDOT/PSS paper gave us the inspiration to mimic the motion of a butterfly.[35] Wings made of cellulose paper were stuck to the edge of the PEDOT/PSS paper and the resulting "butterfly" moves reversibly when a voltage was switched on and off with a frequency of 0.02 Hz, as shown in Figure 2.12.

2.4 Conclusions

In conclusion, Paper coated with highly conductive PEDOT/PSS underwent an anisotropic bending motion in response to an electronic field in ambient air. The PEDOT/PSS papers displayed electromechanical properties that could be tuned by varying the weight of PEDOT/PSS and the frequency of the applied voltage. The PEDOT/PSS papers can undergo intensive bending/unbending motions when the voltage is switched on and off. These bending/unbending motions can also be controlled by changing the RH and applied voltage. Based on this electromechanical response, butterfly-like motion of the PEDOT/PSS paper was demonstrated. The unique actuation performance of this PEDOT/PSS/cellulose paper composite system, coupled with the ease of conformal coating, and its mechanical robustness,

low driving voltage, and good cycling ability, provides the potential to further expand the range of applications of artificial muscles that operate under ambient conditions.[36-38]

References

1. R. E. Mark, C. C. Habeger, J. Borch, M. B. Lyne, *Handbook of Physical Testing of Paper: Volume 1*, 2nd ed.; CRC Press:, 2001.
2. H. Holik, *Handbook of Paper and Board*, 1st ed.; WILEY-VCH Press: Weinheim, 2006 and P. Zugenmaier. *Crystalline Cellulose and Derivatives*, 3rd ed.; CRC Press: Boca Raton, London, New York, 2007.
3. C. N. R. Rao, A. Müller, A. K. Cheetham, *The Chemistry of Nanomaterials, Synthesis, Properties and Applications*, 1st ed.; WILEY-VCH Press: Weinheim, 2004.
4. P. Anderson, D. Nilsson, P. O. Svensson, M. Chen, A. Malmström, T. Remonen, T. Kugler, M. Berggren, Active Matrix Displays Based on All-Organic Electrochemical Smart Pixels Printed on Paper, *Adv. Mater.* **2002**, *14*, 1460-1464.
5. F. Eder, H. Klauk, U. Zschieschang, G. Schmid, C. Dehm, Organic Electronics on Paper, *Apply. Phys.Lett.* **2004**, *84*, 2673.
6. B. Lamprecht, R. Thünauer, M. Ostermann, G. Jakopic, G. Leising, Organic Photodiodes on Newspaper, *Phys. Stat. Sol.* **2005**, *202*, 50-52.
7. G. Nystöm, A. Razaq, M. Strømme, L. Nyholm, A. Mihranyan, Ultrafast All-Polymer Paper-Based Batteries, *Nano Lett.* **2009**, *9*, 3635-3639.
8. L. Hu, J. W. Choi, Y. yang, S. Jeong, F. La mantia, L. F. Cui, Y. Cui, Highly Conductive Paper for Energy-Storage Devices, *Proc. Natl. Acad. Sci. USA.* **2009**, *106*, 21490-21494.
9. D. H. Kim, Y. S. Kim, J. Wu, Z. Liu, J. Song, H. S. Kim, Y. Y. Huang, K. C. Hwang, J. A. Rogers, Ultrathin Silicon Circuits With Strain-Isolation Layers and Mesh Layouts for High-Performance Electronics on Fabric, Vinyl, Leather, and Paper, *Adv. Mater.* **2009**, *21*, 3703-3707.
10. A. W. Martinez, S. T. Phillips, M. J. Buttle, G. M. Whitesides, Patterned Paper as a Platform for Inexpensive, Low-Volume, Portable Bioassays, *Angew. Chem. Int. Ed.* **2007**, *46*, 1318-1320.
11. A. W. Martinez, S. T. Phillips, B. J. Wiley, M. Gupta, G. M. Whitesides, Flash: A rapid Method for Prototyping Paper-based Microfluidic Devices, *Lab. Chip.* **2008**, *8*, 2146-2150.
12. A. M. Martinez, S. T. Phillips, G. M. Whitesides, Three-dimensional Microfluidic Devices Fabricated in Layered Paper and Tape, *Proc. Natl. Acad. Sci. USA.* **2008**, *105*,

19606-19606.

13. E. Carrilho, A. M. Martinez, G. M. Whitesides, Understanding Wax Printing: A Simple Micropatterning Process for Paper-Based Microfluidics, *Anal. Chem.* **2009**, *81*, 7091-7095.
14. J. Kim, S. Yun, Discovery of Cellulose as a Smart Material, *Macromolecules* **2006**, *39*, 4202-4206.
15. J. Kim, W. Jung, H. S. Kim, In-plane Strain of Electro-active Paper under Electric Fields, *Sens. Actuators. A.* **2007**, *140*, 225-231.
16. H. S. Kim. Y. X. Li, J. Kim, Electro-mechanical Behavior and Direct Piezoelectricity of Cellulose Electro-active Paper, *Sens. Actuators. A.* **2008**, *147*, 304-309.
17. M. Elson, J. Lars, L. Magnus, Characterization of PEDOT:PSS Adsorption on Cellulosic Materials, *Cellulose* **2009**, *16*, 807-815.
18. J. H. Johnston, J. Moraes, T. Borrmann, Conducting Polymers on Paper Fibres, *Synth. Met.* **2005**, *153*, 65-68.
19. D. K. Schroder. *Semiconductor Material and Device Characterization*, 3rd ed.; IEEE Press: Hoboken, New Jersey, 2006.
20. L. Hu, M. Pasta, F. L. Mantia, L. F. Cui, S. M. Jeong, H. D Deshazer, J. M. Choi, S. M. Han, Y. Cui, Stretchable, Porous, and Conductive Energy Textiles, *Nano. Lett.* **2010**, *10*, 708-714.
21. L. Kacir, O. Ishai, M. Narkis, Oriented Short Glass-fiber Composites. IV. Dependence of Mechanical Properties on the Distribution of Fiber Orientations, *Polym. Eng. Sci.* **1978**, *18*, 45-52.
22. S. Kirchmeyer, K. Reuter. Scientific Importance, Properties and Growing Applications of Poly(3,4-ethylenedioxythiophene), *J. Mater. Chem.* **2005**, *15*, 2077-2088.
23. J. Y. Ouyang, C. W. Chu, F. C. Chen, Q. F. Xu, Y. Yang. High-Conductivity Poly(3,4-ethylenedioxythiophene):Poly(styrene sulfonate) Film and Its Application in Polymer Optoelectronic Devices, *Adv. Funct. Mater.* **2005**, *15*, 203-208.
24. P. Tehrani, L. O. Hennerdal, A. L. Dyer, J. R. Reynolds, M. Berggren. Improving the Contrast of All-printed Electrochromic Polymer on Paper Displays, *J. Mater. Chem.* **2009**, *19*, 1799-1802.
25. H. Okuzaki, H. Suzuki, T. Ito. Electromechanical Properties of Poly (3,4-ethylenedioxythiophene)/poly(4-styrene sulfonate) Films. *J. Phys. Chem. B.* **2009**,

113, 11378.

26. H. Okuzaki, Y. Harashina, H. Yan. Highly Conductive PEDOT/PSS Microfibers Fabricated by Wet-spinning and Dip-treatment in Ethylene Glycol. *Eur. Polym. J.* **2009**, *45*, 256-261.
27. S. K. M. Jonsson, J. Birgerson, X. Crispin, G. Greczynski, W. Osikowicz, A. W. D. van der Gon, W. R.Salaneck,; M. Fahlman, The Effects of Solvents on the Morphology and Sheet Resistance in Poly(3,4-ethylenedioxythiophene)–Polystyrenesulfonic Acid (PEDOT–PSS) Films, *Synth. Met.* **2003**, 139, 1-10.
28. *Synth. Met.* **2002**, *126*, 311-316.
29. U. Lang, N. Naujoks, J. Dual, Mechanical Characterization of PEDOT:PSS Thin Films, *Synth. Met,* **2009**, 159, 473-479.
30. S. Gerreau, G. Louarn, J. P. Buisson, G. Froyer, S. Lefrant, In situ Spectroelectrochemical Raman Studies of Poly(3,4-ethylenedioxythiophene) (PEDT), *Macromolecules*, **1999**, *32*, 6807-6812.
31. S. Gerreau, M. Leclerc, N. Errien, G. Louarn, Planar-to-nonplanar Conformational Transition in Thermochromic Polythiophenes: A Spectroscopic Study, *Macromolecules*, **2003**, *36*, 692-697.
32. J. Ouyang, C. W. Chu, F. C. Chen, Q. Xu, Y. Yang, High-Conductivity Poly(3,4-ethylenedioxythiophene):Poly(styrene sulfonate) Film and Its Application in Polymer Optoelectronic Devices, *Adv. Funct. Mater.* **2005**, *15*, 203-208.
33. S. Sakamoto, M. Okamura, Z. Zhao, Y. Furukawa, Raman Spectral Changes of PEDOT-PSS in Polymer Light-Emitting Diodes upon Operation, *Chem. Phys. Lett.* **2005**, *412*, 395-398.
34. H. L. Cheng, J. W. Lin, M. F. Jang, F. C. Wu, W. Y. Chou, M. H. Chang, C. H. Chao,Long-Term Operations of Polymeric Thin-Film Transistors: Electric-Field-Induced Intrachain Order and Charge Transport Enhancements of Conjugated Poly(3-hexylthiophene), *Macromolecules* **2009**, *42*, 8251-8259.
35. R. M. Alexander, *Exploring Biomimetics: Animals in Motion,* W. H. Freeman and Company Publish, New York, p.260,1992.
36. Y. Ma, J. Q. Sun, Humido- and Thermo-Responsive Free-Standing Films Mimicking the Petals of the Morning Glory Flower, *Chem. Mater.* **2009**, *21*, 898.
37. T. Mirfakhrai, J. D. Madden, R. H. Baughman, Polymer Artificial Muscles, *Mater. Today*

2007, *10*, 30-38.

38. B. C. Yoseph, *Proc. SPIE Smart Structures and Materials Symposium, EAPAD Conference*, San Diego, CA, March 18-21, 2002.
39. J. D. Madden, Mobile Robots: Motor Challenges and Materials Solutions, *Science* **2007**, *318*, 1094-1097.

Chapter 3

Anisotropic Actuation of PEDOT/PSS Films Containing Aligned Electrospun Nanofibers

Chapter 3 Anisotropic Actuation of PEDOT/PSS Films Containing Aligned Electrospun Nanofibers

Abstract: We demonstrate directional actuation of poly(3, 4-ethylenedioxythiophene)/poly(4-styrene sulfonate) (PEDOT/PSS) composite films containing aligned poly(vinyl pyrrolidone)/poly(methyl methacrylate) (PVP/PMMA) nanofiber assemblies. The aligned nanofiber assemblies showed anisotropic wettability based on the high alignment degree of the nanofibers. The PEDOT/PSS composite film containing aligned nanofibers displayed an anisotropic actuation response when a voltage was applied in air. The orientation of the embedded nanofibers within the PEDOT/PSS matrix leads to the control of actuation direction due to the difference of anisotropic mechanical properties in the composite films.

3.1 Introduction

In chapter 3, we focus on control of anisotropic actuation properties of conjugated polymer films by using aligned electrospun nanofiber assemblies.

Electrospinning is a simple method for producing nanofibers and nanofibrous non-woven mats for various applications. It involves discharging a polymer solution in air from a nozzle under high voltage and producing nanofibers by exploiting electrostatic repulsion of the polymer solution.[1-3] Furthermore, the fiber orientation can be controlled by using modified fiber collectors.[4] Aligned electrospun nanofibers have potential applications in structural reinforcement, tissue engineering, and blood vessel engineering, which often require well-aligned and highly ordered structures.[2, 3] There are only a few reports in the literature on anisotropic actuation based on anisotropic structures. Anisotropic actuation of polypyrrole films was achieved by orientation of polymer backbones through directional stretching.[5]

Uniaxial orientation of nafion, and the subsequent formation of electrode layers to create ionic polymer-metal composites, can also yield anisotropic actuation upon electrical stimulation.[6] Chapter 2 demonstrated anisotropic actuation of PEDOT/PSS coated papers, for which the actuation stress depended on the relative orientation of paper fibers and the loading direction of the coating.[7] The combination of cellulose fiber-based paper and PEDOT/PSS matrix can successfully realize the anisotropic actuation of PEDOT/PSS. In this chapter, we changed the fiber-based material to aligned electrospun nanofiber assemblies. When the aligned nanofiber assemblies were embedded within the conductive polymer matrix, the actuation properties followed the direction of fiber orientation. We selected aligned electrospun nanofibers for anisotropic actuation of conductive polymers. We fabricated aligned PVP/PMMA nanofiber assemblies up to several centimeters in length to realize anisotropic motion of PEDOT/PSS films. The aligned nanofiber assemblies displayed anisotropic wettability due to the high alignment degree of the nanofibers. We further demonstrated anisotropic electromechanical actuation of PEDOT/PSS film by using the aligned PVP/PMMA nanofibers. The composites with incorporated aligned nanofiber assemblies offer new opportunities to achieve anisotropic actuation in soft actuators.

3.2 Experimental Section

3.2.1 Materials

Poly(vinylpyrrolidone) (PVP, Nacalai Tesque, Mw 1,000,000 g mol^{-1}), poly(methyl methacrylate) (PMMA, Wako Chemicals, MW 100,000 g mol^{-1}), ethylene glycol (EG, Wako Chemicals), N,N-dimethylformamide (DMF, Wako Chemicals), tetra-n-butylammonium bromide (TBAB, Wako Chemicals) and fuchsine (Wako Chemicals) were used as received. Poly(vinyl alcohol) (PVA, Mw 140,000 g mol^{-1}) was provided by Kuraray Co. Ltd.

3.2.2 Fabrication of nanofiber by electrospinning.

Nanofiber assemblies were fabricated using a NANON-01A electrospinning machine with a drum collector (MECC Co., Ltd.). PVP/PMMA nanofiber assemblies were produced from 250 mg/ml PVP and PMMA in a DMF solution containing 5 wt% TBAB (relative to PMMA).[8, 9] The mixed solutions for the PVP/PMMA composite nanofibers were prepared by dissolving PVP and PMMA (weight ratio PVP: PMMA=10:90) in DMF. TBAB was used as an organic salt to increase the electrical conductivity of the solution.[9] In the electrospinning process, the prepared solutions were placed in 6 mL disposable plastic syringes and injected through a stainless steel needle (18 gauge, orifice diameter 1.2 mm). The needle was connected to a high-voltage DC power supply. The solutions were continuously fed by a syringe pump through the nozzle at a rate of 0.4 ml/h. A high voltage (14 kV) and a distance of 14 cm between the needle and the drum collector were used. The drum collector, which was connected with the ground and used as a target electrode, was rotated at 50 and 3000 rpm/min to collect nonaligned and aligned nanofiber assemblies, respectively.[4] The relative humidity (RH) in the chamber was maintained at about 35% by flowing N_2.

3.2.3 Dynamic contact angle measurement.

For each experiment, fuchsine solution at a concentration of 1×10^{-5} M was used instead of deionized water to ensure a clear view of droplets. A 0.5 μL droplet was deposited using a micropipette on the surfaces of nanofiber assemblies. Images of the spreading of the droplet were recorded using both a top view KH-7700 digital microscope with an AD-5040L macrolens (Hirox Co., Ltd.) and a side view IUC200-CK2 camera (Trinity Co., Ltd.) at a frame rate of 30 fps. The dynamic contact angle and base diameter were determined with the side view camera. A minimum of 10 drops were examined for each surface.

3.2.4 Deposition of PEDOT/PSS dispersion on PVP/PMMA nanofiber assemblies.

The weights of nonaligned and aligned PVP/PMMA nanofiber mats were 25.4 and 24.4 mg respectively with area 4×7 cm. Each nanofiber mat was placed on a PE film and well-dispersed PEDOT/PSS aqueous dispersion (1.3 wt% solid content, 2.0 g) containing 5 wt% EG was deposited on the nanofiber mat, then the sample was dried at 100 °C for 2 h. EG was used as an additive to enhance the electronic conductivity of PEDOT/PSS.

3.2.5 Measurements.

Morphologies of nanofibers were examined with a VE-8800SP (Keithley Co., Ltd.) scanning electronic microscope (SEM). The angle distribution of the nanofibers was determined from the SEM images using image tools. The nanofiber alignment was quantified by measuring the angles between the desired direction and the longitudinal axes of the nanofibers. 200 fibers were examined from SEM images over an area of 0.18×0.25 mm^2 for each nanofiber mat. The orientation parameter that was originally suggested in the field of fiber composites was adapted to quantitative analysis of the electrospun nanofibers.[10, 11] Mechanical properties were evaluated with a RTC-1250A tension tester (A&D Co., Ltd.) at a constant strain rate of 100% min^{-1} (chuck distance 30 mm). Tensile specimens were prepared with length 30 mm. Young's modulus, tensile strength, and elongation at break were calculated from the stress-strain curves as average values from at least 5 determinations.

The electromechanical properties of PEDOT/PSS films were tested with a ZP-2N force gauge (Imada Co., Ltd.). A composite film specimen with size 40×3 mm was placed in a humidity-controlled chamber. An electric field was applied to the film by a computer-driven PK-80 DC power supply (Matsusada Co., Ltd.) through a pair of copper wires (170 mm)

attached to the PEDOT/PSS film with silver paste; the distance between the electrodes was about 30 mm. The electric currents were monitored with a U1252A digital multimeter (Agilent Co., Ltd.).

3.3 Results and Discussion

3.3.1 Electrospinning of PVP/PMMA nanofibers

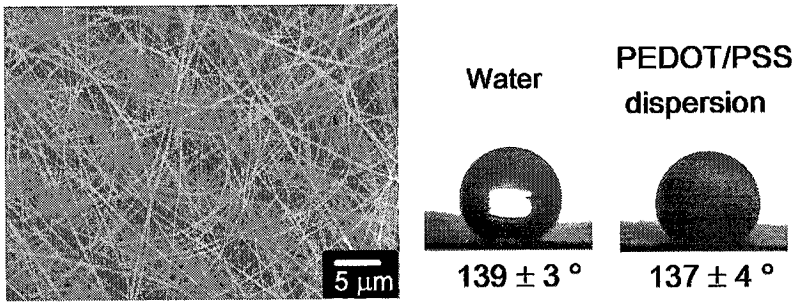

Figure 3.1 SEM image and contact angles of PMMA nanofiber mats.

Electrospinning has been widely investigated as a versatile fiber fabrication method to create nanofibers composed of synthetic polymers, natural polymers, and inorganic oxides. [12, 13] Among the synthetic polymers, PMMA is one of well-investigated polymers to create uniform nanofibers with various sizes by controlling the polymer solution properties including dielectric constant, evaporation rate, viscosity, solution conductivity, and surface tension.[8, 9, 13-16] In this context, we selected PMMA for the construction of anisotropic structures in conductive polymer matrix. The PMMA solution was electrospun into nanofibers and the resulted nanofibers were collected as a nanofiber mat according to the procedure reported by Dong et al.[8, 9] PMMA nanofiber mats were obtained by the electrospinning process of PMMA solution in DMF containing 5 wt% TBAB. In the absence of TBAB, beads are often formed in electrospinning. Addition of TBAB to PMMA solution reduced the formation of beads due to the increase of solution conductivity and formed continuous and smooth fibrous morphology and a narrow diameter distribution. Long and smooth nanofibers

were formed without beads, and the average diameter of PMMA nanofibers was 221±63 nm (Figure 3.1). Electrospun nanofiber mats having high surface roughness provide an ideal candidate for construction of hydrophobic surface on a large scale. Although the contact angle of water on PMMA spin-coated film was 70±2°, the contact angle of water on the PMMA nanofiber mat was found to be 139±3°. The PMMA nanofiber mat contains microscopic air pockets in the interfiber space and the presence of air pockets increases the contact angle of water. The Cassie-Baxter models have been commonly used to explain the wetting behaviors of liquid drops on rough surfaces of pillar structures, textiles, and nanofiber mats.[17-20] The Cassie-Baxter model includes the effect of microscopic air pockets remaining trapped below the liquid droplet, which leads to a hydrophobic interface. The contact angle on air pockets has been estimated by the following Cassie-Baxter equation;

$$\cos \theta_1 = f(1+\cos \theta_2)-1 \qquad (1)$$

where θ_1 is the apparent contact angle on the textured surface, f is the fraction of solid area, and θ_2 is the intrinsic contact angle on a flat surface. The observed average contact angles θ_1 of PMMA nanofiber mat and θ_2 of spin-coated PMMA film were 139° and 70°, respectively. The air pockets on the surface of the nanofiber mat prevented water from contacting the PMMA surface completely by trapping air at the water-PMMA nanofiber interface. The f value in eq. (1) was estimated to be 0.18 by using the observed θ_1 andθ_2, indicating the presence of 82% air pockets in the PMMA nanofiber mats. Wettability of hydrophobic electrospun fiber mat can be tuned by controlling the diameters of nanofibers. The contact angle of water on PMMA nanofiber mats was reduced from 142±3° to 120±2° as the diameter of PMMA nanofiber was increased from 154 nm to 907 nm (Figure 3.2). Hydrophobic property of the PMMA nanofiber mat results in the difficulty for the penetration of

PEDOT/PSS aqueous dispersion within the nanofiber matrix and the coating of nanofiber surface (Figure 3.3).

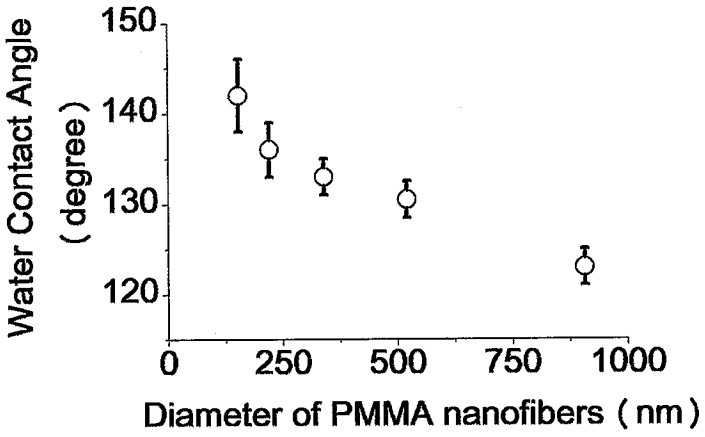

Figure 3.2 The relationship between water contact angle and PMMA nanofiber diameters.

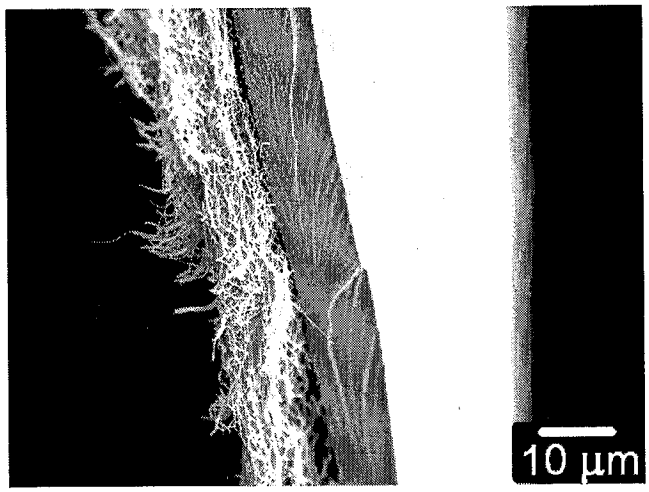

Figure 3.3 SEM image of PEDOT/PSS on PMMA fiber mat

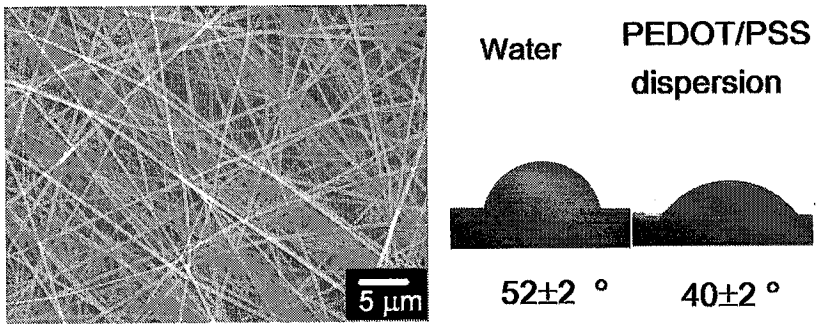

Figure 3.4 SEM image and contact angles PVP/PMMA nanofiber mats

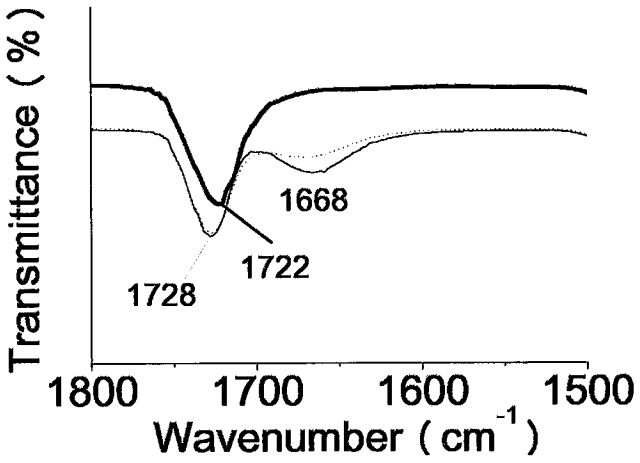

Figure 3.5 IR spectra of PMMA nanofibers (bold line), PVP/PMMA nanofibers (solid line) and water washed PVP/PMMA nanofibers (dashed line).

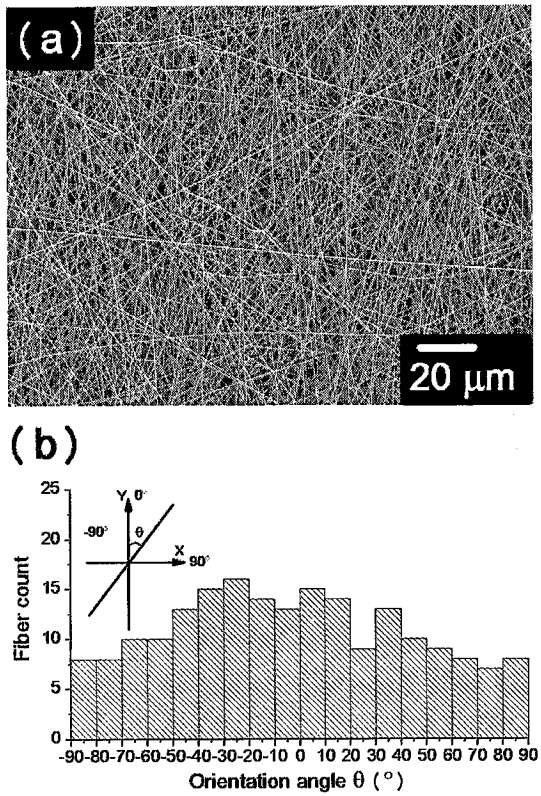

Figure 3.6 (a) SEM image of nonaligned PVP/PMMA nanofibers in an area of 0.18×0.25 mm^2. (b) Histogram of distribution of the PVP/PMMA fiber orientation from (a). The orientation parameters p of the coated nanofibers determined from the histogram is 0.08.

In order to improve the wettability of PMMA nanofibers keeping fiber morphology, water-soluble polymers were introduced within the PMMA nanofibers. The improvement of wettability may change the penetration of aqueous solution within the nanofiber mats.

Non-charged water-soluble PVP was selected as an additive for the wettability improvement of PMMA nanofibers. PVP is an amphiphilic polymer and readily dissolve in water and many organic solvents.[21, 22] In addition, PVP can be miscible with PMMA due to the interaction between carbonyl groups in PMMA and amide groups in PVP.[23, 24] Due to its amphiphilic character and the interaction with PMMA, PVP is a suitable additive to control hydrophilicity of PMMA nanofibers. Figure 3.4 showed the SEM image of PVP/PMMA composite nanofiber mat. The mixed solutions produced continuous nanofibers without the formation of beads under the same condition of PMMA electrospinning process and the average diameters of nanofibers increased from 221±63 nm to 334±54 nm nm by the addition of PVP. The contact angle on PVP/PMMA nanofiber mat was 52°, which was lower than that on the PMMA nanofiber mat. And the water droplet was smoothly penetrated within the nanofiber mats. The origin of this decrease in contact angle is believed to be due to the following two effects; the increase of diameter and the increasing the surface energy of the solid. However, the effect of diameter change is minor since the PMMA nanofiber mat composed of 400 nm diameter nanofibers showed a high contact angle above 120°. The contact angle on PVP/PMMA composite nanofiber mats agreed with that on the spin-coated thin film of PVP/PMMA (θ_2 = 54°), suggesting that the addition of hydrophilic PVP in PMMA results in an increase in the surface energy of nanofiber mats. When the PVP/PMMA nanofiber mats were immersed by water for 8 hours and dried, the diameters of nanofibers and the contact angle on nanofiber mat remained unaltered in water-treated PVP/PMMA nanofiber mats. FTIR spectrum of nanofiber mat after immersion into water displayed a broad peak assigned to amide carbonyl stretching at 1668 cm^{-1} (Figure 3.5), indicating the presence of PVP within the nanofiber mat.[25] Furthermore, the position of C=O stretching band of the PVP/PMMA composite nanofiber mat was shifted by 6 cm^{-1} compared to that of PMMA.[15, 26] These results

support that water-soluble PVP chains are fixed within PMMA and the embedded PVP does not release by immersion into water due to the interaction between carbonyl groups in PMMA and amide groups in PVP. The addition of PVP in PMMA changed wettablity of nanofiber mats by reducing of surface energy keeping fibrous morphology. This orientation parameter of the nonaligned PVP/PMMA nanofiber mat was determined to be 0.08 (Figure 3.6).

3.3.2 Aligned PVP/PMMA Electrospun Nanofiber Assemblies

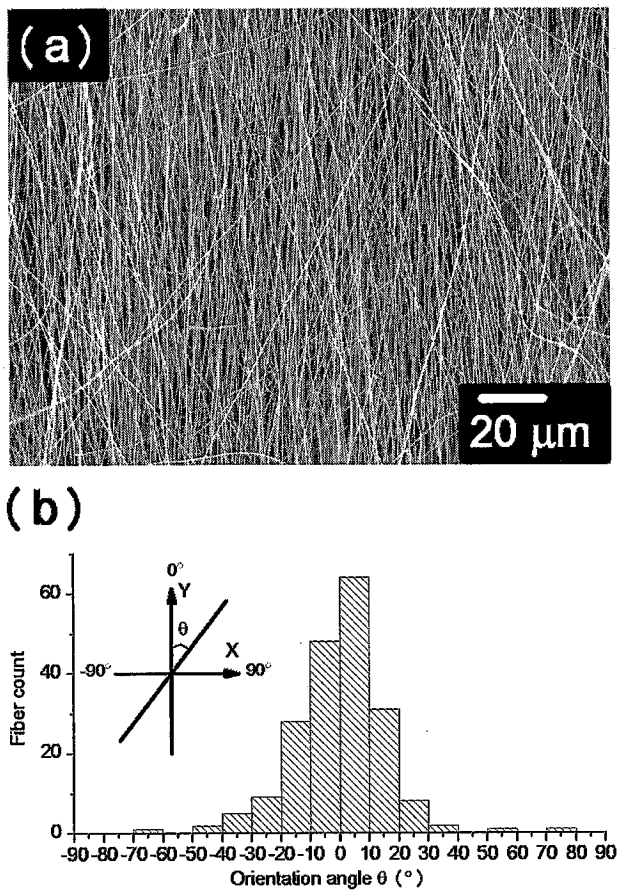

Figure 3.7 (a) SEM image of aligned PVP/PMMA nanofiber assemblies. (b) Histogram of orientation distribution of the PVP/PMMA nanofibers.

Aligned electrospun nanofiber assemblies were prepared from 250 mg/ml PVP/PMMA (weight ratio 10/90) in DMF containing 5 wt% TBAB with respect to PMMA.[22, 23] Electrospun nanofibers were collected on the drum collector rotated at 3000 rpm. The SEM

image of aligned PVP/PMMA nanofiber assemblies shows that nanofibers with average diameter 342±56 nm were well arranged and formed a dense array (Figure 3.7a). The thickness of the aligned nanofiber assembly used in this study was approximately 22 μm. Although substantial misalignment was still observed in the fiber assemblies, it was found that at least 85.5 % of the nanofibers were oriented within ±20° of the preferred direction (Figure 3.7b). The orientation parameter of the nanofiber assembly was estimated to be 0.86 by statistical analysis of the direction histogram.[10, 11] The value obtained is comparable with the reported value for electrospun poly (ethylene oxide) nanofiber assemblies collected at 2500 rpm.[26]

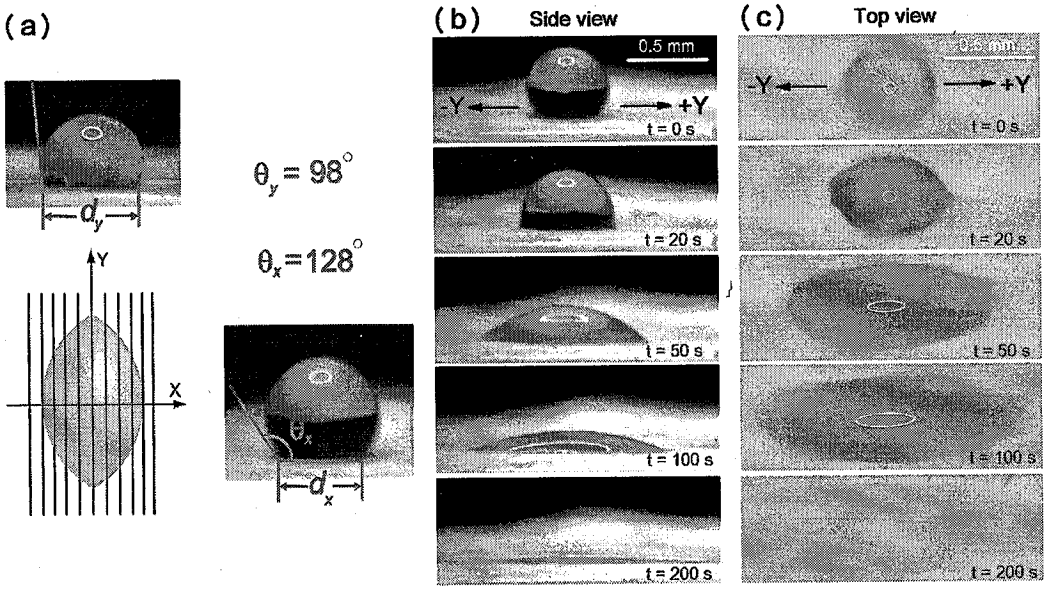

Figure 3.8 (a) Illustration for the directional measurement of contact angles on aligned PVP/PMMA nanofibers. (b) and (c) Time-lapse images of liquid droplet spreading on PVP/PMMA nanofiber mat: (b) side view and (c) top view. A 0.5 μL water droplet (fuchsine concentration: 1×10^{-5} M) were spread on aligned PVP/PMMA nanofiber assemblies. The drop motions are highlighted by the arrows in (b) and (c).

The wettability of these nanofiber assemblies is a key attribute for coating the polymer matrix. During the coating process, polymer solution penetrated into the nanofiber assemblies and covered all surfaces of the nanofibers. A 0.5 μL water droplet spread on the nonaligned nanofiber mat formed a spherical shape and displayed complete isotropic wetting after 4 s. However, the same droplet on aligned nanofiber assemblies showed anisotropic wetting

similar to the behavior of a water droplet on grooved surfaces.[28-30] Figure 3.8 shows the time-course of water droplet deformation on the aligned nanofiber assemblies. The x- and y-directions in Figure 3.8a show the directions of movement of the droplet as parallel and perpendicular to the oriented nanofibers. While the contact angle measured in the x-direction θ_x was 128 °, the contact angle θ_y was found to be 98 °. Both angles were significantly larger than the contact angle for a PVP/PMMA solution cast film (51°). The nanofiber assemblies include the effect of microscopic air pockets trapped below the liquid droplet, which leads to a hydrophobic interface.[17, 18] The addition of water-soluble PVP to PMMA changed the wettability of the nanofiber assemblies by reducing surface energy while maintaining the fibrous morphology. The contact angles in both directions approached zero by penetration of the water droplet into the nanofiber matrix. Time-lapse images of a liquid droplet spreading on aligned PVP/PMMA fiber mat are shown in Figures 3.8b and c. The initially spherical droplet spread on the aligned PVP/PMMA nanofiber assemblies, and was deformed into an ellipsoidal shape. Finally, the droplet penetrated into the nanofiber matrix and achieved complete wetting after 180 s.

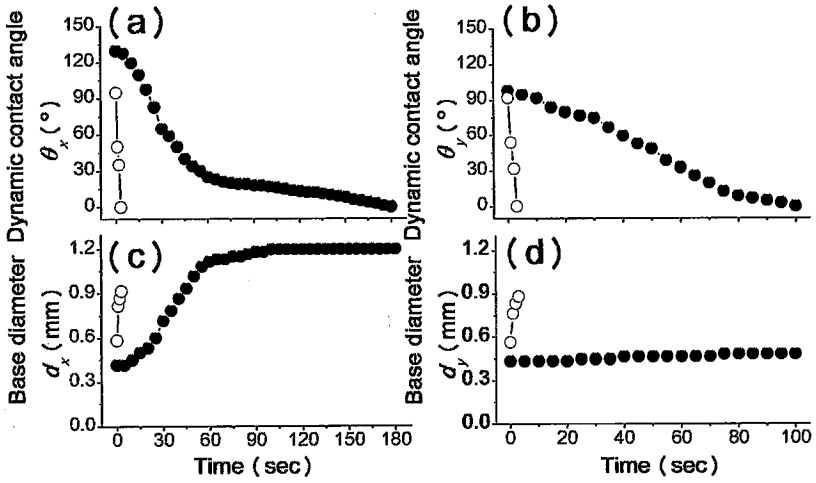

Figure 3.9 (a) and (b) Dynamic contact angle parallel and perpendicular to the y-axis (see the definition in Figure 2a) as a function of time for PVP/PMMA nanofiber mat. (c) and (d) Base diameter perpendicular and parallel to the y-axis as a function of time for PVP/PMMA nanofiber assemblies (●) and nonaligned nanofiber mat (○).

To confirm the role of the contact line pinning of aligned nanofiber assemblies in determining the droplet shape, the dynamic contact angles and base diameter both perpendicular and parallel to the y-axis were measured as a function of time. Figure 3.9 shows the time-courses of the contact angles and base diameters of a water droplet on aligned and

nonaligned nanofiber assemblies. The dynamic contact angles and the base diameters in both directions on a nonaligned nanofiber mat decreased within 4 s. The profiles in the x-axis were comparable with those in the y-axis. By contrast, the aligned nanofiber assemblies required 180 and 100 s, following attainment of the equilibrium contact angles θ_x and θ_y, to reach complete wetting (Figures 3.9a and b). On the aligned nanofiber assemblies, the base diameter d_x increased gradually for 100 s then became constant, while the base diameter d_y was roughly constant during the experiment (Figures 3.9c and d). The final drop elongation, calculated from the diameter ratios in the x and y directions of the ellipsoidal droplet on the aligned nanofiber assembly was 2.5, whereas for the drop on the nonaligned nanofiber mat the elongation was 1.0 (Figures 3.9c and d). Thus, the nonaligned nanofiber mat exhibited isotropic spreading of the droplet and there were no pinning barriers for contact line motion. On the other hand, the aligned nanofiber assembly showed directional spreading of the droplet along the alignment direction of the nanofibers. These results clearly confirmed that the aligned nanofiber assemblies had a high degree of alignment while maintaining their wettability.

3.3.3 Characterization of PEDOT/PSS Film Containning Nanofibers

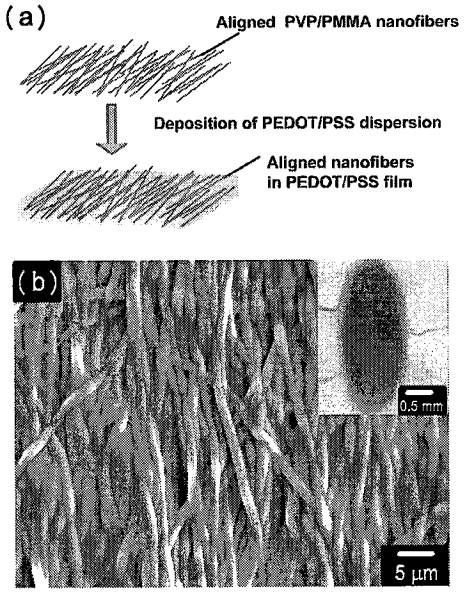

Figure 3.10 (a) Schematic illustration of the preparation of PEDOT/PSS composite film containing aligned nanofiber assemblies. (b) SEM image of the surface of PEDOT/PSS composite film containing aligned PVP/PMMA nanofibers. Inset is optical image of PEDOT/PSS dispersion wetted spot on aligned nanofiber assemblies.

Electroactive PEDOT/PSS films have been found to exhibit excellent isotropic actuation properties as a result of controlling the water-vapor sorption equilibrium in response to an

electric field.[21,31] When the aligned nanofiber assemblies were embedded in the PEDOT/PSS matrix, the anisotropic structure affected the directional actuation of the composite. The procedure for fabrication of aligned nanofiber-embedded PEDOT/PSS composite is shown schematically in Figure 3.10a. PEDOT/PSS aqueous dispersion displayed complete wetting like water on the aligned nanofiber assemblies. It easily penetrated into the aligned nanofiber assemblies and wetted all surfaces of the nanofibers. Figure 3.10b shows an SEM image of the PEDOT/PSS film containing the aligned PVP/PMMA nanofiber mat, showing aligned fibrous morphology after coating. A PEDOT/PSS layer was coated on the surfaces of the aligned nanofibers, and the interspace between nanofibers was filled with PEDOT/PSS. The contour of a PEDOT/PSS wetted spot revealed an elongated and parallel-sided shape (inset to Figure 3.10b) with elongation value 2.1. This shape is typically observed on grooved surfaces, which again confirms that the nanofibers were highly orientated.[27-29] The orientation parameter of the coated nanofibers was determined as 0.82 (Figure 3.11), in agreement with the value for uncoated aligned nanofibers. Inside the PEDOT/PSS layer, the aligned nanofibers were fully covered with PEDOT/PSS (Figure 3.12).

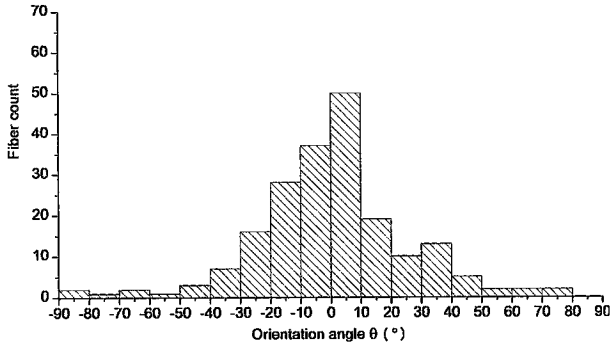

Figure 3.11 Histogram of the orientation distribution for the PEDOT/PSS coated nanofiber. The orientation parameters f_p of the coated nanofibers determined from the histogram is 0.82.

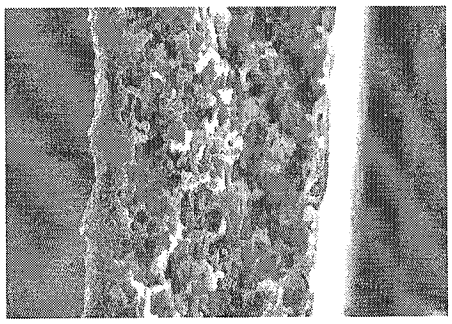

Figure 3.12 Cross-sectional SEM image of PEDOT/PSS layer containing aligned nanofibers.

3.3.4 Anisotropic Actuation of PEDOT/PSS Film Containing Nanofibers

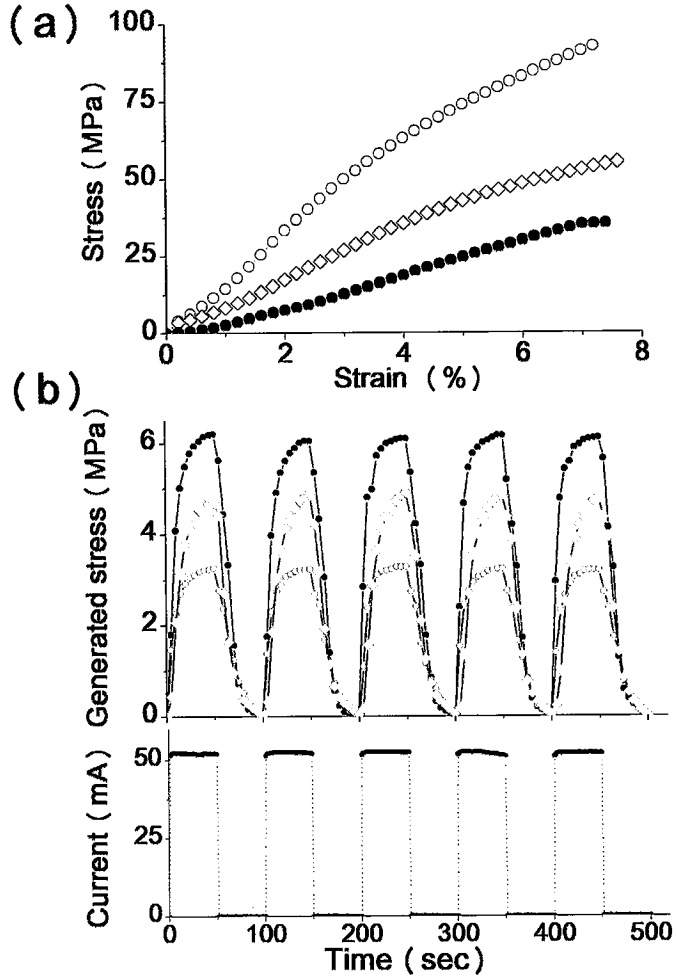

Figure 3.13 (a) Stress-strain curves of PEDOT/PSS composite films with nonaligned and aligned nanofibers and (b) time profiles of the generated stress of loading direction parallel to aligned nanofiber direction (○), loading direction perpendicular to aligned nanofiber direction (●) of PEDOT/PSS composite films with aligned nanofiber assemblies, and PEDOT/PSS film with nonaligned nanofiber mat (◇). (c) Time profile of the current of PEDOT/PSS composite films at 25°C with 50% RH.

Young's modulus of the aligned nanofiber-embedded PEDOT/PSS composite film along the nanofiber orientation direction was 2.2±0.2 GPa, nearly three times than that of nonaligned nanofibers (0.8±0.1 GPa). Moreover, this value was almost five times than the value perpendicular to the nanofiber direction, showing the anisotropic mechanical properties of the composite film (Figure 3.13a).

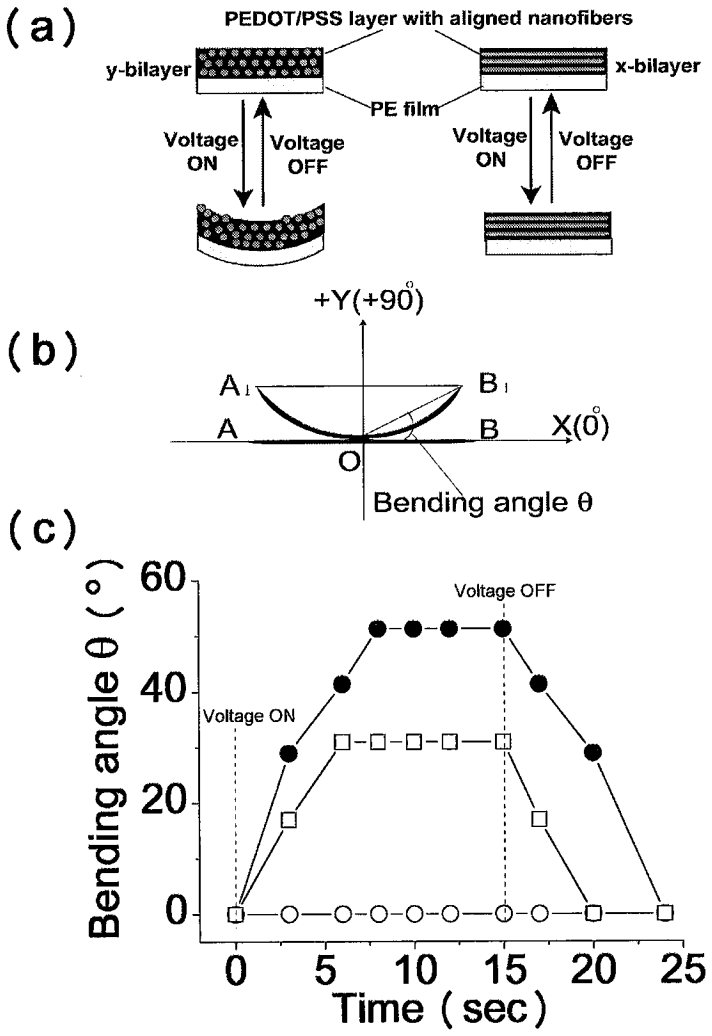

Figure 3.14 (a) Illustration of PEDOT/PSS-PE bilayer with aligned nanofiber assemblies. Left image: y-bilayer, right image: x-bilayer. (b) Schematic illustration of the bending/unbending motions. (c) Time-dependent bending angles of PEDOT/PSS-PE bilayer with aligned nanofiber assemblies ((●) y-bilayer, (○) x-bilayer) and PEDOT/PSS-PE bilayer with nonaligned nanofiber mat (□). The bending actuations are measured under an applied constant current of 53 mA at 25°C with 50% RH.

Bilayer actuators were fabricated by deposition of PEDOT/PSS composite film onto polyethylene (PE) thin film in the same manner that PEDOT/PSS composite film was made. Poly(vinyl alcohol) (PVA) was used as an adhesion interlayer between PE and the PVP/PMMA nanofiber mat to prevent the PEDOT/PSS film from peeling off. The thicknesses of PE film, PVA interlayer, and PEDOT/PSS composite film were 10, 0.55 and 27 μm, respectively. Two PEDOT/PSS-PE bilayers containing the aligned nanofiber assemblies were prepared by cutting the bilayer in two directions. Cross-sectional images of the bilayer

actuators are depicted in Figure 3.14a. The left image shows the aligned nanofiber direction parallel to the loading direction, and is defined as a y-bilayer. The right image shows the aligned nanofiber direction perpendicular to the loading direction, and is defined as an x-bilayer. The y-bilayer displayed a bending/unbending motion in response to an applied voltage of 2.8 V, while no obvious motion of the x-bilayer was observed. Figure 3.14b shows a schematic illustration of the bending/unbending movement of the bilayer actuators. The bending angle (θ) of the bilayer actuator was obtained from the width between the two positions A_1 and B_1. Figure 3.14c shows the time-dependent bending angles of the PEDOT/PSS-PE bilayer. The PEDOT/PSS composite layer on the PE film shrunk by applying a voltage due to water vapor desorption from the electro-active PEDOT/PSS, and the bilayer bent as the result of shrinking of the PEDOT/PSS layer. The y-bilayer bent from 0° to 53° within 8 s of after applying the electrical field, indicating a bending speed of 7.9 °/s. However, the x-bilayer showed no motion on application of the same voltage. Thus the PEDOT/PSS-PE bilayer with incorporated nonaligned nanofiber mat showed an isotropic bending motion on application of the electrical field. It follows that the bending motion is affected by the alignment of the nanofiber structures in the PEDOT/PSS layer, and the difference of Young's modulus in the composite films results in the anisotropic bending actuation.

3.4 Conclusions

Anisotropic actuation properties using electrospun nanofiber assemblies can be obtained by controlling the alignment of the nanofibers and fully covering the nanofibers with electro-active conductive polymers. The orientation of the nanofibers pre-determined an anisotropic generating stress and bending motion. Aligned nanofiber assemblies were prepared by collection of electrospun nanofibers on a rotating drum collector. The alignment

of nanofiber assemblies was evaluated by statistical analysis of the nanofiber direction histogram and anisotropic wettability. PEDOT/PSS composite film incorporating the aligned nanofiber assemblies exhibited anisotropic electromechanical properties due to the anisotropic mechanical properties within the composite film. This study will open prospects for the construction of anisotropic actuators based on directional orientation of nanofibers, and further investigation may lead to fabrication of low-cost, flexible ambient devices with anisotropic actuation properties.

References

1. Y. Dzenis, Spinning Continuous Fibers for Nanotechnology, *Science* **2004**, *304*, 1917-242.
2. A. Greiner, J. H. Wendorff, Electrospinning: A Fascinating Method for the Preparation of Ultrathin Fibers, *Angew. Chem. Int. Ed.* **2007**, *46*, 5670-5703.
3. J. W. Xie, X. R. Li, Y. N. Xia, Putting Electrospun Nanofibers to Work for Biomedical Research, *Macromol. Rapid. Commun.* **2008**, *29*, 1775-1792.
4. P. Katta, M. Alessandro, R. D. Ramsier, G. G. Chase, Continuous Electrospinning of Aligned Polymer Nanofibers onto a Wire Drum Collector, *Nano Lett.* **2004**, *4*, 2215-2218.
5. R. Pytel, E. Thomas, I. Hunter, Anisotropy of Electroactive Strain in Highly Stretched Polypyrrole Actuator, *Chem. Mater.* **2006**, *18*, 861-863.
6. J. K. Park, R. B. Moore, Influence of Ordered Morphology on the Anisotropic Actuation in Uniaxially Oriented Electroactive Polymer Systems, *ACS App. Mater. Interfaces.* **2009**, *1*, 697-702.
7. J. Zhou, T. Fukawa, H. Shirai, M. Kimura, *Macromol. Mater. Eng.* **2010**, *295*, 671-675.
8. H. Dong and W. E., Jr. Jones, Preparation of Submicron Polypyrrole/Poly (methyl methacrylate) Coaxial Fibers and Conversion to Polypyrrole Tubes and Carbon Tubes, *Langmuir* **2006**, *22*, 11384-11387.
9. H. Dong, V. Nyame, A. G. Macdiarmid, W. E. Jones, Polyaniline/Poly(methyl methacrylate) Coaxial Fibers: The Fabrication and Effects of the Solution Properties on the Morphology of Electrospun Core Fibers, *J. Polym. Sci., Part B: Polym. Phys.* **2004**, *42*, 3934-3942.
10. F. Gadala-Maria, F. Parsi, Measurement of Fiber Orientation in Short-Fiber Composites Using Digital Image Processing, *Polym. Composite.* **1993**, *14*, 126-131.
11. L. Liu, Y. A. Dzenis, Analysis of Effects of the Residual Charge and Gap Size on Electrospun Nanofiber Alignment in a Gap Method, *Nanotechnology* **2008**, *19*, 1-7.
12. V. Thavasi, G. Singh, S. Ramakrishma, Electrospun Nanofibers in Energy and Enviromental Applications, *Energy Environ. Sci.* **2008**, *1*, 205-221.
13. J. W. Xie, X. R. Li and Y. N. Xia, Putting Electrospun Nanofiber to Work for Biomedical Research, *Macromol. Rapid. Commun.* **2008**, *29*, 1775-1792.

14. S. Megelski, J. S. Stephens, D. B. Chase and J. F. Rabolt, Micro and Nanostructured Surface Morphology on Electrospun Polymer Fibers, *Macromolecules* **2002**, *35*, 8456-8466.
15. S. Pelfrey, T. Canta, M. R. Papantonakis, D. L. Simonson, R. A. Mcgill and J. Macossay, Microscopic and Spectroscopic Studies of Thermally Enhanced Electrospun PMMA Micro and Nanofibers, *Polym. Chem.* **2010**, *1*, 866-869.
16. X. Y. Sun, L. R. Nobles, H. G. Börner and R. J. Spontak, Field-Driven Surface Segregation of Biofunctional Species on Electrospun PMMA/PEO Microfibers, *Macromol. Rapid. Commun.* **2008**, *29*, 1445-1460.
17. A. Lafuma, D. Quéré, Superhydrophobic States, *Nat. Mater.* **2003**, *2*, 457-460.
18. A. Tuteja, W. Choi, M. L. Ma, J. M. Mabry, S. A. Mazzella, G. C. Rutledge, G. H. McKinley, R. E. Cohen, Designing Superroleophobic Surfaces, *Science* **2007**, *318*,1618-1622.
19. C. Ishino, K. Okumura and D. Quere, Wetting Transitions on Rough Surfaces, *Eurphys. Lett.* **2004**, *68*, 419-425.
20. C. Ishino and K. Okumura, Wetting Transitions on Textured Hydrophilic Surfaces, *Eur. Phys. J. E.* **2008**, *25*, 415-424.
21. P. H. Qiu and C. B. Mao, Biomimetic Branched Hollow Fibers Templated by Self-Assembled Fibrous Polyvinylpyrrolidone Structures in Aqueous Solution, *ACS nano.* **2009**, *3*, 1573-1579.
22. D. Li and Y. N. Xia, Electrospinning of Nanofibers: Reinventing the Wheel, *Adv. Mater.* **2004**, *16*, 1151-1170.
23. E. P. D. Silva and M. I. B.Tavares, Solid State NMR Study of Poly(methyl methacrylate) /Poly(vinyl pyrrolidone) Blends, *Polym. Bull.* **1998**, *41*, 307-310.
24. W. P. Hsu, Effect of Tacticity of Poly(methyl methacrylate) on the Miscibility with Poly(vinyl pyrrolidone), *J. Appl. Polym. Sci.* **2001**, *81*, 3190-3197.
25. Y. Borodko, S. E. Habas, M. Koebel, P. D. Yang, H. Frei and G. A. Somorjai, Probing the Interaction of Poly(vinyl pyrrolidone) with Platinum Nanocrystals by UV-Raman and FTIR, *J. Phys. Chem. B.* **2006**, *110*, 23052-23059.
26. G. Han, B. Guo, L.Zhang and B. Yang, Conductive Gold Films Assembled on Electrospun Poly(methyl methacrylate) Fibrous Mats, *Adv. Mater.* **2006**, *18*, 1709-1712.

27. H. Kusumastmaja, R. J. Vrancken, C. W. M. Bastiaansen, J. M. Yeomans, Anisotropic Drop Morphologies on Corrugated Surfaces, *Langmuir* **2008**, *24*, 7299-7308.
28. J. Yang, F. R. A. J. Rose, N. Gadegaard, M. R. Alexander, Effect of Sessile Drop Volume on the Wetting Anisotropy Observed on Grooved Surfaces, *Langmuir* **2009**, *25*, 2567-2571.
29. D. Y. Xia, S. R. J. Brueck, Strong Anisotropic Wetting on One-Dimensional Nanopatterned Surfaces, *Nano Lett.* **2008**, *8*, 2819-2824.

Chapter 4

Macroporous Conductive Polymer Films Fabricated by Using Electrospun Nanofiber Templates and Their Anisotropic Actuation Properties

Chapter 4 Macroporous Conductive Polymer Films Fabricated by Using Electrospun Nanofiber Templates and Their Anisotropic Actuation Properties

Abstract: We demonstrate a facile method to fabricate macroporous poly(3, 4-ethylenedioxythiophene)/poly (4-styrene sulfonate) (PEDOT/PSS) films with empty channels by using electrospun nanofiber as a sacrificial template. The channels within PEDOT/PSS films were prepared by depositing PEDOT/PSS aqueous dispersion onto poly(vinyl pyrrilidone)/poly(methyl methacrylate) (PVP/PMMA) nanofiber template, and then the nanofibers were removed by solvent extraction. The average diameter of the channels is 313 ± 45 nm, which is almost same as the parent PVP/PMMA nanofibers. The macroporous PEDOT/PSS film with the empty channels showed an enhancement of electromechanical properties compared to the nonporous PEDOT/PSS film.

4.1 Introduction

Macroporous materials having pores greater than approximately 50 nm have attracted considerable attention due to their potential applications, such as catalysis[1], separation[2], sorption[3], optics[4,5], and drug delivery.[6] Filling voids in ordered assembly of spherical templates with metal oxides or cross-linked polymers and subsequent removing the templates can create three-dimensional structures having long-range ordered dielectric periodicity.[4] These macroporous materials have been investigated as photonic band gap crystals for the optical spectrum.[7] The utility of the porous system is a sensitive function of the internal pore diameter, their distribution, and their morphology.[8-11] The synthetic approaches to creating macroporous materials have been demonstrated the creation of internal spherical voids with

monodisperse and controllable diameters. [1, 4, 12, and 13] We focused on the creation of internal one-dimensional channels within the conductive polymer films by removing nanofiber templates without the use of lithography techniques. Long and continuous channels in the materials can provide unique interfaces for transportation and transduction of molecules. The channel structures have been fabricated by top-down techniques using electron beam lithography, focused-ion-beam milling, nanoimprint or template techniques using sacrificial materials of SiO_2[14], ZnO[15], metals[16], and organic fibers[17,18].

Recently, there has been growing interest in developing porous conductive polymers.[19-21] For applications of conductive polymer based sensors and actuators, channel structure is one of the ideal structure that can enhance the device performance by improving surface area and also can bring a range of opportunities for engineering stimuli-responsive properties.[22] The template method provides a versatile approach for the construction of uniform pores and channels within conductive polymer matrix.[23] Porous conductive polymers have been obtained by using various templates. Uniform pores in anodized aluminum oxide membranes have been used as a template to prepare hollow fibers of polyaniline, polypyrrole, poly (3, 4-ethylenedioxythiophene) and poly (3-hexylthiophene).[24-29] Recently, we reported a synthesis of porous conductive polymers having nanometer-scale channels by the amphiphilic surfactant templating approach.[30] However, there are only a few reports in the literatures on preparation of macroporous conjugated polymers with long and continuous channels.

Electrospinning is a simple method for the production of nanofibers and nanofibrous nonwoven mats with various applications.[31-33] The electrospinning process is a method of discharging a polymer solution in air from a nozzle under high voltage and producing nanofibers by exploiting electrostatic repulsion of the polymer solution. Although the electrospinning has been successfully applied to produce conductive nanofibers, the

conductive polymers needs a careful control of spinability because of their low solubility and the fast crystallization, and their mechanical strength of resulted nanofiber mats are weak.[34-40] The deposition of different wall materials on the surface of the electrospun nanofibers was achieved by using various techniques including chemical vapor deposition, sol-gel polymerization, and electroless plating.[41-44] Selective removal of the fiber core leads to the formation of hollow fibrous materials. Laforgue et al. demonstrated the fabrication of hollow conductive nanofibers by the combination of the electrospinning techniques and an adapted vapor-phase polymerization procedure.[42] Dong et al. reported the preparation of polypyrrole/ poly (methyl methacrylate) coaxial fibers using electrospun polymer fibers as template and subsequent formation of conductive wall around polymer fibers.[44] Sacrificial nanofiber templates fabricated by electrospinning offers the advantages to produce hollow nanofibers with submicrometer or even nanometer diameter.

In chapter 3, we fabricated nonaligned and aligned PVP/PMMA nanofibers by electrospinning. These nanofiber mats displayed excellent wetting properties that PEDOT/PSS aqueous dispersion penetrates into the nonwoven nanofiber mat and all nanofibers are decorated with PEDOT/PSS. In this chapter, we report a fabrication method to obtain macroporous poly (3, 4-ethylenedioxythiophene)/ poly (4-styrene sulfonate) (PEDOT/PSS) films with empty channels created by using electospun nanofibers as a sacrificial template. The fabrication procedure for the channels in PEDOT/PSS thin film can be briefly described as follows. First, PEDOT/PSS was deposited on the surface of the nanofiber templates. And subsequently, nanofiber templates are removed by dissolution in an appropriate solvent to create the desired channel structure. A key is a surface design of the nanofiber templates, which should be intact during the deposition process and easily removable in the following removal process. The wall materials need to be robust enough to

retain its morphology during the removal of nanofiber template and construction of the wall of channels.

Conducting polymers transduce the input of chemical or physical energy directly into mechanical work. The PEDOT/PSS films exhibited an excellent actuation through the control of the equilibrium of water vapor sorption in response to the electric filed. In this chapter, we found the enhancement of electromechanical actuation property of macroporous PEDOT/PSS film by the creation of channels. The channels in PEDOT/PSS films may provide transportation interfaces of water vapor and the presence of channels affects the actuation property.

4.2 Experimental Section

4.2.1 Materials

The materials were same with the materals in Chapter 3.

4.2.2 Fabrication of Nanofiber Templates by Electrospinning

The methods were same according to the method described in Chapter 3.

4.2.3 Deposition of PEDOT/PSS Dispersion on PVP/PMMA Nanofiber Mats

The weight of PVP/PMMA nanofiber mat (PVP/PMMA = 10/90 wt %) was 34.4 mg with an area of 4 x 7 cm. The fiber mat was put on the PE film and well-dispersed PEDOT/PSS aqueous dispersion (1.2 wt% of solid content, 3.0 g) containing 5 wt% EG was deposited on the nanofiber mat and followed by drying the sample at 100 °C for 2 hours. EG was used as an additive for the enhancement of electronic conductivity of PEDOT/PSS.

4.2.4 Preparation of Macroporous PEDOT/PSS Films

Macroporous PEDOT/PSS films having numerous channels were prepared by solvent extraction process of sacrificial nanofiber templates. The PEDOT/PSS coated mat was cut into strips with a dimension of 3 mm x 7 cm and then each strip was put into a vessel with 20 ml $CHCl_3$ or toluene. The PEDOT/PSS film was easily peeled off from the PE film in organic solvents after 5 min. PEDOT/PSS film was removed from solution, washed several times by organic solvents to dissolve nanofibers from the PEDOT/PSS matrix, and air-dried.

4.2.5 Measurements

The apparent contact angles were record by an IUC200-CK2 camera (Trinity, INC) within 3s after placing droplets of about 2 μL on spin-coated PMMA films, PVP/PMMA films or nanofiber mats. The average contact angle value was obtained by measuring at five different positions of the same sample. Morphologies of nanofibers, PEDOT/PSS films were evaluated by a VE-8800 scanning electronic microscope (Keithley Co., LTD). FT-IR spectra were obtained using an IR Prestige-21spectrometer (Shimazu Co., LTD).

The actuation performances of PEDOT/PSS films were tested on a ZP-2N force gauge (Imada Co., LTD). Actuation specimen was prepared in size of 30 x 3 mm and settled into a humidity-controlled chamber. The electric field was applied to the film with a computer-driven PK-80 DC power supply (Matsusada Co., LTD) through a pair of copper wires (170 mm) attached to the film with silver paste; the distance between the electrodes was 30 mm. The electric currents were monitored by a U1252A digital multimeter (Agilent Co., LTD). Temperature and humidity in the measuring chamber were monitored by a HMI-31 sensor (VAISALA Co., LTD). The stress and current changes were collected through USB communication to the computer.

4.3 Results and Discussion

4.3.1 Macroporous PEDOT/PSS Films Fabricated by Using Mats of Nonaligned nanofibers

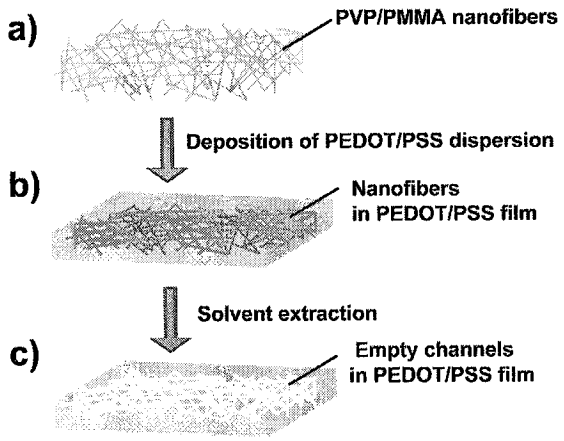

Figure 4.1 Schematic illustration of the preparation of macroporous PEDOT/PSS film.

The fabrication procedures of channels in PEDOT/PSS layer are shown schematically in Figure 4.1. The contact angles of PEDOT/PSS aqueous solution on PMMA and PVP/PMMA composite nanofiber mats were 137±4 ° and 40±2 °, respectively, which were at the same range as those of water. The PEDOT/PSS aqueous dispersion easily penetrated through the nanofiber mat and wet the surface of all nanofibers. When PEDOT/PSS aqueous dispersion containing 5wt% of EG was deposited onto the PVP/PMMA nanofiber mat and dried at 100 °C, a dark blue films were yielded. Finally, PVP/PMMA nanofibers were treated with $CHCl_3$ or toluene to dissolve away PMMA and leave macroporous PEDOT/PSS films as a solid.

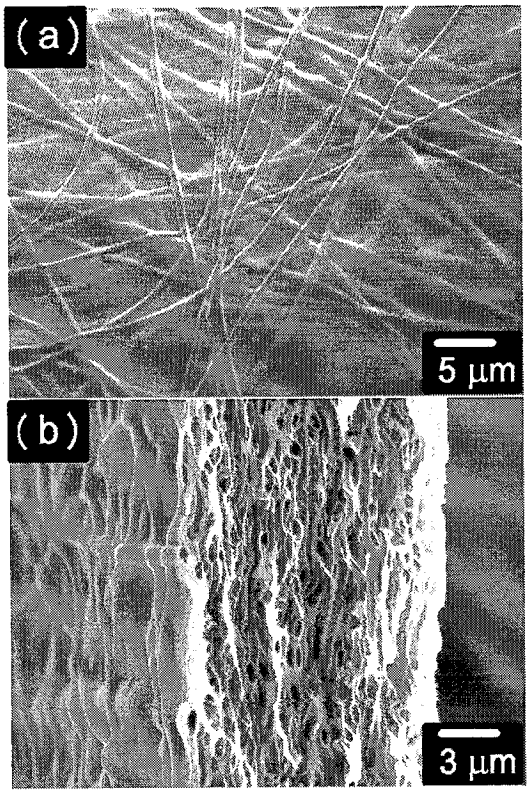

Figure 4.2 SEM images of (a) the surface of PEDOT/PSS film containing PVP/PMMA nanofiber mat and (b) cross section of macroporous PEDOT/PSS film with channel structures.

Figure 4.2a showed a SEM image of PEDOT/PSS film containing the PVP/PMMA nanofiber mat, showing almost no change of fibrous morphology upon coating. The PEDOT/PSS layer was coated on the surface of nanofibers and the interspace among nanofibers was filled with the PEDOT/PSS layer. The diameter of nanofibers and the thickness of the mats were not affected by the wet-coating process, which is expected because PVP/PMMA nanofibers are not swollen in water. The film after the solvent extraction possesses a lot of pores and the thicknesses of PEDOT/PSS wall in the macroporous film are in a range of 20 to 120 nm (Figure 4.2b). The weight decrease after the solvent extraction was above 90 % of weight of nanofiber template. The average diameter of channels measured from the SEM image is 313±45 nm, respectively. The observed pore size was similar to the average diameter of PVP/PMMA nanofibers (334±54 nm). FTIR spectrum of the

macroporous film did not show any peaks of PMMA and PVP, indicating the releasing of PVP/PMMA. TG curve of the macroporous film agreed with that of dried PEDOT/PSS and a steep weight decrease at 400 °C as observed in TG curve of PEDOT/PSS film containing the PVP/PMMA nanofiber mat was disappeared after the solvent extraction (Figure 4.3). These results supported that one-dimensional channel structure was constructed by the deposition of PEDOT/PSS around PVP/PMMA nanofiber mat and the extraction of nanofiber templates from the PEDOT/PSS film.

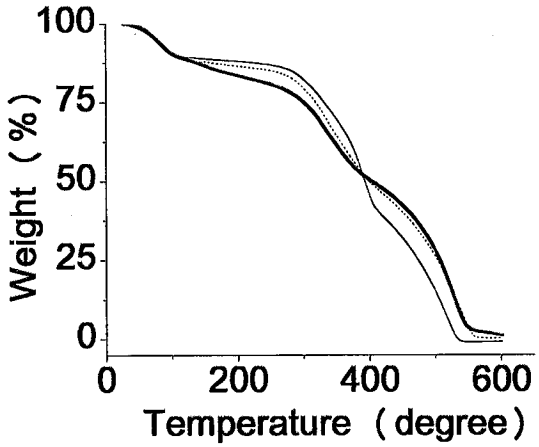

Figure 4. 3 TG curves of nonporous PEDOT/PSS film (bold line), PVP/PMMA nanofiber embedded in PEDOT/PSS film (solid line), and macroporous PEDOT/PSS film (dashed line).

The porosity (P) of PVP/PMMA nanofiber mat was estimated using the following equation [43]:

$$P = (d_0 - d) / d_0 \qquad (2)$$

where d_0 is the density of materials (PMMA and PVP densities are 1.18 and 1.20 g/cm^3. We used 1.18 g cm^{-3} as the density of mixed materials because of a low composition ratio of PVP) and d is the apparent density calculated from weight and volume of nanofiber mat. The volumes were determined by area and average thickness of sample. For maximum accuracy in the thickness variations, the measurements of average thickness were carried out at several points within the same sample. The porosity of nanofiber mat was estimated to be 0.83,

indicating that 17% of volume in sample volume is the nanofiber volume. This volume can convert into a pore volume in the macroporous PEDOT/PSS film. From the nanofiber volume and the average diameter of channels, the specific surface area of macroporous film was estimated to be 4.52 m^2/g. The estimated specific surface area of macroporous PEDOT/PSS film was 14 times compared with that of PEDOT/PSS film without channels (0.32 m^2/g). Macroporous conductive films having a large surface area will provide new opportunity for the fabrication of electronic devices and biosensors by the deposition of functional materials onto the wall of channels and the recognition of giant molecules within the channels.[45, 46]

4.3.2 Actuation Properties of Macroporous PEDOT/PSS Films with Nonaligned Channels

The PEDOT/PSS films have been investigated as electro-active actuators. Okuzaki et al. investigated the electromechanical properties of PEDOT/PSS film actuator in an ambient atmosphere under an electrical field.[47] We also reported the actuation properties of PEDOT/PSS coated cellulose paper, which displayed an anisotropic stress generation according to the orientation of cellulose fibers in the paper. The PEDOT/PSS films exhibited an excellent actuation through the control of the equilibrium of water vapor sorption in response to the electric filed.[48] Conducting polymers transduce the input of chemical or physical energy directly into mechanical work. The introduction of channel structures in PEDOT/PSS films will affect the actuation property. The electromechanical properties of macroporous PEDOT/PSS films were investigated by the generated stress by applying the voltage.

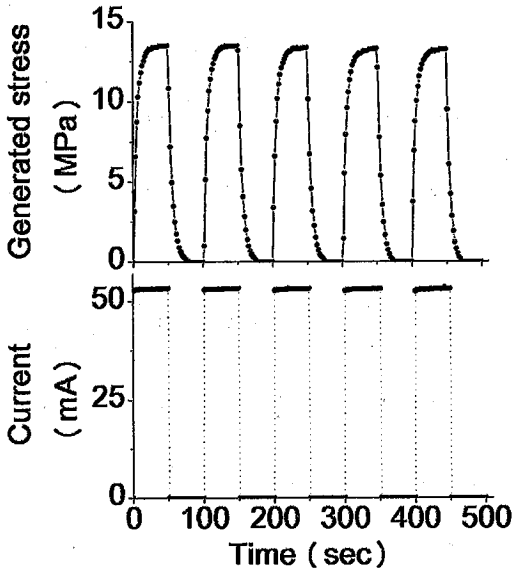

Figure 4.4 Time profiles of the generated stress and electrical current of macroporous PEDOT/PSS film at 50% RH and 25 °C.

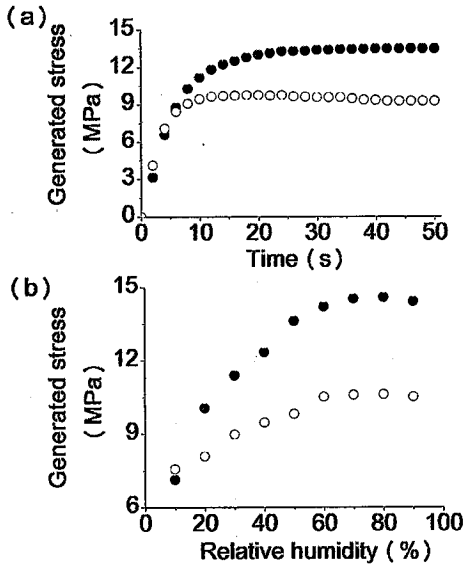

Figure 4.5 (a) Time profiles of the generated stress of macroporous PEDOT/PSS film (●) and nonporous PEDOT/PSS film (○) by applying a voltage of 2.8V at 50 % RH and 25 °C. (b) Generated stresses of macroporous PEDOT/PSS film (●) and nonporous PEDOT/PSS film (○) under various relative humidity at 25 °C.

Time profiles of the generated stress and electronic current of macroporous PEDOT/PSS films at 50% RH and 25 °C are shown in Figure 4.4. When a direct current of 2.8 V was applied to the macroporous PEDOT/PSS film, the film generated significant stress in response to the electric field. Turning off the applied voltage returned the stress to zero. This

generation of stress is attributed to the contraction of PEDOT/PSS layer upon desorption of water.[47] After turning off the electrical field, the film underwent an expansion movement and relaxed to its original configuration. This movement is due to the extension of the PEDOT/PSS film upon adsorption of water. The generated stress after 500 cycles of this experiment was almost unaltered, which indicates good repeatability and reliability of actuation properties. To examine the influence of actuation properties on the presence of pores in PEDOT/PSS films, we prepared nonporous PEDOT/PSS films having same weight and size as the porous films. Although the nonporous PEDOT/PSS film exhibited a generated stress of 9.3 MPa by applying 2.8 V, the generated stress was enhanced to be 13.5 MPa in the macroporous film (Figure 4.5a). The generated stress strongly depended on relative humidity and the macroporous film showed a larger increase of generated stress compared to the nonporous film (Figure 4.5b). The enhancement of generated stress can be driven by the complete adsorption of water vapor within the porous film through a large interface in the macorporous PEDOT/PSS film.

The resistivities of macroporous and nonporous PEDOT/PSS films were measured by a two probe system. The electrical resistivities of two samples were about 6.3×10^{-3} and 10.2×10^{-3} Ω·cm, respectively. We record the dependence of surface temperature on time of these two samples by applying a voltage about 2.8 V on each sample for 100 sec. The currents of both samples were displayed around 53 mA, suggesting that the generated heat of macroposous film is the same as that of nonporous film. The difference of surface temperatures between macroporous and nonporous PEDOT/PSS films was observed. The surface temperature of nonporous PEDOT/PSS film was rise to 46.1 °C by applying 2.8 V for 100 s, which is 15.5 °C higher than macroporous film. This difference in temperatures suggests that air in the pores performs the insulating layer for the heat transduction within the

macroporous PEDOT/PSS films and the heat energy could be stored in the film. As described previously, the porosity of the film with channel structures was estimated to be about 17%. The total heat transfer through a porous material can be simplified as the sum of the heat transfer through solid phase and air phase.[49] The thermal conductivity (K) of the macroporous PEDOT/PSS film can be described by a thermal resistor model,[50] which consists of PEDOT/PSS and air;

$$K = K_p V_p + K_a V_a \qquad (3)$$

where K_p and K_a are the thermal conductivities of a PEDOT/PSS and air, V_p and V_a represent the volume percentage of PEDOT/PSS and air. The reported thermal conductivity of PEDOT/PSS film (Clevios P) and air are 0.17 and 0.025 W/ (m K), respectively.[49, 51] Overall thermal conductivity of PEDOT/PSS with channel structures is 0.14 W/ (m K). The thermal conductivity of macroporous film was reduced compared with the nonporous PEDOT/PSS film. Air in the channel structures act as thermal insulation component, which prevent the heat from transferring to the air outside.

4.3.3 Bending Actuation Properties of Macroporous PEDOT/PSS-PE Bilayer with Nonaligned Channels

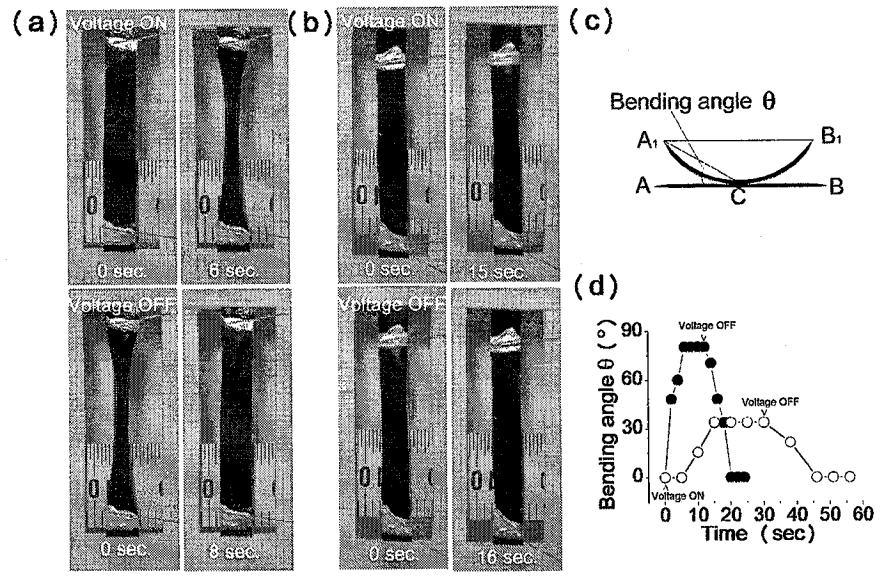

Figure 4.6 Time profiles of bending/unbending movement of (a) macroporous PEDOT/PSS-PE bilayer and (b) nonporous PEDOT/PSS-PE bilayer actuator. (c) Schematic illustration of the bending/unbending movement, (d) Time-dependent bending angles of macroporous (●) and nonporous (○) PEDOT/PSS-PE bilayer actuators.

Previously we demonstrated a bending motion of the PEDOT/PSS coated paper when the voltage switching between on and off. The mechanism of this bending motion also lines in shrinking of PEDOT/PSS layer by applying voltage. However, the response time of this bending motion was slow; one cycle for the bending/unbending motion needs over 50s. Construction of channels in PEDOT/PSS film results in the creation of porous materials having high surface area and these materials may provide continuous pathways of water molecular into and out of the polymer matrix. Bilayer actuators were fabricated by the deposition of macroporous PEDOT/PSS film onto polyethylene (PE) thin film as the same preparation manner of macroporous PEDOT/PSS films to control the bending direction. Poly (vinyl alcohol) (PVA) was used as an adhesion interlayer between PE and PVP/PMMA

nanofiber mat to prevent PEDOT/PSS film from peeling off. The thicknesses of PE film, PVA interlayer, and macroporous PEDOT/PSS film are 10, 0.55, and 6.3 μm, respectively. The bending/unbending movements of the bilayer actuators were recorded by a digital video camera recorder by applying a constant current of 53 mA. The sample was nearly flat at room temperature (25°C) with a 50% RH. The macroporous PEDOT/PSS-PE bilayer actuator exhibited a large bending motion as soon as the electrical field was applied (Figure 4.6). In contrast, the nonporous bilayer actuator showed a small bending and a slow response compared to the macroporous PEDOT/PSS-PE bilayer actuator. Figure 4.6c shows the schematic illustration of the bending /unbending movement of bilayer actuator. The bending angles (θ) of the bilayer actuator were obtained from the width between A_1 and B_1 by monitoring the camera redorder. Figure 4.6d shows the time-dependent bending angles of macroporous and nonporous PEDOT/PSS-PE bilayer actuators. The nonporous bilayer actuator needs 15 sec to reach the bending angle at 34° after applying the electrical field. In contrast, the macroporous PEDOT/PSS-PE bilayer actuator shows a large and fast deformation to reach a deflection angle of 80.4°. The bending motion of the macroporous PEDOT/PSS-PE bilayer actuator can be repeated 100 times without any damage. These results also support the rapid desorption and sorption of water vapor within the macroporous actuator. The construction of channels in the PEDOT/PSS layer is promising for fabricating the fast-response conductive polymer actuators.

4.3.4 Bending Actuation Properties of Macroporous PEDOT/PSS-PE Bilayer with Aligned Channels

In our previous section, we improved the bending/unbending actuation of PEDOT/PSS-PE bilayer by introduction of channel structures in PEDOT/PSS layers. These channel structures were constructed by nonaligned PVP/PMMA fibers with an orientation parameters $f_p = 0.08$.

These nonaligned channels largely enhanced the specific surface area of PEDOT/PSS film and resulted in a rapid desorption and sorption of water vapor, thus, improved actuation of PEDOT/PSS-PE bilayer with a intensive bending/unbending motion and a fast response speed.[34,35]

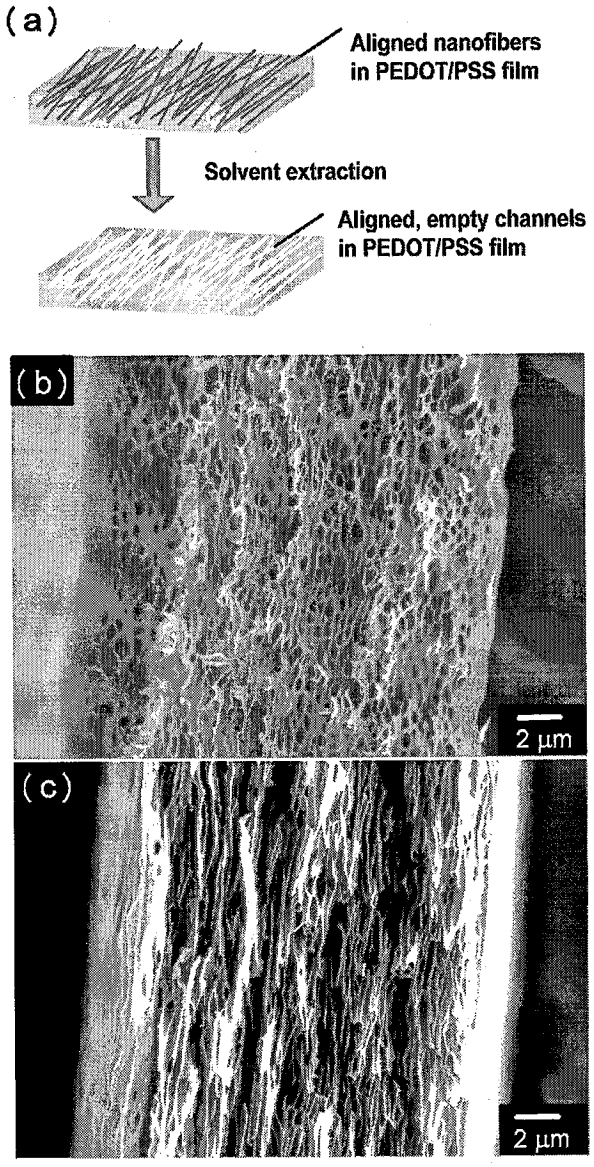

Figure 4.7 (a) Schematic illustration of the preparation of PEDOT/PSS film with aligned channels in PEDOT/PSS layer. (b) SEM image of macroporous PEDOT/PSS film with channel arrays (perpendicular to the channel direction) and (c) SEM image of macroporous PEDOT/PSS film with channel arrays (parallel with the channel direction).

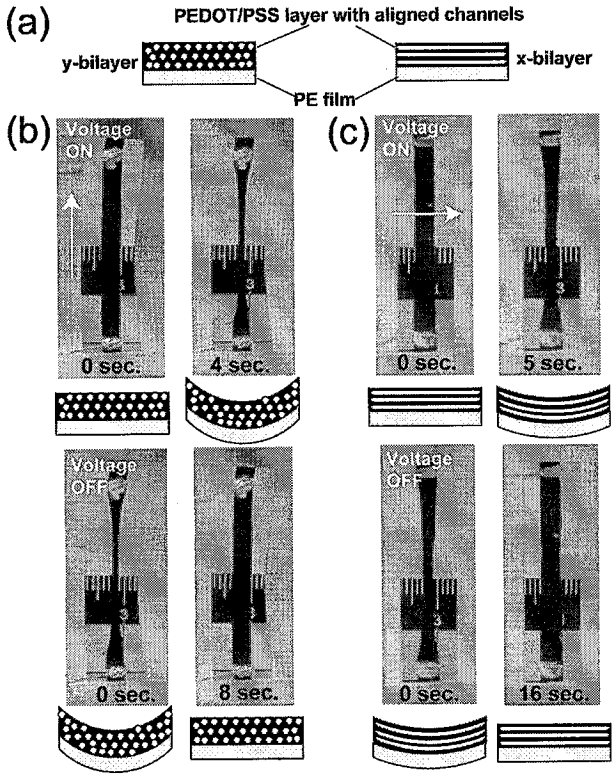

Figure 4.8 (a) Illustration of macroporous PEDOT/PSS-PE bilayer. Left image: y-bilayer, right image: x-bilayer. (b), (c) Time-lapse images of bending/unbending movement of Macroporous PEDOT/PSS-PE bilayer actuators, the channel orientations are highlighted by the arrows in (b) and (c). The images below each time-lapse image are the cross section illustrations of the PEDOT/PSS-PE bilayers. The thicknesses of the PE film, PVA interlayer, and macroporous PEDOT/PSS layer are 10, 0.55, and 5.3 μm. The actuations are measured under an applied constant current of 53 mA at room temperature (25°C) with a 50% RH.

The anisotropic configuration of this macroporous PEDOT/PSS might affect the actuation properties. As a result, we prepared the two PEDOT/PSS-PVA bilayers by cutting the bilayer in two different directions. The cross section illustration images of configurations are clearly depicted in Figure 4.8a. The left image indicates the aligned channel direction parallels to the loading direction and is defined as y-bilayer. The right image indicates the aligned channel direction perpendiculars to the loading direction and is defined as x-bilayer. Figure 4.8b and c show the time-lapse images of bending/unbending movement of these macroporous PEDOT/PSS-PE bilayer actuators. The aligned channel directions are highlighted by the

arrows in Figure 4.8b and c. The images below each time-lapse image are the cross section illustrations of the PEDOT/PSS-PE bilayers. The y-bilayer exhibits a large bending motion by bending to a strong curving configuration from PE film to PEDOT/PSS layer as soon as the electrical field is applied. This motion is highly reversible when the applied voltage is turned off (Figure 4.8b). The x-bilayer showed a small bending from a flat configuration to a curving configuration after applying electrical field. This motion is also highly reversible when the applied voltage is turned off and the bilayer returned to a flat configuration (Figure 4.8c).

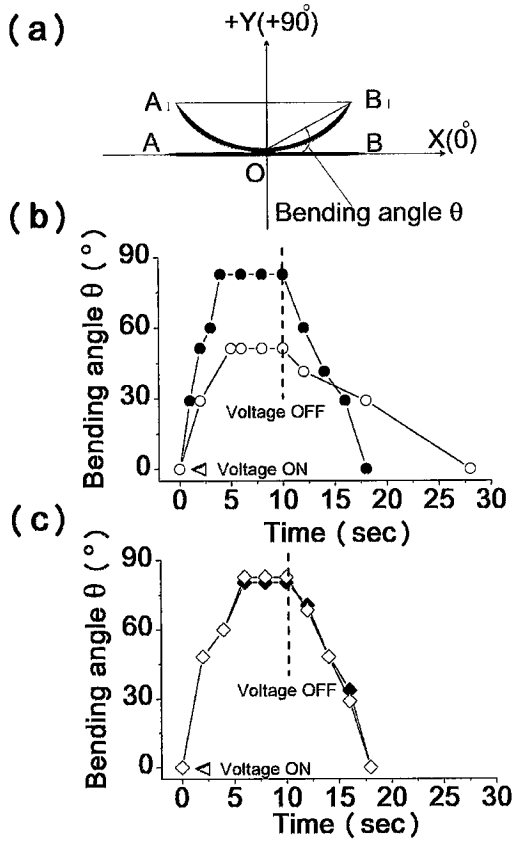

Figure 4.9 (a) Schematic illustration of the bending/unbending movements. (b) Time-dependent bending angles of macroporous PEDOT/PSS-PE bilayer actuators with aligned channels ((●) y-bilayer, (○) x-bilayer,). The thicknesses of the PE film, PVA interlayer, and macroporous PEDOT/PSS layer with aligned channel are 10, 0.55, and 5.3 μm. (c) Time-dependent bending angles of macroporous PEDOT/PSS-PE bilayer actuators with nonaligned channels. The thicknesses of the PE film, PVA interlayer, and macroporous PEDOT/PSS layer with aligned channel are 10, 0.55, and 6.3 μm. The actuations are measured under an applied constant current of 53 mA at room temperature (25°C) with a 50% RH.

Figure 4.9a shows a schematic illustration of the bending/unbending movement of the bilayer actuators. The bending angle (θ) of the bilayer actuator was obtained from the width between A_1 and B_1 monitored by camcorder. Figure 4.9b shows the time-dependent bending angles of the y-bilayer and x-bilayer. The y-bilayer takes 4 s to bend from 0° to 83° after applying the electrical field, indicating a bending speed of 21°/sec. The value is higher than that of bilayer with nonaligned channels (13.4°/sec) and is about 10 times than that of bilayer without channels (2.3°/sec).[24] In contrast, x-bilayer takes 5 s to bend from 0° to 51° after applying the electrical field, indicating a bending speed of 10.2°/sec. However, the bilayer with nonaligned channels shows an isotropic bending motion when it was tested by cutting the bilayer in different directions. Thus, the bending actuations of these two bilayers with aligned channels indicate that the bending motion of the bilayer actuators is affected by the alignment of the channel structures in PEDOT/PSS layer. This phenomenon has some similarity with PEDOT/PSS coated papers, which shows anisotropic electromechanical motion induced from the orientation of cellulose fibers in the paper.[48] Bilayers with aligned nanofibers in PEDOT/PSS layer also show an anisotropic bending motion when an electric field is applied The aligned nanofibers act as filler which reinforce PEDOT/PSS film in the main orientation of the nanofibers(Figure 4.9). The Young's modulus along the nanofiber direction is about twice than that of perpendicular to the nanofiber direction (Figure 3.13a). As a result, the bending motion along the fiber direction is limited. After removing the nanofibers by solvent extraction, the Young's modulus difference in these two direction is still obvious, which indicates the alignment direction of the channel affect the mechanical property of PEDOT/PSS film and finally results in the anisotropic bending actuation of PEDOT/PSS-PE bilayer. The bending motion of these two bilayer actuators with aligned channel structures are highly reversible and can return to their original configuration after

turning of the electrical field. These bending/unbending motions can be repeated over 100 times without any damage to both of the two bilayer actuators. These results suggest that construction of aligned channel in PEDOT/PSS layer can achieve anisotropic bending actuation of the bilayers. These results also lead to fabricate the fast-response conductive polymer with intensive bending actuation.

4.4 Conclusions

In summary, we developed a simple method for constructing channel structures in conductive PEDOT/PSS film by using PVP/PMMA nanofiber template which fabricated in chapter 3. PEDOT/PSS aqueous dispersion penetrates into the nonwoven nanofiber mat and all nanofibers are decorated with PEDOT/PSS. The nanofibers are robust enough to retain its morphology during the deposition process and can be easily removed by the solvent extraction process. The channels in PEDOT/PSS film provide an adsorption interface of water vapors because of its surface area and improve the actuation properties. Moreover, PEDOT/PSS-PE bilayer having this aligned channels in PEDOT/PSS layer displayed an anisotropic bending actuation compared with the bilayer having nonaligned channels. The alignment of the channels replicating the morphology of the aligned PVP/PMMA nanofibers and plays an important role to affect the anisotropic bending actuation of PEDOT/PSS-PE bilayer. Construction of channels in conductive polymer provides new possibilities for fabricating lightweight, low-cost, and flexible ambient devices having improved electromechanical properties.

References

1. K. Lewandowski, P. Murer, F. Svec, J. M. J. Frechet, The Design of Chiral Separation Media Using Monodisperse Functionalized Macroporous Beads: Effects of Polymer Matrix, Tether, and Linkage Chemistry, *Anal. Chem.* **1998**, *70*, 1629-1638.
2. J. E. G. J. Wijnhoven, W. L. Vos, Preparation of Photonic Crystals Made of Air Spheres in Titania, *Science* **1998**, *281*, 802-804.
3. D. B. Akolekar, A. R. Hind, S. K. Bhargava, Synthesis of Macro, Meso and Microporous Carbon from Natural and Synthetic Sources, and Their Application as Adsorbents for the Removal of Quaternary Ammonium Compounds from Aqueous Solution, *J. Colloid Interface Sci.* **1998**, *199*, 92-98.
4. P. Jiang, K. S. Hwang, D. M. Mittleman, J. F. Bertone, V. L. Colvin, Template-Directed Preparation of Macroporous Polymers with Oriented and Crystalline Arrays of Voids, *J. Am. Chem. Soc.*, **1999**, *121*,11630-11637.
5. J. D. Joannopoulos, P. R. Villeneuve, S. H. Fan, Photonic Crystals: Putting an New Twist on Light, *Nature* **1997**, *386*, 143-149.
6. M. R. Abidian, D. H. Kim, D. C. Martin, Conducting-Polymer Nanotubes for Controlled Drug Release, *Adv. Mater.* **2006**, *18*, 405-409.
7. P. V. Braun, P. Wiltzius, Macroporous Materials-Electrochemically Grown Photonic Crystals, *Curr. Opin. Coll. Int. Sci.* **2002**, *7*, 116-123.
8. G. Widawski, M. Rawiso, B. Francois, Self-organized Honeycomb Morphology of Star-polymer Polystyrene Films, *Nature* **1994**, *369*, 387-389.
9. A. Imhof, D. J. Pine, Ordered Macroporous Materials by Emulsion Templating, *Nature* **1997**, *389*, 948-951.
10. A. Imhof, D. J. Pine, Uniform Macroporous Ceramics and Plastics by Emulsion Templating, *Adv. Mater.* **1998**, *10*, 697-700.
11. M. B. Tennikov, N. V. Gazdina, T. B.Tennikova, F. Svec, Effect of Porous Structure of Macroporous Polymer Supports on Resolution in High-performance Membrane Chromatography of Proteins, *J. Chromatogr. A.* **1998**, *798*, 55-64.
12. O. D. Velev, T. A. Jede, R. F. Lobo, A. M. Lenhoff, Porous Silica via Colloidal Crystallization, *Nature* **1997**, *389*, 447-447.

13. S. H. Park, Y. Xia, Fabrication of Three-Dimensional Macroporous Membranes with Crystalline Lattices of Polymer Beads as Templates, *Chem. Mater.* **1998**, *10*, 1745-1747.

14. R. Fan, R. Karnik, M. Yue, D. Li, Y. A. Majumdar, P. D. Yang, DNA Translocation in Inorganic Nanotubes, *Nano Lett.* **2005**, *5*, 1633-1637.

15. S. H. Choi, G. Ankonina, D. Y. Youn, S. G. Oh, J. M. Hong, A. Rothschild, I. D. Kim, Hollow ZnO Nanofibers Fabricated Using Electrospun Polymer Templates and Their Electronic Transport Properties, *ACS nano*. **2009**, *3*, 2623-2631.

16. A. J. Yin, J. Li, W. Jian, J. A. Bennett, J. M. Xu, Fabrication of Highly Ordered Metallic Nanowire Arrays by Electrodeposition, *Appl. Phys. Lett.* **2001**, *79*, 1039-1041.

17. D. A. Czaplewski, J. Kameokaa, R. Mathers, G. W. Coates, H. G. Craighead, Nanofluidic Channels with Elliptical Cross Sections Formed Using a Nonlithographic Process, *Appl. Phys. Lett.* **2006**, *83*, 4386-4388.

18. M. Wang, N. Jing, C. B. Su,, J. Kameokaa, Electrospinning of Silica Nanochannels for Single molecule detection, *Appl. Phys. Lett.* **2006**, *88*, 033106-1-033106-3.

19. S. I. Cho, S. B. Lee, Conducting Polymer Nanotubes. In *Dekker Encyclopedia of Nanoscience and Nanotechnology*. Contescu, C. I. Putyera, K. Eds. 2nd edition CRC Press: Boca Raton, 2009; Volume I, pp 965-973.

20. A. D. W. Carswell, B. P. Grady, One-Dimensional Electrically Conducting Polymeric Nanostructures. In *Dekker Encyclopedia of Nanoscience and Nanotechnology*. Contescu, C. I. Putyera, K. Eds. 2nd edition; CRC Press: Boca Raton, 2009; Volume V, pp 3243-3250.

21. J. S. Jang, X. L. Li, J. H. Oh. Facile Fabrication of Polymer and Carbon Nanocapsules Using Polypyrrole Core/Shell Nanomaterials, *Chem. Commun.* **2004**, *7*, 794-795.

22. M. A. C. Stuart, W. T. S. Huck, J. Genzer, M. Muller, C. Ober, M. Stamm, G. B. Sukhorukov, I. Szleifer, V. V. Tsukruk, M. Urban, *et al.* Emerging Applications of Stimuli-Responsive Polymer Materials, *Nat. Mater.* **2010**, *9*, 101-113.

23. R. Xiao, S. I. Cho, R. Liu, S. B. Lee, Controlled Electrochemical Synthesis of Conductive Polymer Nanotube Structures, *J. Am. Chem. Soc.* **2007**, *129*, 4483-4489.

24. Y. Z. Long, L. J. Zhang, Y. J. Ma, Z. J. Chen, N. L. Wang, Z. Zhang, M. X. Wan, Electrical Conductivity of an Individual Polyaniline Nanotube Synthesized by a Self-Assembly Method, *Macromol. Rapid. Commun.* **2003**, *24*, 938-942
25. Y. Z. Long, L. J. Zhang, Z. J. Chen, K. Huang, Y. S. Yang, H. M. Xiao, M. X. Wan, A. Z. Jin, C. Z. Gu, Electronic Transport in Single Polyaniline and Polypyrrole Microtubes, *Phys. Rev. B.* **2005**, *71*, 1654121-1654127.
26. B. H. Kim, D. H. Park, J. Joo, S. G. Yu, S. H. Lee, Synthesis, Characteristics, and Field Emission of Doped and Dedoped Polypyrrole, Polyaniline, Poly(3, 4-ethylenedioxythiophene), *Synth. Met.* **2005**, *150*, 279-284.
27. S. I. Cho, S. B. Lee, Fast Electrochemistry of Conductive Polymer Nanotubes: Synthesis, Mechanism, and Application, *Acc. Chem. Res.* **2008**, *41*, 699-707.
28. C. R. Martin, Template Synthesis of Electronically Conductive Polymer Nanostructures, *Acc. Chem. Res.* **1995**, *28*, 61-68.
29. T. A. Skotheim, J. R. Reynolds, Eds., Handbook of Conducting Polymers,3rd edition, CRC Press, Boca Raton 2007; Volume I, pp 308-309.
30. M. Kimura, T. Osawa, N. Adachi, Y. Tatewaki, T. Fukawa, H. Shirai, Preparation of Porous Conjugated Polymers Using Amphiphilic Triblock Copolymers PEO–PPO–PEO as Structure-directing Agents, *Chem. Lett.* **2009**, *38*, 250-251.
31. A. Greiner, J. H. Wendorff, Electrospinning: A Fascinating Method for the Preparation of Ultrathin Fibers, *Angew. Chem. Int. Ed.* **2007**, *46*, 5670-5703.
32. J. Xie, X. R. Li, Y. N. Xia, Putting Electrospun Nanofibers to Work for Biomedical Research, *Macromol. Rapid Commun.* **2008**, *29*, 1775-1792.
33. V. Thavasi, G. Singh, S. Ramakrishna, Electrospun Nanofibers in Energy and Environmental Applications, *Energy Environ. Sci.* **2008**, *1*, 205-221.
34. M. Li, Y. Guo, Y. Wei, A. G. MacDiarmid, P. I. Lelkes, Electrospinning Polyaniline-contained Gelatin Nanofibers for Tissue Engineering Applications, *Biomaterials* **2006**, *27*, 2705-2715.
35. A. G. MacDiarmid, W. E. Jones, I. D. Norris, J. Gao, A. T. Johnson, N. J. Pinto, J. Hone, B. Han, F. K. Ko, H. Okuzaki, M. Llaguno, Electrostatically-generated Nanofibers of Electronic Polymers, *Synth. Met.* **2001**, *119*, 27-30.

36. I. S. Chronakis, S. Grapenson, A. Jakob, Conductive Polypyrrole Nanofibers via Electrospinning: Electrical and Morphological Properties, *Polymer* **2006**, *47*, 1597-1603.

37. S. Chuangchote, T. Srikhirin, P. Supaphol, Color Change of Electrospun Polystyrene/MEH-PPV Fibers from Orange to Yellow through Partial Decomposition of MEH Side Groups, *Macromol. Rapid. Commun.* **2007**, *28*, 651-659.

38. A. Laforgue, L. Robitaille, Fabrication of Poly-3-hexylthiophene/Polyethylene Oxide Nanofibers, *Synth. Met.* **2008**, *158*, 577-584.

39. S. Lee, G. D. Moon, U. Jeong, Continuous production of uniform poly(3-hexylthiophene) (P3HT) nanofibers by electrospinning and their electrical properties, *J. Mater. Chem.* **2009**, *19*, 743-748.

40. O. Martinez, A. G. Bravo, N. J. Pinto, Fabrication of Poly(vinylidene fluoride–trifluoroethylene)/Poly(3,4-ethylenedioxythiophene)–Polystyrene Sulfonate Composite Nanofibers via Electrospinning, *Macromolecules* **2009**, *42*, 7924-7929.

41. B. W. Jensen, K. West, Vapor-Phase Polymerization of 3,4-Ethylenedioxythiophene: A Route to Highly Conducting Polymer Surface Layers, *Macromolecules* **2004**, *37*, 4538-4543.

42. A. Laforgue, L. Robitaille, Production of Conductive PEDOT Nanofibers by the Combination of Electrospinning and Vapor-Phase Polymerization, *Macromolecules* **2010**, *43*, 4194-4200.

43. A. Laforgue, L. Robitaille, Deposition of Ultrathin Coatings of Polypyrrole and Poly(3,4-ethylenedioxythiophene) onto Electrospun Nanofibers Using a Vapor-Phase Polymerization Method, *Chem. Mater.* **2010**, *22*, 2474-2480

44. H. Dong, W. E. J. Jr Jones, Preparation of Submicron Polypyrrole/Poly(methyl methacrylate) Coaxial Fibers and Conversion to Polypyrrole Tubes and Carbon Tubes, *Langmuir* **2006**, *22*, 11384-11387.

45. X. Hou, L. Jiang, Learning from Nature: Building Bio-Inspired Smart Nanochannels, *ACS nano*. **2009**, *3*, 3339-3342.

46. P. Abgrall, N. T. Nguyen, Nanofluidic Devices and Their Applications *Anal. Chem.* **2008**, *80*, 2326-2341.

47. H. Okuzaki, H. Suzuki, T. Ito, Electromechanical Properties of Poly (3, 4-ethylenedioxythiophene)/Poly(4-styrene sulfonate) Films, *J. Phys. Chem. B.* **2009**,

113, 11378-11383.

48. J. Zhou, T. Fukawa, H. Shirai, M. Kimura, Anisotropic Motion of Electroactive Papers Coated with PEDOT/PSS, *Macromol. Mater. Eng.* **2010**, *295*, 671-675.
49. B. E. Yoldas, M. J. Annen, J. Bostaph, Chemical Engineering of Aerogel Morphology Formed under Nonsupercritical Conditions for Thermal Insulation, *Chem. Mater.* **2000**, *12*, 2475-2484.
50. D. Y. Kim, Y. S. Kim, K. W. Choi, J. C. Grunlan, C, H. Yu, Improved Thermoelectric Behavior of Nanotube-filled Polymer Composites with Poly(3,4-ethylenedioxythiophene)/poly(styrenesulfonate), *ACS Nano*, **2010**, *4*, 513-523.
51. B. Zhang, J. Sun, H. E. Katz, F. Fang, R. L. Opila, Promising Thermoelectric Properties of Commercial PEDOT:PSS Materials and Their Bi_2Te_3 Powder Composites, *ACS Appl. Mater. Interfaces*. **2010**, *2*, 3170-3178.

Chapter 5

Conclusions and Outlook

Chapter 5 Conclusions and Outlook

This chapter highlights the topics obtained from the devolopment of PEDOT/PSS-based actuators with anisotropic actuations. These conclusions drawn from the results learned both at the material and the structure levels. The upcoming sections follow the course of research that occurred in this study and this thesis, progressing from design to fabrication, and to characterization of the PEDOT/PSS-based anisotropic actuators. This final section summarizes the achieved results and makes the outlook for future research in this area.

5.1 Thesis Conclusion

This thesis was directed at the development of PEDOT/PSS-based actuators for anisotropic actuation. The anisotropic actuation allows more efficient control of independent structure and could largely improve structural control performance. Thus, there is a need for development of anisotropic actuation of conductive polymer based actuators. This thesis provided a strong motivation for the construction of PEDOT/PSS-based actuators for anisotropic actuation. This study highlighted the difference in the origins of actuator anisotropy. And showed the actuation anisotropy which stems from different in-plane Young's modulus, contributes to an actuator's ability to generate unequal stresses.

Chapter 2 started with a Paper coated with highly conductive PEDOT/PSS paper can generate different stresses within the plain of the paper in accordance with the fiber orientation. It indicated that the coated paper has a higher degree of compliance at cross direction than the machine direction. The generated stress transformation will turn out to be easier when the testing is carried out to the off-principal directions where the main fiber orientation does not coincide with the loading direction. Moreover, the PEDOT/PSS paper underwent an anisotropic bending motion in response to an electronic field in ambient air. The subtasks indentified in this study, the effect of weight of PEDOT/PSS, relative humidity,

voltage and frequency on actuation properties, have been carried out in order to understand the goal. The mechanics of the anisotropic actuation of the PEDOT/PSS papers are now understood.

Chapter 3 followed the anisotropic actuator design in chapter 1 and had some similarity with the design in chapter 2. However, the cellulose fiber-based paper (in chapter 2) has been changed into electrospun nanofibers. Chapter 3 showed that the goal of anisotropic actuation of PEDOT/PSS film can also be realized by using electrospun nanofibers. PEDOT/PSS composite film incorporating the aligned nanofiber assemblies exhibited anisotropic electromechanical properties due to the anisotropic mechanical properties within the composite film. Moreover, the PEDOT/PSS-PE bilayer with incorporated aligned nanofiber mat showed an anisotropic bending motion on application of the electrical field. It follows that the bending motion is affected by the alignment of the nanofiber structures in the PEDOT/PSS layer, and the difference of Young's modulus in the composite films results in the anisotropic bending actuation.

By using the electrospun nanofiber templates which were fabricated in chapter 3, chapter 4 proceeded to fabricate macroporous PEDOT/PSS films with channel structures. The nanofibers are robust enough to retain its morphology during the deposition process and can be easily removed by the solvent extraction process. The channels in PEDOT/PSS film provide an adsorption interface of water vapors because of its surface area and improve the actuation properties. Moreover, PEDOT/PSS-PE bilayer having this aligned channels in PEDOT/PSS layer displayed an anisotropic bending actuation compared with the bilayer having nonaligned channels. The alignment of the channels replicating the morphology of the aligned PVP/PMMA nanofibers and plays an important role to affect the anisotropic bending actuation of PEDOT/PSS-PE bilayer.

5.2 Outlook

The future work will involves enhancement of actuation aimed at material level and at structural level. For the macroporous PEDOT/PSS film with channels, it is possible to manipulate the diameter, shape, density and alignment of the channels in conductive polymer films by controlling the template nanofibers through different electrospinning conditions. These factors might finally affect the actuation properties.

Publications

1. Zhou, J.; Fukawa, T.; Shirai, H.; Kimura, M. Anisotropic Motion of Electroactive Papers Coated with PEDOT/PSS, *Macromol. Mater. Eng.* **2010**, *295*, 671-675.
2. Zhou, J.; Kimura, M. Electromechanical Actuation of Highly Conductive PEDOT/PSS-coated Cellulose Papers, *SEN'I GAKKAISHI* **2011**, *67*, 125-131.
3. Zhou, J.; Gao, Q.; Fukawa, T.; Kimura, M. Macroporous Conductive Polymer Films Fabricated Using Electrospun Polymer Templates and Their Electromechanical Properties, *Nanotechnology* **2011**, *22*, 275501.
4. Zhou, J.; Fukawa, T.; Kimura, M. Directional Electromechanical Properties of PEDOT/PSS Films containing Aligned Electrospun Nanofibers, *Polymer Journal.* **2011,** doi:10.1038/pj.2011.62

International Conferences

1. Zhou, J.; Gao, Q.; Kimura, M. "Macroporous Conductive Polymer Films with Channels and Its Application," *International Conference on Materials for Advanced Technologies (ICMAT 2011)*, Singapore, June 2011.
2. Zhou, J.; Kimura, M. "Construction of Conductive Polymer Channels," *The 5th Nagoya University-UCLA International Symposium (Global COE Joint Symposium)*, Ueda, Japan, August 2010.
3. Zhou, J.; Kimura, M. "Construction of Three-dimensional Nanochannels in PEDOT/PSS Film," The 10th *International Conference of Future Textile*, Ueda, Japan, July 2010.
4. Kimura, M.; Lin, B. J.; Zhou, J. "Foldable Textile Electronic Devices Using All-organic Conductive Fibers," The 10th *International Conference of Future Textile*, Ueda, Japan, July 2010.
5. Zhou, J.; Kimura, M. "Porous Conductive Polymer Materials Having Continuous

Nanochannels," *International Symposium on Polymer Chemistry*, Suzhou, China, June 2010.

6. Zhou, J.; Kimura, M. "Electroactive EG-treated PEDOT/PSS Paper Actuator Working in Air," *The 1st FAPS Congress*, Nagoya, Japan, October 2009.
7. Zhou, J.; Kimura, M. "Electroactive PEDOT/PSS-coated Cellulose Paper Actuator Working in Air," Extended abstract, *The 10th Asian Textile Conference,* Ueda, Japan, July 2009.
8. Zhou, J.; Kimura, M. "Electroactive PEDOT/PSS Film Actuator Working in Air," The *7th East Asian Symposium on Polymers for Advanced Technology*, Ueda, Japan, May 2009.

Acknowledgements

I would like to take this opportunity to thank many people who made this research possible.

First and foremost, I would like to thank my advisor Professor Mutsumi Kimura for his support and guidance. I am constantly amazed by his depth on science, which he always shared with me. He has provided me with an scientific environment filled with possibilities that inspired my mind and enticed my imagination.

I would like to acknowledge the members of my thesis committee, Prof. Toshihiro Hirai, Prof. Hidenori Okuzaki, Prof. Kousaku Ohkawa, Prof. Yuichi Hirada. Great thanks to them for looking through my thesis carefully and providing great advices to improve my work.

I am grateful for Mr. Fukawa for all of his support and positive outlook on my research. I would also like to thank him for his expertise on physics, material science, electronics and experimental set-ups. I highly respect his opinions. Great thanks to Mr. Bangjia Lin who provide all his kindness help on the first six months when I start my life in Japan. Thanks again to Mr. Bangjia Lin for his effort to teach me on lots of measurements such as SEM, TG, DSC, IR and so forth. Thanks to Qiang Gao for always being there for discussion on no matter experiments or new crazy ideas. And also I appreciate for his expertise on electrospinning, his advise greatly accelerates my research process. Thanks to Junko Takizawa and Seiko Sato for their technical supports on my experiments. Thanks for my tutor Shigenori Kamada who teaches me Japanese, and meaurements like Raman and UV. Other menbers in our lab like Otsuji Satoshi, Masayoshi Karazawa, Mei Yokokawa, Keisuke Takemoto, Hiroki Yamagiwa and Althiery Anne-Claire have had the arduous task of working with me and their help and discussions certainly enriched my knowledge. There are so many memories that I will cherish because of them: barbecues, hanamis, small trips. Their friend ship has made these three years a wonderful experiences.

Thanks for the financial support of Global COE Program for "International Center of Excellence on Fiber Engineering". My sincere gratitude goes out to Ms. Yamashita, Ms. Miyazaki, Ms. Yamamoto and Ms. Kubota for their work on daily issues like research fees and conference expenses.

I would like to thank my parents in China. They have stood by me throughout the years and offered their encouragement, patience and support no matter where I am. I am so grateful to have such a loving family.

And finally, to my wife Xuezhu Xu, thank you for being with me in this long journey and lighting up my life. Thank you for giving me the motivation to my research and help me set the goals that have become important in my life.

Anisotropic Properties of Fiber-embedded Soft Materials **September 2011** **Jian Zhou**